# Optical Frequency Transfer via Telecommunication Fiber Links for Metrological Applications

Von der Fakultät für Mathematik und Physik der
Gottfried Wilhelm Leibniz Universität Hannover

zur Erlangung des Grades

Doktor der Naturwissenschaften
Dr. rer. nat.

genehmigte Dissertation

von

Stefan Droste
geboren am 11. September 1984 in Münster

2014

# Zusammenfassung

Für die vorliegende Arbeit wurde die Übertragung hochstabiler optischer Frequenzen über Glasfaserverbindungen großer Reichweite untersucht. Derartige Frequenzen stehen dank der enormen Fortschritte in der Entwicklung optischer Frequenzstandards mittlerweile mit nie dagewesener Genauigkeit zur Verfügung. In Zukunft werden optische Frequenzstandards daher nicht nur die gegenwärtigen, auf Mikrowellen basierenden Primärstandards zur Zeitmessung ablösen, sondern auch als Messwerkzeuge für unterschiedlichste Experimente in der Grundlagenforschung, der Geowissenschaft, der Astronomie und weiteren Forschungsgebieten Verwendung finden.

Da jedoch weltweit nur wenige Exemplare solcher hochgenauen optischen Atomuhren existieren, die zudem aufgrund ihres komplexen Aufbaus nicht oder nur mit enormem Aufwand transportabel sind, werden Verfahren benötigt, um die Frequenzinformation der optischen Standards zu möglichen Anwendern zu transferieren. Satellitengestützte Verfahren sind zwar in der Lage, die Frequenzen der gegenwärtigen Mikrowellenstandards ohne nennenswerte Genauigkeitsverluste zu übertragen. Für optische Frequenzen ist die erreichbare Genauigkeit mit der bisherigen Technik jedoch nicht mehr ausreichend, sodass neue Verfahren wie die in dieser Arbeit beschriebene Übertragung mit Hilfe von Glasfaserverbindungen benötigt werden.

Während dieser Dissertation wurde die Frequenzübertragung mit Hilfe von Laserlicht mit einer stabilen optischen Trägerphase über zwei 920 km lange Glasfaserleitungen untersucht, welche das Max-Planck-Institut für Quantenoptik (MPQ) in Garching mit der Physikalisch-Technischen Bundesanstalt (PTB) in Braunschweig verbinden. Schwankungen der optischen Weglänge müssen zunächst detektiert und anschließend aktiv kompensiert werden, um eine stabile und genaue Übertragung der optischen Frequenz zu gewährleisten. In einem ersten Experiment konnte eine relative Restinstabilität der übertragenen Frequenz von $5 \times 10^{-15}$ in 1 s und weniger als $10^{-18}$ nach 1000 s demonstriert werden. Zudem zeigte die transferierte Frequenz keine Abweichung von der Originalfrequenz innerhalb einer Unsicherheit von $4 \times 10^{-19}$ oder 80 $\mu$Hz.

In einem zweiten Experiment wurden die beiden 920 km langen Glasfasern in Reihe hintereinander geschaltet, um eine 1840 km lange Faserschleife zu erzeugen, die vom MPQ aus bis zur PTB und zurück zum MPQ führt. Auch hierüber wurde eine optische Trägerphase erfolgreich übertragen, wobei eine Restinstabilität von $3 \times 10^{-15}$ in 1 s und $4 \times 10^{-19}$ nach lediglich 100 s erzielt wurde. Die Abweichung der transmittierten Frequenz von der Originalfrequenz betrug weniger als $3 \times 10^{-19}$ oder 60 $\mu$Hz. Diese Faserverbindung ist die bei Weitem längste Faserstrecke, die jemals für den Transfer von hochstabilen Frequenzen untersucht wurde. Die Länge von 1840 km reicht aus, um nahezu alle sich mit Präzisionsmessungen beschäftigenden Institute in Europa

miteinander zu verbinden, was den Vergleich von Atomuhren sowie die Durchführung von Hochpräzisionsexperimenten ermöglichen würde.

Trotz der hervorragenden Resultate, die mit Faserverbindungen erreicht werden können, sind die satellitenbasierten Systeme weiterhin die Methode der Wahl für Anwendungen, die nicht allerhöchste Ansprüche an Stabilität und Genauigkeit stellen. Aus diesem Grund wurde eine auf dem Global Positioning System (GPS) basierende Satellitenverbindung zwischen MPQ und PTB mit Hilfe einer der 920 km Faserstrecken charakterisiert. Diese GPS-Verbindung, welche eine Basislänge von 450 km hat, zeigte eine Instabilität von $3 \times 10^{-13}$ in 30 s und $5 \times 10^{-16}$ nach 20.000 s. Die Unsicherheit der übertragenen Mikrowellenfrequenz wurde zu $6 \times 10^{-16}$ bestimmt. Im Gegensatz zu den meisten bisherigen Untersuchungen zu GPS-Verbindungen erlaubte die Verwendung der Faserstrecke die Charakterisierung dieser GPS-Verbindung unabhängig vom Einfluss der involvierten Frequenzstandards. Die erzielten Ergebnisse zeigen, dass bei Verwendung geeigneter Hardware der Vergleich von Mikrowellenuhren über eine GPS-Verbindung bis zu einem Niveau von etwa $5 - 6 \times 10^{-16}$ nicht durch das Rauschen dieser Verbindung limitiert ist. Somit kann ein Großteil der sich heute im Einsatz befindlichen Mikrowellenuhren über eine GPS-Verbindung verglichen werden. Für Fontänenuhren, welche eine Genauigkeit von etwa $2 - 3 \times 10^{-16}$ erreichen, reicht die erzielbare Übertragungsgenauigkeit einer solchen GPS-Verbindung jedoch nicht aus. Darüber hinaus liegt die demonstrierte Genauigkeit der GPS-Verbindung etwa drei Größenordnungen überhalb der einer Faserverbindung vergleichbarer Länge, was für einen Vergleich optischer Frequenzstandards eindeutig unzureichend ist.

**Stichworte:** Faserverbindung, Frequenztransfer, Atomuhr

# Abstract

This thesis reports on the characterization of ultra-stable optical frequency transfer via long-haul telecommunication fiber links. Optical frequencies like this are provided by stable laser systems which are used in optical atomic frequency standards that allow for the generation of frequencies with unprecedented stability and accuracy. These frequency standards not only constitute high-performance time keeping devices but can also be seen as measurement tools for various experiments in fundamental research, geoscience, astronomy, and other fields.

However, the most precise atomic clocks are operated at only a handful of locations around the world and they can hardly be transported from one location to another due to their highly complex nature. Consequently, methods of transmitting the frequency information of atomic clocks to distant places like metrology institutes are required. Traditionally, satellite based systems are used to link the majority of precision measurement laboratories around the world. While these systems demonstrate respectable performances which are sufficient for the dissemination of most microwave atomic clock signals, novel techniques are required to transfer the unprecedented stable and accurate optical clock signals.

In the course of this work, the transmission of a frequency reference with a stable optical carrier-phase through two 920 km fiber links that connect the Max-Planck-Institut für Quantenoptik (MPQ) in Garching and the Physikalisch-Technische Bundesanstalt (PTB) in Braunschweig is investigated. Fluctuations of the optical path length are detected and actively compensated in order to achieve a stable and accurate frequency transfer. In this first experiment, residual instabilities of the transferred frequency of $5 \times 10^{-15}$ in 1 s and less than $10^{-18}$ after 1000 s are achieved. Moreover, the transmitted frequency shows no deviation from the original frequency within an uncertainty of $4 \times 10^{-19}$ or 80 $\mu$Hz.

In a second experiment, the two 920 km links are connected in series to create an 1840 km fiber link loop that reaches from MPQ to PTB and back to MPQ. Successful transmission of an optical carrier is demonstrated over this link with residual instabilities of $3 \times 10^{-15}$ in 1 s and $4 \times 10^{-19}$ after only 100 s. Deviations of the transmitted frequency are constrained to $3 \times 10^{-19}$ or 60 $\mu$Hz. This fiber link is by far the longest link investigated for frequency transfer up to date. It's length approaches continental scale distances which demonstrates that all of the major precision measurement laboratories within Europe can be connected to exchange highly stable optical frequencies for the purpose of atomic clock comparisons as well as for high precision experiments.

Despite the superior performance achievable with fiber links, the traditional satellite links still remain the dominant method for most frequency transfer applications to date

due to their high degree of flexibility and availability. Therefore, a satellite link based on the Global Positioning System (GPS) between MPQ and PTB is characterized in a third experiment. The characterization is accomplished by using one of the 920 km fiber links mentioned above. This GPS link, having a baseline of 450 km, shows an instability of $3 \times 10^{-13}$ in 30 s and a floor of $5 \times 10^{-16}$ after 20,000 s. The uncertainty of the transferred microwave frequency is determined to be $6 \times 10^{-16}$. Unlike most previous GPS link characterization experiments, the use of the fiber link allows the unambiguous determination of the GPS link performance without any contribution from the involved frequency standards. The demonstrated results imply that the comparison of most microwave frequency standards over a GPS carrier-phase link is not limited by the noise of the frequency transfer link itself. For the comparison of fountain clocks, which achieve an accuracy of $2 - 3 \times 10^{-16}$, the performance of a GPS carrier-phase link is, however, insufficient. Furthermore, the demonstrated performance of a GPS carrier-phase link is about three orders of magnitude worse than a fiber link of a comparable distance which is clearly inadequate for the comparison of state-of-the-art optical frequency standards.

**Keywords:** Fiber link, frequency transfer, atomic clock

# Contents

# Chapter 1

# Introduction

Time is commonly thought of as the definition for the duration of a physical process and a means to characterize the consecutive order in which events occur. Time by itself is absolutely passive. It exists independent of any material or physical process. At the same time, all events and processes occurring in the world are subject to it. Our understanding of nature is, to a large extent, based on time and dynamic processes, which makes it particularly prominent not only in the context of science but also in our everyday life.

Our ability to count the oscillations of electromagnetic waves nowadays makes the measurement of frequencies, the inverse of time, a particularly easy task. In fact, no other physical quantity can be measured with higher accuracy than frequencies. Additionally, we are able to construct devices capable of generating incredibly accurate frequencies. Those devices are typically referred to as frequency standards, while a clock in the common sense comprises an oscillator and a device that is capable of counting the cycles of the oscillation and a means of displaying the result.

Already at the end of the $19^{\text{th}}$ century scientists suggested the idea of using an atomic transition to measure time [1] but it would take another 70 years until the first atomic clock was built in the middle of the past century [2]. Since then, relentless developments have led to microwave atomic clock systems whose accuracy increased with about one order of magnitude every decade until the end of the last century. Time is expressed by the unit "second" in the international system of units (SI). The second is defined by a microwave transition between two hyperfine states in cesium and therefore cesium clocks are often titled as *primary* frequency standards. Accordingly, other frequency standards, for example based on rubidium, are called *secondary* frequency standards.

During the second half of the last century, cesium clocks constituted the state-of-the art in the context of precise frequency generation. Although it was well known that higher oscillator frequencies potentially offer better performance, the development of clocks operating at frequencies significantly above the microwave region was hindered by the electronics needed to count the fast oscillations. Scientists addressed this issue by constructing complex and sophisticated phase-coherent frequency chains that connect an optical frequency with a microwave frequency from a primary frequency standard to

allow for optical frequency measurements referenced to the unit Hertz. The first absolute frequency measurement in the visible part of the optical spectrum was accomplished in the middle of the 1990s [3].

The complicated frequency chains were superseded by the invention of the optical frequency comb technique [4] at the beginning of this century which finally brought a breakthrough by down-converting optical frequencies with more than $10^{15}$ cycles per second to countable microwave frequencies. The first clocks based on optical rather than microwave atomic transitions had already been proposed in 1982 [5]. Suddenly, however, constructing a functional optical clock became a manageable task. Since then, intense research and ingenious techniques have led to a whole variety of optical clocks with outstanding performance.

Meanwhile, optical clocks routinely demonstrate significantly better performance, surpassing even the best cesium clocks and thereby the SI unit Hertz. Whereas the best cesium clock accumulates a deviation of about 20 ps per day, which is approximately 1 s every 140 million years, the best optical clock today accumulates 1 s in about 20 billion years. The characterization of frequency standards requires a comparison to a second standard, with similar or ideally better performance. A comparison of two frequency standards always reveals the performance of the worse of the two standards as its noise is dominating the comparison. Therefore, optical clocks can only be characterized by comparing them among each other. It is expected that the definition of the second will at some point in the future be changed from cesium to an optical standard [6]. Numerous comparisons between the different species of optical clocks are necessary to find a suitable candidate to serve as a next primary frequency standard.

Comparisons of atomic clocks that are separated by more than a few hundred meters are nowadays performed by either the reception of signals from Global Navigation Satellite Systems (GNSS) or by sending and receiving signals through geostationary satellites [7]. Both methods use microwave signals with carrier frequencies of a few Gigahertz. Sophisticated technology has been invented to increase the performance of such a satellite link. However, the achievable stability and accuracy is severely limited due to various effects for satellite based frequency transfer. Therefore, optical clocks cannot be compared at the level of their intrinsic uncertainty using satellites. Consequently, novel time and frequency transfer and dissemination techniques have to be developed.

The present work describes the transfer of optical frequencies over long-haul optical fiber links. An optical carrier emitted by a continuous-wave (cw) laser is sent through underground glass fibers that span a large part of Germany. Originally installed for telecommunication purposes, the fibers are used as a transfer medium to coherently transmit highly stable optical frequencies. As will be discussed later, this concept allows the comparison of optical clocks and consequently, frequency transfer via fiber links has attracted substantial attention in recent years [8–13].

Chapter 2 gives an overview over state-of-the-art frequency standards operating in the microwave as well as in the optical regime after introducing some basics about the characterization of clocks. Additionally, important relationships between clock characteristics and phase noise are introduced for further use throughout this work. Currently

used long-distance time and frequency dissemination techniques are discussed in Chapter 3. Their limitations are laid out in detail to emphasize the need for novel fiber-based methods which are introduced subsequently. Additionally, the principles of fiber based frequency transfer are introduced in this chapter.

In Chapter 4, fiber links with a total length of 920 km and 1840 km are investigated. Here, the experimental setup of these links as well as the characterization of the frequency transfer is described. Additionally, the key components that enable the high-stability transfer of optical frequencies are discussed in detail. Chapter 5 deals with phase noise types that have not been considered up to date but which are present in the systems presented in Chapter 4. The response of the Allan deviation and modified Allan deviation to those noise types is investigated and discussed as well.

As an application of the frequency transfer via fiber link, a GPS carrier-phase frequency transfer link is characterized with the help of the fiber link. The performance of the GPS link is demonstrated by analyzing the stability and accuracy achievable when transferring a microwave frequency over a distance of 450 km. The results are presented in Chapter 6.

Within the framework of this thesis, the borders of existing technology have been pushed to transfer optical frequencies over continental scale distances with unprecedented performances. Previous limitations were overcome in order to enable frequency metrology with 19 digits accuracy. The investigation of fiber link noise properties led to a substantial reduction in averaging time needed to reach superior frequency stabilities. In an optical clock comparison, this means that the noise contribution of the fiber link frequency transfer becomes negligible after a few seconds. Consequently, the fast reduction of the frequency instability potentially also offers the determination of gravitational potential differences with centimeter accuracy within minutes of averaging time.

The high-stability frequency transfer via fiber links not only allows atomic clock comparisons but can rather be seen as an enabling technology. Various applications touching our everyday life like mobile broadband internet or satellite navigation as well as countless scientific experiments from precision spectroscopy to tests of fundamental physics rely on highly accurate reference frequencies. All of those applications directly profit from the availability of ultra stable reference frequencies that this work helps to provide.

# Chapter 2

# Frequency Standards

## 2.1 Introduction

The measurement of time or frequency has a wide range of applications. Devices, that produce highly stable frequency references, or in other words, allow us to measure time intervals, are known as frequency standards. Modern atomic clocks constitute the most common means for a frequency standard today. They provide extremely stable and accurate output frequencies that are used to answer some of the most fundamental questions in physics. Atomic frequency standards play an important role even in our everyday life as the timing signal of an atomic clock that generates the SI-second is distributed country wide in order to synchronize clocks at television and radio broadcasters, station clocks as well as private radio-controlled clocks. Higher demands on accurate frequency references are set by research groups around the world that are aiming to validate Einstein's theory of relativity with an ever increasing precision, to verify theoretical predictions from quantum electrodynamics, or to search for slow temporal variations of natural constants [14–16].

The latest generation of atomic frequency standards take advantage of a significantly higher operating frequency. Those so called optical atomic clocks use optical transitions in atoms or ions instead of microwave transitions. Besides major advances in trapping and cooling of particles the increase in frequency allows a dramatically improved performance with relative uncertainties on the order of one part in $10^{18}$ [17]. Scientists working in fundamental science, in astronomy, in geoscience and other fields of research are expecting to push their experiments to a new level using those novel frequency standards. Also the definition of the SI-second, currently bases on a microwave transition in cesium, is expected to be changed to an optical transition frequency in the future [6].

This chapter gives an introduction to the properties of frequency standards and their characterization. Various high-performance oscillators that are common in most precision measurement laboratories are discussed and an overview of today's best frequency standards is given. Some selected applications of frequency standards are also highlighted in the end of this chapter.

## 2.2   Clock characterization

Any clock consists of a frequency source or oscillator that produces a stable output frequency and a device to count this frequency. The output of the frequency counter can then be used to generate a timing signal. In other words, a frequency counter quantifies the output of a frequency source by counting the oscillating cycles of the frequency. In general, anything from a pendulum to a quartz oscillator or an atomic transition can serve as a frequency source. In the framework of this thesis the focus lies on the most stable existing frequency sources, namely on atomic clocks. Here, atoms or ions are used as an oscillator with a specific transition frequency $\nu(t)$. This frequency is inevitably subject to fluctuations $\Delta\nu(t)$ whose magnitude depends on the individual clock system. More advanced systems decrease the magnitude of those fluctuations to a large extent but they cannot be suppressed entirely. Additionally, the output frequency of an oscillator may be shifted by $\Delta\nu_{shift}$ from its unperturbed value $\nu_0$ due to systematic effects. To characterize a clock both the fluctuations as well as a possible shift are of interest.

Typically, different oscillators operate at different carrier frequencies $\nu_0$. For a carrier frequency independent comparison of all kinds of oscillators it is convenient to define the normalized frequency deviation $y(t)$ as:

$$y(t) = \frac{\Delta\nu(t) + \Delta\nu_{shift}}{\nu_0} = \frac{1}{2\pi\nu_0}\frac{d\phi(t)}{dt} \tag{2.1}$$

where $\phi(t)$ represents the signal's instantaneous phase [18]. The oscillators stability is determined by $\Delta\nu(t)$ while its accuracy is limited by $\Delta\nu_{shift}$. In the following sections the mathematical formalisms to describe both are laid out in greater detail.

### 2.2.1   Stability

**Time domain description**

A time sequence of the fluctuating frequency signal $y(t)$ is measured with the help of a frequency counter. This results in a reduction of the continuous function $y(t)$ into a discrete series of consecutive measurements averaged over the measurement time $\tau$:

$$\overline{y}(t) = \frac{1}{\tau}\int_{t_i}^{t_i+\tau} y(t)\ dt \tag{2.2}$$

The frequency instability of a signal is commonly expressed by the so called *Allan Variance* $\sigma_y^2(\tau)$ (AVAR) or its square root the *Allan standard deviation* $\sigma_y(\tau)$ (ADEV) [19]:

$$\sigma_y^2(\tau) = \left\langle \sum_{i=1}^{2}\left(\overline{y}_i - \frac{1}{2}\sum_{j=1}^{2}\overline{y}_j\right)^2 \right\rangle = \frac{1}{2}\langle(\overline{y}_2(t) - \overline{y}_1(t))^2\rangle \tag{2.3}$$
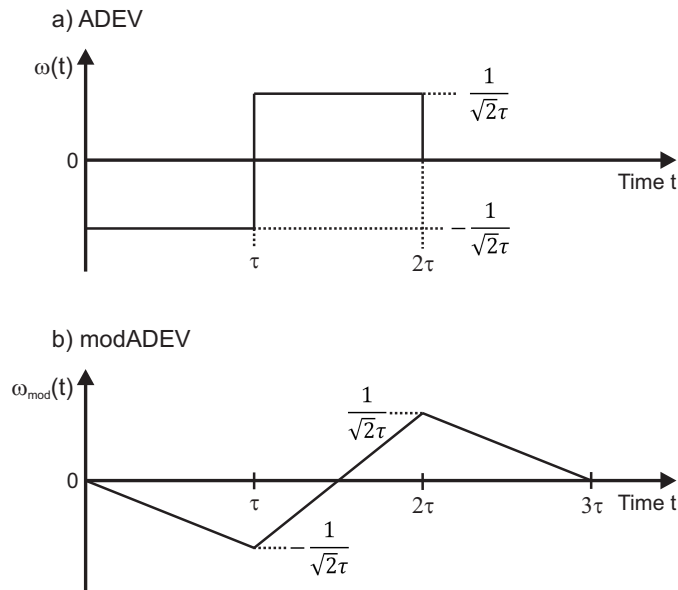
FIGURE 2.1: Filter functions associated with a) the Allan deviation and b) the modified Allan deviation. See also Equation 2.5 and Equation 2.6.

As it can be seen, the ADEV is based on differences of adjacent frequency values rather than on frequency differences from the mean value, as is the normal standard deviation. The confidence of the instability estimate for long averaging times is significantly improved by choosing overlapping samples [20]. This results in the so called overlapping ADEV which is standardly used throughout this thesis.

Equation 2.3 can be rewritten as a weighted integral [21] as

$$\sigma_y^2(\tau) = \left\langle \left( \int_{-\infty}^{\infty} y(t') \, \omega(t-t') \, dt' \right)^2 \right\rangle \tag{2.4}$$

by introducing a filter function $\omega(t)$:

$$\omega(t) = \begin{cases} -\frac{1}{\sqrt{2}\tau} & \text{for} \quad 0 < t \le \tau \\ \frac{1}{\sqrt{2}\tau} & \text{for} \quad \tau < t \le 2\tau \\ 0 & \text{elsewhere} \end{cases} \tag{2.5}$$

which is illustrated in the upper plot of Figure 2.1.

It should be pointed out that the ADEV formalism requires consecutive frequency measurements without dead time, that is, either multiple (for instance two in the simplest case) coordinated frequency counters or one frequency counter capable of performing dead time free measurements has to be used.

The ADEV shows a characteristic response to a number of different contributing noise types. The slope of the ADEV as a function of $\tau$ can therefore be used to identify the
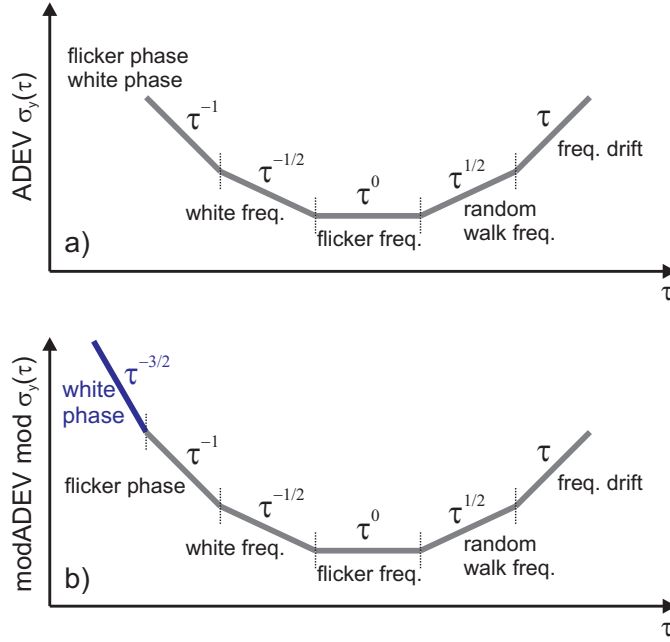
FIGURE 2.2: Response of a) the Allan deviation and b) the modified Allan deviation to the most common noise types. The Allan deviation shows the same $\tau$-dependency for white and flicker phase noise while the modified Allan deviation can be used to distinguish between these two noise types unambiguously.

dominating noise type of a frequency signal. However, the ADEV cannot distinguish between the two common noise types flicker phase and white phase noise (both show a $\tau^{-1}$-dependency). To overcome this deficiency, the so called *modified Allan deviation* (modADEV) has been introduced which features a higher sensitivity to white phase noise [22]. The modADEV is calculated in analogy to Equation 2.3 but with a triangular rather than a constant weighting function [23]:

$$
\omega_{mod}(t) = \begin{cases} -\frac{1}{\sqrt{2}\tau^2}t & \text{for} \quad 0 < t \le \tau \\ \frac{1}{\sqrt{2}\tau^2}(2t - 3\tau) & \text{for} \quad \tau < t \le 2\tau \\ -\frac{1}{\sqrt{2}\tau^2}(t - 2\tau) & \text{for} \quad 2\tau < t \le 3\tau \\ 0 & \text{elsewhere.} \end{cases}
\tag{2.6}
$$

A graphical representation of Equation 2.6 is given in the lower plot of Figure 2.1.

The advantage of the modADEV is its ability to distinguish between more noise types as compared to the ADEV. White phase noise, for instance, averages as $\tau^{-3/2}$ and flicker phase noise as $\tau^{-1}$ in the modADEV (see Figure 2.2). Furthermore, the instability of a frequency that is dominated by white phase noise decreases faster in a given measurement time. Thus, the modADEV is a more universal tool as it provides more comprehensive information about an oscillator's noise in a shorter period of time.

**Frequency domain description**

The time domain analysis of a signal's frequency instability is advantageous as it is easily calculated from a time series of frequency counter measurements and it allows a very fast comparison among various signals. This convenience, however, comes at the cost of restrained information about the frequencies at which the noise arises. More information can therefore be obtained by analyzing an oscillator signal in the frequency domain. A frequency domain analysis clearly reveals the Fourier frequencies of the underlying noise which is essential for identifying noise sources.

To characterize phase or frequency fluctuations it is most common to measure the corresponding power spectral densities (PSD) $S_\phi(f)$ and $S_y(f)$. They represent the amount of power that is spread away from the carrier. The PSD of phase fluctuations is defined by

$$S_\phi(f) = |\tilde{\phi}(2\pi f)|^2 \tag{2.7}$$

with $\tilde{\phi}(f)$ being the Fourier transform of the signal's phase $\phi(t)$. The relation between phase and (fractional) frequency fluctuations is simply

$$S_y(f) = \frac{f^2}{\nu_0^2} S_\phi(f) \tag{2.8}$$

Analysis of various frequency sources from quartz oscillators to atomic frequency standards revealed that the measured PSDs can be reasonably well approximated by a superposition of five independent noise processes. More specifically, a power law model is often used where the spectral densities vary as a power of $f$ [24, 25]:

$$S_\phi(f) = \sum_{\alpha=-2}^{2} h_\alpha f^{\alpha-2} \tag{2.9}$$

with the coefficients $h_\alpha$ as a measure of the noise level. Depending on the particular oscillator two or three terms are typically dominant in different frequency regimes. The most common noise types present in real systems are giving in Table 2.1.

**Conversion from frequency to time domain**

The knowledge of the phase or frequency fluctuations allows to derive the Allan deviation through the relation

$$\sigma_y(\tau)^2 = 2 \int_0^\infty S_y(f) \frac{\sin^4(\pi\tau f)}{(\pi\tau f)^2} \, df \tag{2.10}$$

| Noise Type | $S_y(f)$ | $S_\phi(f)$ | $\sigma_y(\tau)$ | mod $\sigma_y(\tau)$ |
|---|---|---|---|---|
| Random walk frequency noise | $h_{-2}f^{-2}$ | $\nu_0^2 h_{-2}f^{-4}$ | $\propto \tau^{1/2}$ | $\propto \tau^{1/2}$ |
| Flicker frequency noise | $h_{-1}f^{-1}$ | $\nu_0^2 h_{-1}f^{-3}$ | const. | const. |
| White frequency noise | $h_0 f^0$ | $\nu_0^2 h_0 f^{-2}$ | $\propto \tau^{-1/2}$ | $\propto \tau^{-1/2}$ |
| Flicker phase noise | $h_1 f^1$ | $\nu_0^2 h_1 f^{-1}$ | $\propto \tau^{-1}$ | $\propto \tau^{-1}$ |
| White phase noise | $h_2 f^2$ | $\nu_0^2 h_2 f^0$ | $\propto \tau^{-1}$ | $\propto \tau^{-3/2}$ |

TABLE 2.1: Common noise types present in most systems and the corresponding frequency dependence of the power spectral densities together with the $\tau$-dependency of the ADEV and the modADEV.

It should be mentioned that in contrast to Equation 2.10 the calculation of the PSD from the ADEV requires a solution of the integral which is possible only in simple cases when the shape of the PSD is well known [18]. In analogy to Equation 2.10 also the modADEV can be derived from the PSD through [25]

$$\text{mod } \sigma_y^2(\tau) = 2 \int_0^\infty S_y(f) \frac{\sin^6(\pi f \tau)}{(\pi n \tau)^2 \, \sin^2(\frac{\pi \tau f}{n})} \, df \tag{2.11}$$

with the number of samples $n$ used to determine $S_y(f)$ ($n$ drops out as it goes to infinity).

### 2.2.2 Accuracy

As mentioned at the beginning of this chapter, the frequency deviation of an oscillator is not only determined by the frequency fluctuations that are represented by the PSD or the ADEV. The output frequency of a source can also be subject to systematic effects that lead to frequency shifts. If such a shift has no frequency dependence, that is, is constant in time, it does not contribute to the instability of an oscillator. The systematic
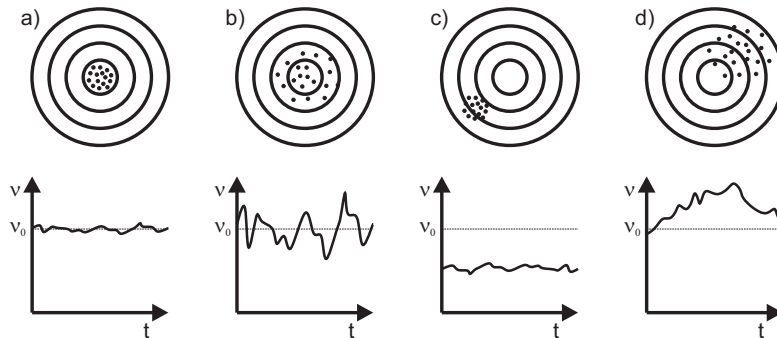


FIGURE 2.3: Simplified illustration of the terms stability and accuracy. Upper row: bullet holes on a target, lower row: temporal evolution of frequency measurements of a source with nominal frequency $\nu_0$. a) stable and accurate, b) accurate but not stable, c) stable but not accurate, d) not stable and not accurate. Figure adapted with permission from [18].

uncertainty or accuracy, however, is the main characteristic of any oscillator. In atomic clock systems the accuracy depends on the uncertainty in the determination of its atomic transition frequency which can be distorted by various effects. The absolute accuracy with respect to the SI unit Hertz can only be determined by linking the oscillator to a primary frequency standard which today are cesium clocks.

Terms like stability and accuracy are commonly used in the context of the characterization of frequency sources. A visualization of these terms is given in Figure 2.3 by comparing the output of an oscillator with bullet holes on a target. The sequence of firing bullets is replaced by consecutive frequency measurements where the distance between each bullet hole from the center corresponds to the deviation of the measured frequency from the center frequency $\nu_0$.

### 2.2.3 Measurement of phase and frequency noise

The noise of an oscillator frequency is measured with electronic frequency counters in the time domain. Those counters perform a comparison between the phase of the unknown signal and a reference phase over a certain time interval which is denoted as the gate time $\tau$. The number of cycles within this gate time then reveals the frequency of the unknown signal.

Care has to be taken when using frequency counters as the way the counter processes the data internally can vary from manufacturer to manufacturer and even from model to model. Some counters exhibit a dead time in between subsequent measurement windows. This dead time leads to a loss of coherence and needs to be avoided if continuous phase information is required (see [23] and Section 2.2.1).

#### 2.2.3.1 Π-type frequency counters

Traditional frequency counters perform single phase measurements at the beginning and at the end of the measurement window, while in between these measurements the zero-crossings of the input signal are counted [26]. This working principle can be expressed with a rectangular weighting function of the form
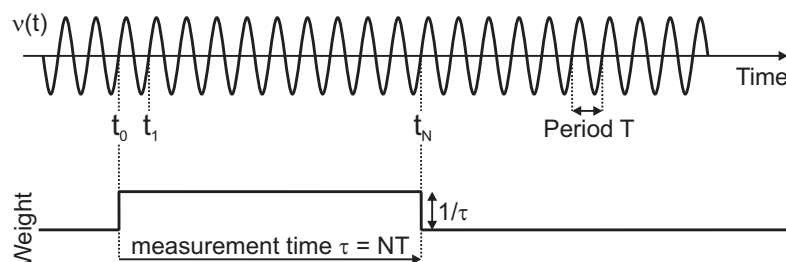


FIGURE 2.4: Rectangular averaging mechanism in Π-type frequency counters.

$$\omega_{\Pi}(t) = \begin{cases} 1/\tau & \text{for} \quad 0 < t < \tau \\ 0 & \text{elsewhere.} \end{cases} \tag{2.12}$$

Internally, the $\Pi$-type counter estimates the frequency of a signal by counting all periods occurring during the time interval $\tau$ as illustrated in Figure 2.4. The estimated frequency is simply the average of the number of cycles over the measurement time and an interpolation of the fraction of an oscillation at the beginning and at the end of each measurement window.

Applying Equation 2.3 to a time series of frequency measurements from a $\Pi$-type frequency counter yields the standard ADEV $\sigma_y(\tau)$ as described in Section 2.2.1, provided that no dead time is introduced by the counter. If dead time is present between consecutive frequency measurements, the instability of the signal can still be calculated with the help of Equation 2.3. The resulting frequency instability, however, may not be denoted as the ADEV and it might have a different dependency of the measurement time [20].

### 2.2.3.2   $\Lambda$-type frequency counters

As described in the previous chapter a $\Pi$-type counter only performs phase measurements at the beginning and at the end of the measurement window, thereby ignoring the time spacing of the zero-crossings in between. Some modern counters improve the measurement resolution by using the information contained in the spacing of the zero-crossings [27]. In these so-called $\Lambda$-type frequency counters hundreds or even thousands of individual phase measurements are performed within a single measurement window. In particular, the average phase over the first half of the measurement window is subtracted from the average phase of the second half. This is equivalent to a moving average of a series of traditional $\Pi$-type counter measurements that are shifted by a time $\tau_0$ as is



FIGURE 2.5: Triangle averaging mechanism in $\Lambda$-type frequency counters.

sketched in Figure 2.5. The working principle can be approximated with an overlapping triangular weighting function of the form

$$
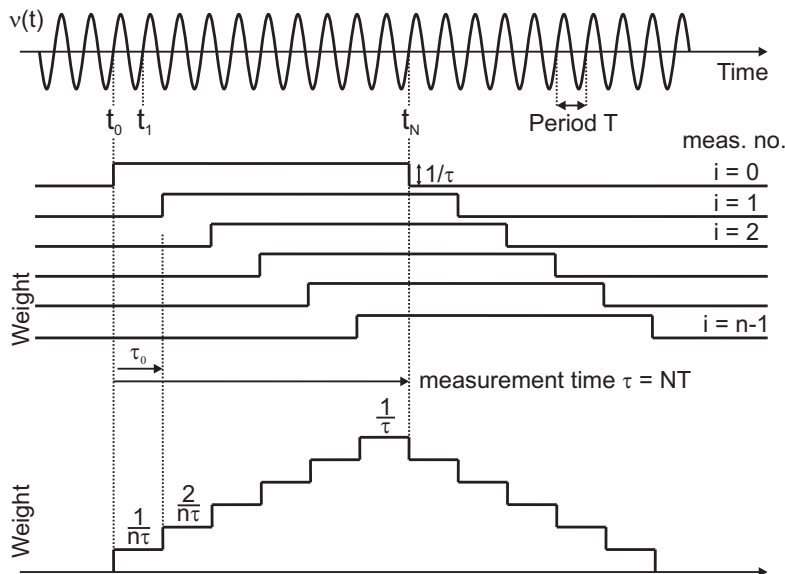\omega_\Lambda(t) = \begin{cases} t/\tau & \text{for} \quad 0 < t < \tau \\ 2 - t/\tau & \text{for} \quad \tau < t < 2\tau \\ 0 & \text{elsewhere.} \end{cases} \tag{2.13}
$$

Applying Equation 2.3 to a time series of frequency measurements derived from an overlapping $\Lambda$-type counter therefore yields the modADEV rather than the standard ADEV [23]. While both, $\Pi$- and $\Lambda$-type counters deliver the same mean frequency, the use of the latter one is preferred due to the increased frequency resolution. A dead time free $\Pi$-type counter, however, is required if the frequency instability should be expressed by the standard ADEV.

## 2.3 Microwave frequency standards

Microwave frequency standards are today's best established clocks and their well defined output finds a broad range of applications in research as well as in our everyday life. Even commercial systems show impressively low instabilities of below $1 \times 10^{-14}$ on long timescales and accuracies around $5 \times 10^{-13}$ [28]. Various different microwave frequency standards have been developed over the past decades, with the most important ones described in greater detail in this chapter.

### 2.3.1 Cesium atomic clocks

Due to the definition of the SI-second cesium atomic clocks are one of the most important devices in the context of frequency standards and the generation of time scales. A beam-type cesium clock uses a beam of thermal ($\approx 100\,^{\circ}$C) $^{133}$Cs atoms which are vaporized in an oven. Subsequently, a strong magnetic field serves as a state-selector, separating the atoms by their effective magnetic moment. The selected atoms then pass through a microwave cavity in which the atoms are interacting with a microwave field generated by a quartz oscillator. The interaction time is typically on the order of a few milliseconds. Here, a Ramsey pulse sequence [29] followed by another state-selecting magnetic field is used to discriminate the atoms that made a state transition from the rest. This way, only atoms that undergo the desired clock transition between the $F = 4$ and $F = 3$ hyperfine ground-states reach the detector. The detector output serves as a feedback signal which is used to continuously steer the quartz oscillator thereby locking it closely to the cesium resonance. The transition frequency between the two participating energy states is about 9.2 GHz. Thermal beam cesium clocks demonstrated instabilities of $8 \times 10^{-13}$ after a measurement time of 100 s and a residual uncertainty of below $1 \times 10^{-14}$ [30].

In the latest and most advanced version of cesium clocks the thermal beam of cesium atoms is replaced by a cloud of laser-cooled [31] ($\approx 1\,\mu$K) atoms. This cloud is launched

vertically upwards 1 m until it comes to a rest under the action of gravity, followed by a descent back to its starting position [32, 33]. This configuration gave this clock its name cesium fountain clock. The Ramsey interaction region is passed twice while the cesium atoms travel up- and downwards. This increases the interaction time from a few milliseconds to about 1 s, yielding a significant enhanced measurement resolution. Fountain clocks are not commercially available which is why they are mostly found in scientific environments.

Cesium fountain clocks provide a dramatically better performance over thermal beam cesium clocks. They demonstrated instabilities of $4 \times 10^{-15}$ after 1 s of measurement time and uncertainties of a few parts in $10^{16}$ [33–36].

### 2.3.2  Masers

A maser as the microwave counterpart of a laser generates coherent microwaves by stimulated emission in a resonator [2]. The most important type of maser is a hydrogen maser that uses atomic hydrogen as the gain medium. An RF discharge produces atomic hydrogen which is then passed through a magnetic field that works as a state-selector. Only atoms in the upper of two hyperfine energy levels make it into a microwave cavity. The cavity is tuned to the transition frequency and a standing wave builds up. A small fraction of the 1.4 GHz microwave is coupled out and amplified while a high performance quartz oscillator is phase-locked to it. The quartz oscillator then provides the actual output of the maser (typically 10 MHz, 100 MHz and 1 GHz).

Commercial hydrogen masers nowadays are extremely reliable devices which show typical short-term instabilities of $1 \times 10^{-13}$ after 1 s and a few parts in $10^{15}$ on medium time scales [37]. Drifts of the microwave cavity cause the maser output frequency to drift which leads to an increase of the instability on long times scales. Hydrogen masers are the workhorses among atomic frequency standards and help to make up the International Atomic Time (see Section 2.5.1). It should be pointed out, however, that hydrogen masers only produce a very stable but not an accurate frequency. Two identical masers can produce stable output frequencies with comparably large offsets between each other.

### 2.3.3  Rubidium atomic clocks

The most compact, inexpensive and widely used type of atomic clock is based on rubidium atoms. A hyperfine transition in $^{87}$Rb at a frequency of about 6.83 GHz is used as the clock transition. Light from a discharge lamp with a wavelength around 800 nm passes through a vapor cell filled with rubidium gas. The rubidium atoms absorb the light which leads to a population of an excited electronic state at the clock transition. A photodiode behind the vapor cell detects the transmitted light intensity. The rubidium gas is housed in a resonance cell to which a microwave frequency from a voltage-controlled oscillator (VCO) near the atomic transition is applied. By frequency modulating the output of the VCO the resonant absorption of the rubidium atoms is monitored and a phase-sensitive detection is used to derive a correction signal. This

signal is then used to steer the output of the VCO, thus providing a stable frequency which serves as the clock signal [38].

Due to its simplicity and robustness the rubidium atomic clock is found in various applications. The telecommunication industry, for example, relies to a large extent on rubidium clocks. Additionally, most of the navigation satellites are equipped with one or more clocks of this type. Commercial rubidium clocks reach a frequency instability of a few parts in $10^{12}$ in 1 s which averages down to the lower $10^{-13}$ level in a few hours. In analogy to cesium clocks, also rubidium fountain clocks have been developed which have been shown to achieve even better stabilities and accuracies compared to the cesium fountain clocks due to smaller collision shifts in rubidium. A frequency instability of $6 \times 10^{-17}$ after $10^7$ s has been demonstrated for such a rubidium fountain clock [39].

### 2.3.4 Cryogenic sapphire oscillators

Another important high-performance oscillator uses a mono-crystalline sapphire cylinder to generate highly stable microwaves. The sapphire cylinder is kept in a cryostat at a temperature close to 6 K, where the frequency-temperature dependence conveniently features a minimum. Microwaves generated by a loop oscillator [40] are coupled into the sapphire resonator in which they excite whispering gallery modes. The quality factor for some of these modes can be as high as $10^9$. Cryogenic sapphire oscillators typically operate at a frequency of around 10 GHz, depending on the particular resonant mode that is chosen.

The short-term frequency instabilities achievable with cryogenic sapphire oscillators are the lowest among today's microwave frequency standards. Frequency instabilities of below $2 \times 10^{-15}$ after 1 s and $5 \times 10^{-16}$ after a few seconds have been demonstrated [41]. Slow drifts of about $5 \times 10^{-14}$ per day lead to an increase in the frequency instability on long times scales.

### 2.3.5 Frequency comb assisted microwave generation

A relatively novel approach compared to the previously described microwave frequency standards makes use of the high frequency stability achievable with optical systems to generate extremely stable microwaves. A continuous-wave (cw) laser that is stabilized to a high-finesse Fabry-Pérot cavity can produce optical frequencies with relative instabilities in the lower $10^{-16}$ range for averaging times of 1-10 s [42]. An optical frequency comb [43] can be used as a frequency divider, therewith transferring the high stability from the optical to the microwave domain [44, 45]. After having stabilized the offset frequency $f_{ceo}$ of a mode-locked laser that produces the frequency comb, the $n$th tooth of the comb is phase-locked to the cw laser. This transfers the stability of the cw laser to the mode spacing and thereby to the repetition rate of the mode-locked laser. The fundamental repetition rate of mode-locked lasers is typically in the 100 MHz to 1 GHz range. Higher microwave frequencies can be chosen by selecting the corresponding harmonics.

The microwave frequencies generated by frequency division from the optical domain show excellent instabilities as low as $8 \times 10^{-16}$ after 1 s. Fabry-Pérot cavities drift due to temperature and aging effects of the spacer material [46] which is then transferred to the microwave signal. This leads to an increase in the frequency instability on long time scales.

## 2.4  Optical frequency standards

Continuous improvements have reduced the fractional frequency uncertainty $\frac{\Delta \nu_{shift}}{\nu_0}$ of cesium fountain clocks to a level on the order of a few times $10^{-16}$ (see Section 2.3.1). As most of the systematic frequency shifts are independent from the transition frequency, higher operating frequencies yield the potential for lower frequency uncertainties. In addition to the formalism discussed in Section 2.2.1, the fractional frequency instability can be written as

$$\sigma_y(\tau) \approx \frac{\Delta \nu}{\nu_0 \sqrt{N\tau}} \tag{2.14}$$

where $\Delta \nu$ is a narrow atomic resonance, $\nu_0$ the transition frequency and $N$ the total number of oscillators (atoms or ions) measured in the total measurement time $\tau$. Making the transition from $\nu_0 = 9.2$ GHz of a cesium clock to the optical regime with several hundreds of terahertz should therefore improve the fractional instability by 4-5 orders of magnitude [47].

The experimental foundation for an optical atomic clock was already laid in the 1980s [5] when single ions were successfully trapped in Paul traps and a technique to reduce the thermal motion of atoms known as laser-cooling was developed [31, 48]. Another milestone in the development of optical clocks was reached with the invention of the femtosecond frequency comb technique [43], which enables the counting of optical frequencies, necessary to operate an optical clock.

Today, two different concepts of realizing an optical clock are competing in reaching the highest accuracy. While one concept utilizes a large array of neutral atoms the other one employs just a single ion. Both concepts have in common that they use cold and trapped atoms or ions to reduce Doppler shifts due to atomic motion and to achieve a small spatial confinement. The following sections give an overview over today's state-of-the-art optical clocks.

### 2.4.1  Neutral atom clocks

Today's best performing neutral atom optical clocks are based on optical lattices that are generated by two or more counter-propagating laser beams. A large amount of atoms ($N \approx 10^3 - 10^6$) is trapped in the lattice achieving a high spatial confinement (so-called Lamb-Dicke regime) [49]. An advantage of using an optical lattice in contrast
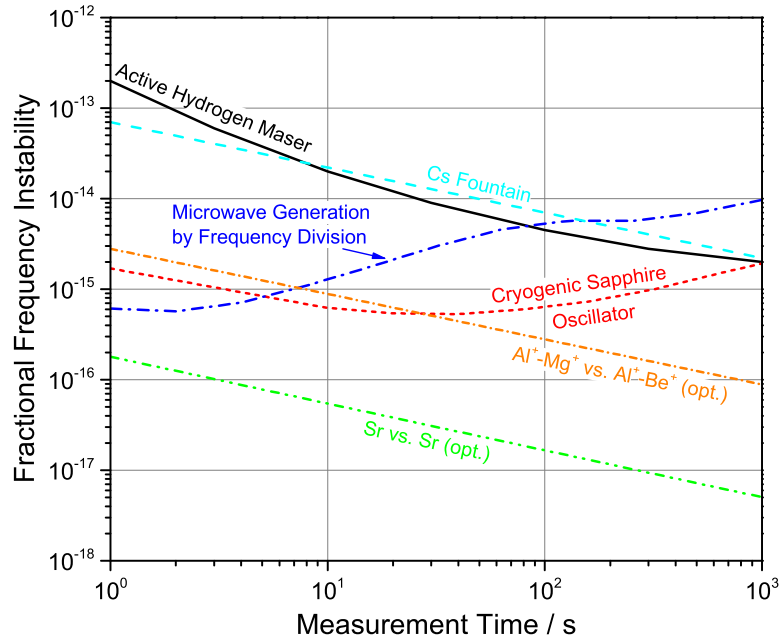
FIGURE 2.6: Fractional frequency instability of the most prominent as well as best performing microwave frequency standards [7, 36, 44, 53]. Also shown are state-of-the-art optical frequency standards [17, 54]. All data expressed as the ADEV. For details see Section 2.3.1 - 2.4.2.

to a cold atom cloud in a magneto-optical trap (MOT) is that each atom is located in its own potential well, thereby eliminating interatomic interactions which can perturb the clock transition by collision shifts. While the first optical clocks appeared in the 1980s [50, 51], the first optical lattice clock has only been demonstrated in 2005 with the discovery of a magic wavelength for which the Stark shift of the energy levels is exactly equal for the two states of the clock transition [52]. Optical clocks in general are based on laser spectroscopy in which the atoms or ions of interest are excited by a narrow linewidth interrogation laser. The laser is frequency-scanned over the atomic transition, thus exciting the atoms from the ground to an excited state. Resonance is detected by monitoring the ground and the excited state population, which is then used to feed back to the interrogation laser in order to keep it on resonance.

According to Equation 2.14 a large number of atoms $N$ dramatically improves the clock stability. Therefore, neutral atom optical clocks might offer the potential of ultimately achieving better performance compared to single ion optical clocks. Optical lattice clocks have demonstrated a fractional frequency instability of about $1.8 \times 10^{-16} / \sqrt{\tau}$ (see Figure 2.6) with a residual uncertainty of $1.6 \times 10^{-18}$ [17].

## 2.4.2 Single ion clocks

In contrast to neutral atoms, single trapped ions of elements such as mercury, ytterbium or aluminum can also serve as a source for highly stable optical frequencies. The transition frequencies of interest in those singly trapped ions possess the advantage of being highly immune to external field perturbations [15, 55]. As discussed above, increasing

| Clock Type | Published Uncertainty |
|---|---|
| Cesium fountain clock | $2.3 \times 10^{-16}$ [35] |
| Ytterbium neutral atom clock | $3.4 \times 10^{-16}$ [57] |
| Ytterbium ion octupole clock | $7.1 \times 10^{-17}$ [55] |
| Mercury ion clock | $1.9 \times 10^{-17}$ [15] |
| Aluminum ion quantum logic clock | $8.6 \times 10^{-18}$ [54] |
| Strontium neutral atom clock | $1.6 \times 10^{-18}$ [17] |

TABLE 2.2: Relative frequency uncertainty of state-of-the-art optical clocks and one of the best cesium fountain clocks for comparison.

the number of oscillators $N$ yields lower frequency instabilities. The number of trapped ions that can be used for extracting a stable optical frequency, however, is limited to one due to strong Coulomb interactions between the ions [52]. The achievable frequency instability of a single ion clock is therefore limited.

On the other hand, the strong Coulomb interaction can also be an advantage for constructing a unique type of single ion optical clock. $Al^+$ is of particular interest in the context of optical clocks due to its low sensitivity to electromagnetic perturbations and its narrow natural linewidth of 8 mHz. However, the absence of an atomic transition for laser cooling and detection accessible with existing laser systems prevented any serious investigation of $Al^+$ in the past. This obstacle was circumvented by introducing the quantum logic spectroscopy [56] where an auxiliary logic ion with accessible cooling and detection transitions is trapped together with the clock ion. The logic ion then sympathetically cools the $Al^+$ ion via Coulomb interaction and additionally enables the internal state detection of the $Al^+$ clock state. $Al^+$ optical clocks have demonstrated a fractional frequency instability of $2.8 \times 10^{-15}/\sqrt{\tau}$ and an accuracy of $8.6 \times 10^{-18}$ [54], making them one of the most accurate clocks among all frequency standards to date.

An overview over the demonstrated uncertainties of today's best performing clocks is given in Table 2.2. It is believed that optical clocks have the potential to reach accuracies significantly below $1 \times 10^{-18}$. As the research on optical clocks is work in progress, it is not possible to point out what kind of clock and what kind of atom/ion species will eventually offer the best performance.

## 2.5  Applications of high-performance clocks

Being able to measure dynamic processes helps us to understand the regularities of nature. Additionally, time (or frequency) can be measured with an extraordinary high precision like no other physical property. The high measurement precision also allows for the construction of time keeping devices that reach unprecedented accuracies. Today, atomic clocks constitute indispensable tools in solving some of the most challenging questions in fundamental physics. However, their applications are not limited to the field of research. Whenever the measurement of time is required, atomic clocks often

find its way into those applications. Satellite navigation, telecommunication systems such as cellphone services or the internet and even electrical power grids rely on the high performance of modern atomic clocks [58].

In this chapter, a few applications of atomic clocks are described in greater detail. All of these applications require a linking of the participating clock systems. The challenge of linking clocks grows with the physical distance between them, while the distance in turn depends on the actual application.

### 2.5.1  Realization of the SI second and international time scales

According to the definition of the SI second [59], cesium atomic clocks are used as a primary standard of time. Commercial as well as cesium fountain clocks are operated by precision measurement institutes around the world. While the fountain clocks certainly give the best representation of the second (see Section 2.3.1), their complex nature makes them difficult to be operated continuously. This issue is typically solved by combining the high accuracy of the fountain clocks with the high stability and reliability of commercial hydrogen masers (see Section 2.3.2). Commonly, an ensemble of masers is calibrated by a cesium fountain clock and their weighted average is used as a national time scale. Performance variations of the clocks in such an ensemble are typically taken into account by applying weights that are inversely proportional to the standard deviation of the clock [60].

By combining the output of more than 300 stable oscillators like masers and cesium clocks from about 60 institutes worldwide, the international time scale *Temps Atomique International* (TAI) is generated. The *International Bureau of Weights and Measures* (BIPM) in France is in charge of calculating TAI and the results are monthly published in Circular T [61]. An acronym of the timing institute generating the time scale is typically added, e.g. TAI(PTB) where PTB in this case identifies the Physikalisch-Technische Bundesanstalt. The better known *Coordinated Universal Time* (UTC) differs from TAI by an integer number of leap seconds to compensate for the slowing of the earth's rotation and to keep the time of the day close to the mean solar time. The atomic clocks on board of the satellites of the Global Positioning System (GPS) are set to GPS time which is not corrected to match the rotation of the earth, that means no leap seconds are added. Currently, the deviation of GPS time and UTC is 16 seconds.

As time scales are based on the comparison of independent clocks, ways of exchanging time or frequency information between the clocks had to be found. While national time scales are generated by clocks which are typically located in the same or a neighboring laboratory, international time scales require the comparison of distant clocks. This in turn requires the linking of clocks which are separated by hundreds or thousands of kilometers. Today, this task is solved by using satellite based systems capable of transmitting stable microwave frequencies. Those systems are introduced and discussed in great detail in Section 3.3.

### 2.5.2 Geodesy

Geodesy is the scientific discipline of studying the shape and the size of the surface of the earth that includes the geometric figure, the orientation in space as well as the gravitational field of the earth [62]. Geodesy is a broad research area with many branches and covers the study of crustal and polar motions as well as the determination of the mean sea level, which often serves as a reference for elevation indications.

The study of earth rotation, tectonic plate movements and other types of geodesy has been revolutionized with the invention of an interferometer technique that allows position determinations with millimeter accuracy. This technique is called very-long-baseline interferometry and uses radio telescopes to observe distant astronomical radio sources such as quasars [63]. While multiple telescopes simultaneously observe the same source, differences in the arrival time of events are measured. Thus, the position determination is accomplished via timing measurements. Consequently, the whole system relies on a common time or frequency reference that all telescopes are connected to. As the resolution in position determination grows with the physical separation of the participating telescopes, frequency dissemination systems capable of bridging large distances are required.

Global-scale geodesy was and still is the task of various satellite missions such as GOCE and GRACE. Both missions have in common that the satellites fly in a low earth orbit where they experience the force by the gravitational field of the earth [64]. This force is either measured with sensitive accelerometers (GOCE) or the absolute distance between two chasing satellites is measured constantly which varies if the satellites fly over regions with slightly stronger or weaker gravity (GRACE). Combined with precise positioning measurements from GPS the gravitational potential of the earth can be calculated.

### 2.5.3 Fundamental physics

**Tests of quantum electrodynamics**

The quantum field theory that describes the interactions of charged particles with electromagnetic fields is known as quantum electrodynamics (QED). It is one of the most successful physical theories that has been devised so far due to its extremely accurate predictions, which have been verified in high-precision spectroscopy experiments. Hydrogen, as the simplest of all atoms, allows a comparison between theory and experiment with an unprecedented level of accuracy.

The spectroscopy of atomic hydrogen reveals the transition frequencies between various energy levels from what, for example, the Rydberg constant or the Lamb shift can be extracted. The $1S$-$2S$ transition at a wavelength of around 121 nm is a prominent example due to its narrow natural linewidth. The determination of those transition frequencies requires a stable reference frequency. Decades of intense research led to a measurement accuracy with 15 digits [16], which is only enabled by the use of cesium fountain clocks (see Section 2.3.1). Further advances in high-precision experiments like this may require the use of optical clocks in the future.

One important parameter for the test of QED is the size of the proton which has been determined by electron-proton scattering experiments in the past. Recent spectroscopy experiments based on muonic hydrogen revealed a significantly lower value for the proton charge radius [65]. The discrepancy of the results between the scattering and the spectroscopy experiments is of unknown origin up to date. However, the uncertainty with which the proton charge radius can be determined is significantly higher in the spectroscopy of muonic hydrogen. Further experiments will have to be conducted to solve the so called proton size puzzle.

**Temporal variations of fundamental physical constants**

The physical constants that we know today provide the foundation of all physical systems in both theory and experiments. As those constants cannot be deduced theoretically, they have been determined in countless experiments over hundreds of years with ever increasing accuracy [66]. One of the cornerstones of physics in general is the assumption that constants have no temporal dependency as the name implies. The measurement of any variation of a physical constant would however have profound implications for our understanding of fundamental physics. The accuracy with which a constant can be determined sets an upper limit to a possible slow drift of that constant in time. Thus, the measurement accuracy has to be increased in order to lower this limit.

Of particular interest are dimensionless constants that do not depend on any units. These constants are known as *fundamental* constants out of which the fine-structure constant $\alpha$ is a common example. Spectroscopic investigations on atomic systems reveal the fine-structure constant and repeated measurements over time yield constraints on possible temporal variations of it [67–69]. Recent experiments using optical clocks constrain a potential drift of $\alpha$ to $\dot{\alpha}/\alpha = (-1.6 \pm 2.3) \times 10^{-17}$ / year which is consistent to zero drift [15]. The ongoing research on improving the optical clocks is expected to further decrease this limit.

**Test of general relativity and relativistic geodesy**

The framework of Einstein's general relativity describes the gravitational time dilation which implies that time is coupled to gravitational potentials. As a result, a clock that is located closer to a gravitational mass goes slower as compared to an identical clock that is located in a greater distance from the mass. A direct consequence of the time dilation is the gravitational redshift which describes the shift of a frequency that passes through different gravitational potentials. Two identical clocks that show no difference in their output frequencies while they are kept in the same gravitational potential will exhibit a frequency difference with respect to the other clock as soon as one of the clocks is moved to another gravitational potential. The fractional frequency shift is calculated by

$$\frac{\Delta\nu}{\nu_0} = \frac{g\Delta h}{c^2} \tag{2.15}$$

with $\nu_0$ being the operating frequency of the clock, $g$ the gravitational acceleration, $c$ the speed of light and $\Delta h$ the height difference in the earth's gravitational field. Quantum gravity and string theory postulate a violation of the universality of the gravitational redshift [70]. The comparison of high performance clocks that are placed in different gravitational potentials can be used to constrain any possible violation. Today, optical clocks and spaceborne hydrogen masers have confirmed the universality of the gravitational redshift to a level of $7 \times 10^{-5}$ [14, 71].

In contrast to assuming certain gravitational potentials and putting general relativity to a test, the opposite approach opens a new field of geodesy. By assuming the correctness of general relativity, atomic clocks can be used to map out different gravitational potentials through the gravitational redshift. This relatively young field of research is denoted as relativistic geodesy due to the contribution of relativistic effects. According to Equation 2.15, a height difference of 1 m leads to a frequency shift of $1 \times 10^{-16}$. Modern optical clocks with their high operating frequencies and superior performance can resolve a height difference of just a few centimeters [14]. With future generations of optical clocks, relativistic geodesy on the millimeter level seems feasible.

On the other hand, the same effects that enable relativistic geodesy may constitute a limitation in the context of remote clock comparisons. With relative accuracies on the order of $10^{-18}$ or below it will become challenging to separate potential clock differences from gravity variations.

As highlighted above, the characterization of frequency standards requires comparisons with frequency references of comparable performance. The generation of time scales even relies entirely on frequent clock comparisons. In the following chapter, methods that allow remote comparisons of atomic clocks by disseminating or transferring stable frequencies are introduced while their limitations are pointed out.

# Chapter 3

# Time and Frequency Dissemination

## 3.1  Introduction

Any measurement of some physical property is a comparison with a known reference. In the context of high-performance oscillators the characterization is done by comparing the oscillator under test with one or several, ideally more stable, reference oscillators. A comparison between oscillators that share a common location typically does not constitute any serious technological challenge. National and international oscillator comparisons, however, require access to a common frequency reference or the transfer of one of the frequency signals to the reference oscillator (or vice versa). Currently, those issues are addressed by using satellites that either provide a common frequency source to all oscillator locations or for the frequency transfer itself. Those well-established techniques reach instabilities of a few parts in $10^{16}$ after one day of measurement time, which is sufficient for the comparison of the majority of microwave frequency standards. The dissemination or comparison of state-of-the-art optical frequency standards on the other hand requires more advanced techniques. This chapter gives an overview over existing technology used for long-distance time and frequency transfer while demonstrating its capabilities as well as its limitations. Optical fibers as a transfer medium for stable frequencies are also introduced together with some important considerations.

## 3.2  Portable atomic clocks

The most intuitive approach of getting access to a stable reference frequency from a remotely located clock is simply to transport the frequency standard itself. For a long time, especially before the existence of satellites that can provide stable frequencies, portable clocks were the only way to transfer the accuracy of a remote frequency standard. Often times those transfer oscillators were transported to a national metrology institute to calibrate it against a primary frequency standard before it could serve as a

reference in an experiment. At MPQ, a portable cesium fountain clock has been used multiple times for the performance of precision hydrogen spectroscopy experiments [16]. With the invention of satellite based frequency dissemination techniques those portable transfer oscillators became somewhat obsolete. However, the challenging transfer of frequencies that support the comparison of state-of-the-art clocks has triggered the development of portable optical frequency standards in several research groups worldwide [72]. First demonstrations of fully functioning portable optical clocks are expected in the near future. Nevertheless, frequent comparisons between stationary optical clocks are and will still be desired as portable optical clocks are expected to remain a unique version of their high-performance stationary counterparts.

## 3.3    Satellite based techniques

Satellites play a major role in time and frequency metrology due to their ability to transmit frequency or timing information to almost every point on the surface of the earth. To date, two different techniques are used which have in common that they both use microwave frequencies. One of them employs a Global Navigation Satellite System (GNSS) such as the Global Positioning System while the other makes use of geostationary telecommunication satellites for a Two-Way Satellite Time and Frequency Transfer (TWSTFT).

### 3.3.1    Global Navigation Satellite System

Out of a few realized and planned Global Navigation Satellite Systems, the Global Positioning System (GPS) is currently the satellite based time and frequency dissemination system with the widest usage [73]. GPS was originally developed to provide precise location and timing information of objects anywhere on the earth. Alternative systems like GLONASS (Russia) or GALILEO (European Union) use or will be using techniques similar to GPS [74, 75].

GPS is designed in a way so that from every point on the earth a minimum of four satellites are simultaneously in view. To achieve that, a total number of 31 GPS-satellites are in operation. Each of these satellites houses one or more microwave frequency standards, typically a rubidium and/or a cesium clock, to generate an on-board frequency reference. The satellite clocks are steered by the U.S. Naval Observatory (USNO), which generates a stable time reference with an ensemble of high-performance cesium clocks and hydrogen masers [76]. Leap seconds, however, are not applied to the GPS time.

Each GPS satellite broadcasts at two carrier frequencies, 1.575 GHz (L1 signal) and 1.227 GHz (L2 signal) that are generated by the on-board clock. To distinguish between the different satellites, the carrier frequencies are phase-modulated with a pseudo-random noise code, uniquely associated with each satellite. GPS receivers are aware of these pseudo-random codes, allowing them to reconstruct the actual message that, among others, contain information of the timing offset between the satellite's clock and

the common system time. Thus, a GPS receiver is able to perform measurements of the propagation time between the receiver location and the satellite. A comparison between two or more remote clocks is achieved by exchanging the measurement data a posteriori, thereby the instability contribution of the satellites' clocks cancel out[1]. The principle of clock comparisons via GNSS is schematically shown in Figure 3.1 a).

### 3.3.1.1   Common View (CV) vs. All-in-View (AV)

For time and frequency comparisons using GNSS two configurations can be employed and are commonly used. In the common view (CV) mode the two remote receivers record the data from the same satellite simultaneously [77]. Clock errors due to fluctuations in the ionosphere are well correlated and cancel in this configuration, which greatly simplifies the frequency transfer process. In principle, for a CV clock comparison the signal of one single satellite is sufficient. As the same satellite has to be in view from both remote sites, the maximum distance that can be covered in the CV mode is approximately 10,000 km [78].

In the all-in-view (AV) mode two receivers track the signals from all satellites in view [79]. The number of satellites that are in view simultaneously depends on the geographical location and is typically around 7-8 for Germany. The received signals are first compared to the GNSS time for each receiver individually and their differences are calculated based on these data. The maximum distance that can be bridged in the AV mode is larger compared to the CV mode and amounts to about 20,000 km. Thus, clocks on the opposite side of the earth can be compared in the AV mode.

Out of these two configurations, the CV methods has originally been used to compare national time scales in order to generate international time scales such as UTC. In the mean time, AV has often replaced CV as it has been shown to provide better performance on some baselines. For example, CV and AV show equivalent performances for baselines of 2500 km while AV shows an improved stability on a baseline of 5000 km [80]. Therefore, AV is considered to provide equal or better performance over CV for most applications [81, 82].

### 3.3.2   Two-Way Satellite Time and Frequency Transfer

An alternative time and frequency transfer method using satellites is called Two-Way Satellite Time and Frequency Transfer (TWSTFT). In contrast to the one-way GNSS technique, information is exchanged between two remote locations by simultaneously sending and receiving the timing signals as sketched in Figure 3.1 b). The main advantage of TWSTFT is that the propagation delay (and thus errors arising from fluctuations of the same) of the signals cancels to a large extent, thus no knowledge of the actual

---

[1]This statement holds for the case, when the two GPS receivers involved track the same satellites during the time of interest. If a particular satellite is tracked by only one of the receivers, noise from the on-board clock does not cancel.
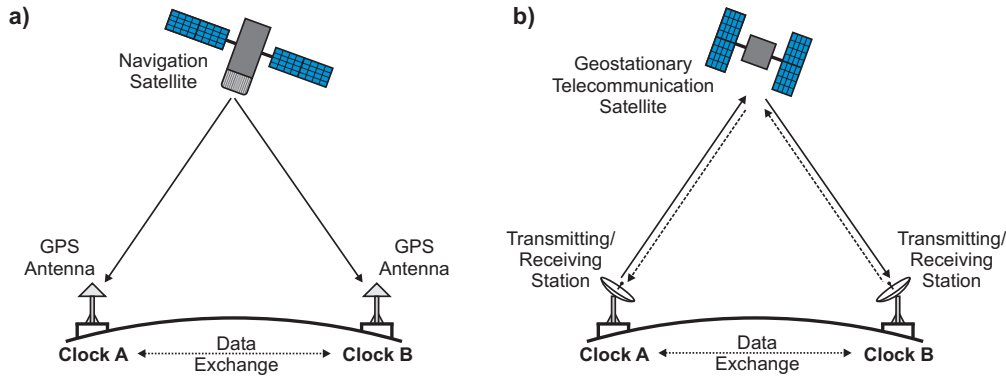
FIGURE 3.1: Schematic of time and frequency transfer via a) navigation satellites and b) Two-Way Satellite Time and Frequency Transfer. Only receivers are needed when using navigation satellites while the two-way method requires receiving and transmitting equipment.

clock or satellite locations is required. For this reason, TWSTFT provides better performance over GNSS (see chapter 3.3.3). The main disadvantage of this technique is that all remote clock locations need to be equipped with transmitting and receiving hardware. TWSTFT is also more expensive compared to the GNSS technique due to costs for satellite time since usually commercial telecommunication satellites are used [83].

Similar to GNSS, a pseudo-random noise code is modulated on the transmission carrier frequencies of 11 GHz and 7 GHz for the down link and 14 GHz and 8 GHz for the up link in the Ku-band and X-band, respectively. In analogy to the GNSS CV method, the satellite used for the timing information exchange has to be in view at both clock locations, thereby limiting the maximum clock distance to about 10,000 km.

### 3.3.3   Limitations

The instability of GNSS based frequency dissemination methods is strongly limited by path length fluctuations between the satellite and the ground clocks. Fluctuations in the troposphere and ionosphere induce path length and therefore signal delay variations. Intense work has been put into modeling the atmospheric layers for which geographic and climate conditions are used [84]. Also relativistic effects such as the gravitational red-shift and the first and second-order Doppler shift due to the motion of the satellite and the earth have to be taken into account.

Using the TWSTFT method, many of the above mentioned effects cancel to a large extent. However, limitations are set by other effects such as the Sagnac effect or path length differences due to the satellite motion. Also some nonreciprocal delays are inevitable in electronic components in the ground station or in the satellite itself.

Both, the GNSS and the TWSTFT methods described above use pseudo-random noise codes modulated on carrier frequencies at a few Gigahertz to transfer the timing information. Alternatively, the carrier-phase (CP) of the transmission frequencies can be measured directly which provides a frequency resolution enhancement of about a factor
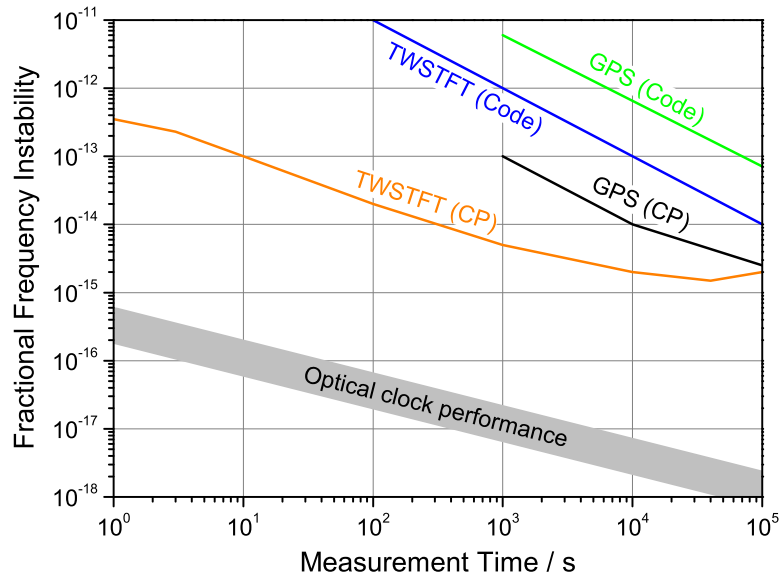
FIGURE 3.2: Fractional frequency instability of satellite based time and frequency dissemination techniques used to date. The pseudo-random noise code (Code) or the carrier-phase (CP) method can be used for both the CV and the AV mode [7, 73, 82, 86, 88]. For comparison, the typical performance of today's optical clocks is depicted.

1000 compared to the code measurements [85]. The CP method thus provides better performance in a remote clock comparison experiment compared to the code-based method.

The frequency instabilities achievable with the mentioned satellite based techniques are shown in Figure 3.2. It can be seen that the lowest instability is a few parts in $10^{15}$ after one day of averaging time [86]. However, it has to be pointed out, that all investigations of the instability limit of satellite based frequency transfer methods of Figure 3.2 were done by comparing two microwave frequency standards that exhibited a noise floor around or above $1 \times 10^{-15}$. Therefore, the achievable frequency instability of the frequency standards partially coincide with the stated instability limit of the transfer methods. It is therefore difficult to distinguish between noise contributions originating from the frequency standards or from the transfer method itself. Recently, a comparison between two hydrogen masers with the help of a GPS carrier-phase link and a TWSTFT link revealed an instability of $4 \times 10^{-16}$ after $10^5$ s [87]. In Chapter 6, a GPS carrier-phase link is investigated in detail in which the limitation imposed by the frequency standards is overcome, thereby allowing a full characterization. Figure 3.2 gives an idea of the frequency instability achievable with satellite based frequency dissemination techniques. It is obvious, that they do not reach the required stability for the dissemination of state-of-the-art optical frequency standards within an adequate measurement time. Achieving higher performance in transferring stable frequencies requires the transition from microwave to optical frequency based methods.

## 3.4   Optical fiber based frequency dissemination

For the last several years, experiments on the transfer of frequencies via optical fibers
have been performed with ever increasing performance and fiber lengths. Different meth-
ods using optical signals for the transfer of frequencies have been investigated. An optical
signal provided by a cw laser can be amplitude modulated before it is sent through a fiber
link [89], thereby transferring a microwave frequency. A combined transfer of microwave
and optical frequencies can be achieved by transmitting pulses from a mode-locked laser
[90]. Femtosecond pulses can also be use in combination with an optical cross-correlation
technique to deliver a stable timing signal to a remote location [91, 92]. Furthermore,
an optical carrier wave can be disseminated by transferring the light of a stable cw
laser. While for short distances up to a few tens of kilometers all four methods show
respectable performances, the latter one is superior in long distance frequency transfer
due to the high carrier frequency and since no dispersion management is required. The
high carrier frequency also provides the femtosecond resolution of optical clocks.

### 3.4.1   Principles of carrier wave fiber based frequency transfer

In order to transfer a highly stable frequency over long distances, two things should
be considered: 1. The transfer medium should ideally not add a significant amount of
noise to the signal to be transmitted and 2. Higher carrier frequencies potentially offer
better stability performance. Nowadays, optical signals with extremely high fractional
instabilities below $10^{-15}$ in 1 s are readily generated. Additionally, the telecommuni-
cation industry did tremendous pioneering work by investigating the transmission of
light through glass fibers. The well developed countries in Western Europe feature an
enormously large and dense glass fiber network that is mainly used for internet data traf-
fic. Therefore, using glass fibers to coherently transmit an optical carrier is an obvious
approach.

One important application for the optical frequency transfer described here is the com-
parison of (optical) atomic clocks. The way such a comparison is achieved with a fiber
link is schematically shown in Figure 3.3. One laboratory that operates an atomic clock
uses an optical frequency comb to link the phase stability of this clock and an ultra-
stable cw transfer laser that serves as an intermediate oscillator. The light of this transfer
laser is transmitted through the fiber link to a remote laboratory housing another atomic
clock. A similar setup featuring an optical frequency comb is used to link the stability
of the second clock and an ultra-stable cw laser. A heterodyne beat between the light
of the local cw laser and the transmitted one then offers the comparison of both clocks
that are involved. In the following, the different components that are required for the
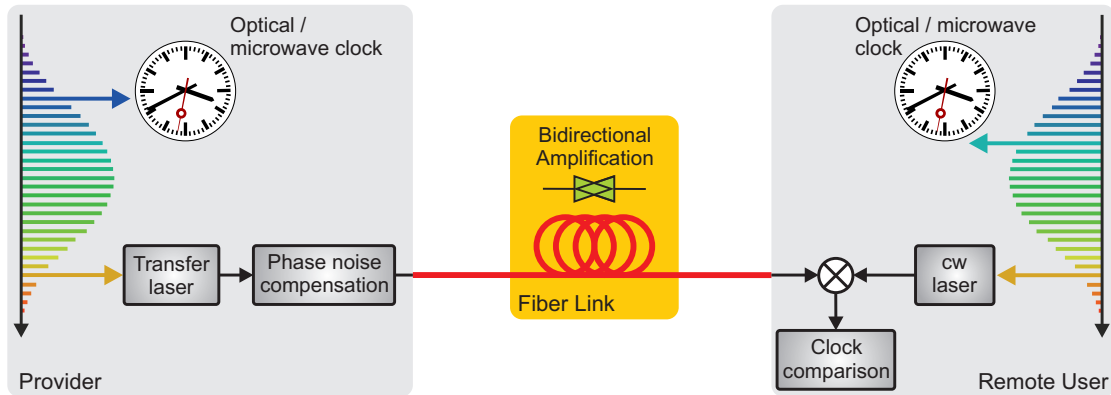optical frequency transfer are described in detail.

FIGURE 3.3: Principle of an atomic clock comparison by fiber link. The phase stability of an atomic clock at a provider site is linked to an ultra-stable intermediate oscillator (transfer laser) with the help of an optical frequency comb. This signal is transmitted to a remote user on an actively noise compensated fiber link. A second intermediate oscillator (cw laser) is used to link the transmitted signal to a second atomic clock and thereby allowing the comparison of the two clocks.

### 3.4.2 Transfer laser systems

The optical frequency to be transferred is provided by a cw laser which can, in principle, operate at any wavelength where glass fibers are transparent. Ideally, however, a wavelength near 1550 nm is chosen as standard telecommunication fibers show the lowest attenuation here. As a high stability of the transferred frequency is desired, the cw laser has to generate a stable and therefore spectrally narrow output.

The frequency stabilization of laser systems has become an intense field of research and new stability records are routinely achieved. State-of-the-art stable lasers employ high-finesse Fabry-Perot resonators that serve as a reference to which the laser is stabilized. If great care is take, special materials, shapes and elaborate mounting of the resonators can lead to residual short term instabilities of a few parts in $10^{16}$ [42]. This corresponds to resonator length variations on the order of a few femtometers, which can only be accomplished by perfect isolation against the environment as well as minimizing the effect of residual perturbations.

The most common way to suppress temperature induced length variations is to use a spacer material that features a thermal expansion coefficient equal to zero at a particular temperature. An example of such a material is called *Ultra-low Expansion* glass (ULE, manufacturer: Corning) with zero thermal expansion at room temperature. Additionally, special spacer geometries and mountings reduce the sensitivity to accelerations, for instance from vibrations [93]. Combining those methods results in a nearly ideal isolation and extremely high length stability of the resonator.

### 3.4.3 Frequency comb systems

An optical frequency comb can be generated by different mechanisms – for instance by a phase/amplitude modulated cw laser [94] or by four-wave mixing in microresonators

[95]. In the field of frequency metrology, however, almost all optical frequency combs are generated by mode-locked lasers that emit a periodic train of laser pulses in the time domain. In the frequency domain, this is equivalent to an optical spectrum which consists of equidistantly spaced spectral lines (or frequencies). The total width of the emitted spectrum can reach from a few nanometers to over 100 nm while the center wavelength is given by the particular laser system.

The frequency of each comb line is determined by only two microwave frequencies. The repetition rate, $f_{rep}$, of the laser determines the spacing between each comb tooth while the whole comb can be offset by the carrier-envelope-offset frequency, $f_{ceo}$. The frequency of an individual comb tooth can be addressed by $\nu_n = n \cdot f_{rep} + f_{ceo}$, where $n$ is an integer typically on the order of $10^5 \ldots 10^6$. An unknown optical frequency $\nu$ within the spectral range of the comb can be determined with high accuracy by measuring the beat frequency between $\nu$ and the nearest comb tooth, resulting in

$$\nu = (n \cdot f_{rep} + f_{ceo}) + f_{beat} \tag{3.1}$$

The integer $n$ is often referred to as the mode number which has to be determined separately. The easiest way to accomplish this is with the help of a high-resolution wavemeter. In the experiments discussed in this work, commercial erbium fiber laser based frequency combs (Menlo Systems GmbH) were used [96, 97]. To link the frequencies of the comb lines to an absolute reference, the repetition rate of the comb is locked to some sort of frequency standard, for example a hydrogen maser.

### 3.4.4 Signal amplification

Glass fibers constitute the best known medium for long distance transfer of optical signals due to their flexibility, the excellent noise properties and especially the low optical attenuation of only 0.23 dB/km around 1550 nm. It is the latter that allows to bridge distances of up to 100 km without intermediate signal amplification. For comparison, a radio frequency exhibits an attenuation of typically 70 dB/km at 100 MHz and 200 dB/km at 1 GHz in a standard coaxial cable (RG-6). However, if an optical signal has to be transmitted over a distance that significantly exceeds 100 km, additional amplifiers have to be used to compensate for the fiber-induced attenuation.

There are different techniques for amplifying an optical signal in the wavelength around 1550 nm. The most widespread one is an erbium-doped fiber amplifier (EDFA) that uses a section of active fiber to provide the gain for the signal to be amplified. This amplifier technique provides moderate gain of up to 25 dB and a wide gain bandwidth covering $\approx$ 1530 - 1580 nm. Signal amplification can also be achieved by using stimulated Raman scattering (SRS) [98] in optical fibers. Such a Raman amplifier can provide gain comparable to that of an EDFA while the gain bandwidth depends on multiple parameters like pump wavelength, pump power, fiber type and others [99]. A third amplifier technique makes use of stimulated Brillouin scattering (SBS) [100] and consequently, these amplifiers are often referred to as fiber Brillouin amplifiers (FBA) [9]. A total

gain of up to 50 dB can be achieved with FBAs while the gain bandwidth of just about 20 MHz is significantly narrower compared to the afore mentioned amplifiers. All of these amplifiers can be used to amplify a signal in both directions along the fiber.

### 3.4.5 Fiber induced phase fluctuations

In contrast to sending light over free-space [91], light transmission through fibers experiences less perturbations which enables better performance. Nevertheless, deployed fibers are, to some extent, inevitably subject to the environment that can affect the properties of the light that travels through them. The most prominent perturbations on optical fibers are thermal fluctuations and acoustic vibrations. Those perturbations lead to variations of the physical fiber length and to fluctuations of the fiber's refractive index. This in turn changes the optical path length and causes phase shifts often referred to as Doppler noise. These phase fluctuations set limits on the achievable stability and accuracy of the transmitted signal.

Temperature fluctuations over time change the optical path length of the fiber with refractive index $n$ and length $L$ as

$$\frac{d(nL)_T}{dt} = \left( L \frac{dn}{dT} + n \frac{dL}{dT} \right) \frac{dT}{dt}. \tag{3.2}$$

The thermo-optic coefficient $\frac{dn}{dT}$ and the thermal expansion coefficient $\frac{dL}{dT}$ are listed in the literature and are equal to $1 \times 10^{-5}$ K$^{-1}$ and $6 \times 10^{-7}$ m K$^{-1}$ for fused silica, respectively [101]. A signal with carrier frequency $\nu_0$ and vacuum wavelength $\lambda_0$ experiences a fractional frequency shift of

$$y(t) = \frac{1}{\nu_0 \lambda_0} \frac{d(nL)_T}{dt}. \tag{3.3}$$

If, for instance, a 1000 km long standard single-mode fiber ($n = 1.468$) is affected by a temperature variation of 1 K during the course of one day, a signal at a wavelength of 1542 nm will experience a fractional frequency shift of about $4 \times 10^{-13}$ which is equal to about 80 Hz. A perturbation like this can easily be corrected with the help of an acousto-optic frequency shifter.

Equation 3.2 only takes into account the fluctuations of the optical path length due to temperature variations. Acoustic waves acting on the fiber can induce stress through pressure, $P$, changes which also lead to phase fluctuations of a signal. In analogy to Equation 3.2, the temporal optical path length fluctuations due to a pressure changes can be expressed as

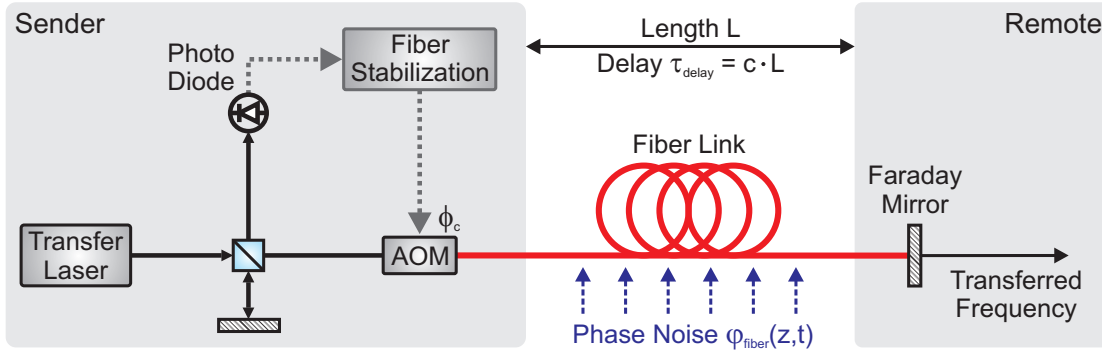$$\frac{d(nL)_P}{dt} = \left( L \frac{dn}{dP} + n \frac{dL}{dP} \right) \frac{dP}{dt}. \tag{3.4}$$

FIGURE 3.4: Simplified sketch for the fiber induced phase noise detection and compensation. A fiber with length $L$ introduces a signal delay $\tau_{delay}$. The fiber phase noise $\varphi_{fiber}(z, t)$ is a function of the position $z$ and time $t$.

The coefficients $\frac{dn}{dP}$ and $\frac{dL}{dP}$ can be found in the literature and amount to $5 \times 10^{-11}$ Pa$^{-1}$ and $\approx 10^{-11}$ m Pa$^{-1}$, respectively [11, 102]. An acoustic pressure change of 0.01 Pa, for instance, causes a fractional frequency shift of a signal at 1542 nm of up to $1.5 \times 10^{-14}$ or 3 Hz in a 1000 km long single-mode fiber. Again, this frequency shift can easily be corrected using optical frequency shifters.

### 3.4.6 Active fiber noise cancellation

Even for a well isolated underground fiber link as investigated in this work the fiber induced phase shifts discussed in Section 3.4.5 are on the order of a few parts in $10^{14}$. To reach better performance of the transferred frequency, those fiber induced phase fluctuations need to be detected and compensated. An interferometric scheme similar to the one described in [103] is used for the noise detection and a phase-locked loop (PLL) at the sender site is employed to suppress the optical path length fluctuations at the remote site.

A simplified sketch of the phase noise compensation system is shown in Figure 3.4. The detection of the fiber induced phase noise is done in a Michelson interferometer. The light of a transfer laser is split into a short ($\approx$ 60 cm) reference arm and long arm that consists of the actual fiber link. An acousto-optic modulator (AOM) that acts as a frequency shifter is inserted in the beam path at the sender site. A Faraday mirror at the remote site reflects a portion of the transferred light whereby it rotates the signal polarization by 90° so that any polarization fluctuations occurring along the link are compensated to a large extent to allow for a beat note with stable amplitude [104]. The retro-reflected light is guided to a photo diode after it reached the sender site again. A heterodyne beat is generated in the radio-frequency domain between the returning round-trip light and a local copy of the original signal. This beat contains information about the accumulated fiber-induced phase noise, $\varphi_{fiber}(z, t)$. The knowledge about the fiber noise can then be used to steer an AOM in order to compensate for it. More details about the electronics used for the fiber link stabilization are given in Section 4.2.3.

### 3.4.6.1 Self-heterodyning

The light emitted by the transfer laser is compared with a time delayed copy of itself as described above. This method is known as self-heterodyning [105]. The coherence length, $L_c$, of a laser is a function of its output spectrum and can be calculated by $L_c = \frac{c}{\pi \Delta \nu} = c\tau_c$ where $\Delta \nu$ is the spectral linewidth of the laser, $c$ is the speed of light in the fiber and $\tau_c$ is the coherence time. In a self-heterodyning setup, two cases can be considered:

1. The long interferometer arm is significantly longer than the coherence length of the laser. In this case, the overlapping beams are essentially uncorrelated and the spectrum of the beat signal could be used to retrieve the laser output spectrum. For the fiber noise cancellation this means that the beat signal at the photo diode contains noise components from the fiber link (long interferometer arm) as well as from the transfer laser itself.

2. The long interferometer arm is shorter than the coherence length of the laser. In this case, the overlapping beams are still correlated so that common mode noise from the laser itself is suppressed. The beat signal at the photo diode is dominated by noise arising in the fiber link.

For the fiber link stabilization discussed here, the latter case is aspired as the beat signal is assumed to carry only the noise from the link. The transfer laser used throughout this work exhibits a linewidth of about 1.5 Hz (FWHM), resulting in a coherence length of over 64,000 km. Thus, the information from the heterodyne beat can safely be used for the compensation of the fiber induced phase noise.

### 3.4.6.2 Phase noise suppression

The fiber noise detection relies on sending a signal to the remote end of the link and receiving the returning light. The finite velocity of the light in the fiber therefore imposes a fundamental limit on the achievable degree of phase noise suppression as the presence of noise is detected only after the light traveled the entire fiber link twice. This directly affects the control bandwidth of the noise cancellation loop so that noise at higher Fourier frequencies cannot be suppressed. Another effect of the propagation delay is that the light exits the fiber end before any correction can be applied. As a result, the fiber noise on the one-way signal cannot be suppressed entirely. In addition, the phase noise cancellation system relies on the fact that the noise in the forward direction is identical to the noise in the backward direction so that the detected signal contains precisely twice the one-way phase noise. Hence, any differential noise between the forward and the backward direction leads to an imperfect cancellation at the remote end.

When no noise compensation is applied, the light traveling through the fiber from the sender site ($z = 0$) to the remote site ($z = L$) accumulates noise. The phase noise $\varphi_{fiber}$ at the exit of the fiber at time $t$ can be expressed as [8, 106]

$$\varphi_{fiber}(t) = \int_0^L \delta\varphi\left(z, t - (\tau_{delay} - \frac{z}{c})\right) \, dz \tag{3.5}$$

where $\tau_{delay}$ is the propagation delay in the fiber and $\delta\varphi(z,t)$ is the phase perturbation at position $z$ and time $t$. Consequently, the phase noise of the round-trip light exiting the fiber at time $t$ is

$$\varphi_{fiber,RT}(t) = \int_0^L \left( \delta\varphi(z, t - \frac{z}{c}) + \delta\varphi\left(z, t - (2\tau_{delay} - \frac{z}{c})\right) \right) \, dz \tag{3.6}$$

in which the first term under the integral represents noise that affects the light traveling towards the sender while the second term represents noise that affects the light traveling away from the sender.

If the phase noise compensation is active, a phase correction $\phi_c$ is applied through the AOM. Assuming a perfect phase locked loop (PLL), the correction is equal to the phase perturbation so that

$$\varphi_{fiber,RT}(t) - \left( \phi_c(t) + \phi_c(t - 2\tau_{delay}) \right) = 0. \tag{3.7}$$

Consequently, at the remote site of the link one obtains

$$\varphi_{fiber}(t) - \phi_c(t - \tau_{delay}) = \frac{z}{c}\frac{d\varphi}{dt}. \tag{3.8}$$

From Equation 3.8 it can be seen that the phase noise at the remote end of the fiber link only vanishes in steady state (no time dependence) or at $z = 0$. In other words, the delay of the round-trip light which is used for the fiber noise compensation leads to an imperfect cancellation of the one-way phase noise. Even if the round-trip phase noise is perfectly canceled, the one-way light still suffers from phase noise which is often referred to as *delay-unsuppressed noise*.

The delay-unsuppressed noise is a fundamental limit of the stabilization techniques used in this work. Hence, it is worth to investigate the consequences of this effect. Taking the Fourier transform of Equation 3.5 yields the power spectral density (PSD) of phase fluctuations for the one-way light

$$S_{fiber}(\omega) = \langle |\tilde{\varphi}_{fiber}(\omega)|^2 \rangle \tag{3.9}$$

under the assumption that the fiber noise is independent of position. $S_{fiber}(\omega)$ is denoted as the phase noise of the free-running fiber link throughout this thesis. A certain loop filter function [107] is introduced to the phase fluctuations of the round-trip signal

| Country | Link length | Demonstrated instability | Remarks |
|---------|-------------|--------------------------|---------|
| Germany | 480 km | $2 \times 10^{-18}$ @ $10^4$ s | single-span [9] |
| Japan | 90 km | $5 \times 10^{-18}$ @ $10^3$ s | single-span [10] |
| France | 540 km | $7 \times 10^{-19}$ @ $10^4$ s | single-span [108] |
| Italy | 47 km | $4 \times 10^{-21}$ @ $10^4$ s | two-way phase transfer [109] |
| USA | 251 km | $6 \times 10^{-19}$ @ $10^2$ s | partially spooled fiber [106] |

TABLE 3.1: Existing fiber links for frequency transfer applications and achieved long term instability.

through the PLL. After applying some control theory and algebraic conversions [8] the PSD of the stabilized one-way light can be derived to

$$S_{remote}(f) = \frac{4}{3}(\pi f \tau_{delay})^2 S_{fiber}(f) \qquad (3.10)$$

where position as well as time independence of the noise has been assumed. Equation 3.10 only holds for low Fourier frequencies well within the control bandwidth of the noise compensation PLL. Note, however, that this effect is not related to any bandwidth limitation of the PLL. It is rather intrinsic to the fact that the round-trip signal is used to stabilize the one-way light at the remote end of the link.

Equation 3.10 assumes that the noise of the transfer laser is well below that of the fiber link and that the noise floor of the interferometer does not contribute to the performance of the frequency transfer. Under the assumption of $S_{fiber}(f)$ being dominated by white frequency noise and a uniform noise distribution along the link, the obtainable frequency instability of the transferred frequency scales with $L^{3/2}$ [8] (see Section 4.4.4). This demonstrates that a low inherent fiber noise is favorable and additionally the frequency stability degrades nonlinear with increasing fiber link length.

## 3.5 Existing fiber links for frequency transfer applications

The progress in the development of optical frequency standards in various institutions around the world and consequently the demand for transmitting highly stable optical frequencies accelerated the research on fiber links. In the mean time, several European countries as well as Japan, the United States and Australia established fiber link connections to compare their high-performance clocks or for other applications requiring timing synchronization. As an example, Figure 3.5 shows the frequency instability achieved by transferring an optical carrier over fiber links in Germany, France and Japan over the last years. Research on fiber links is also conducted in Italy, Poland, England and other countries around the world with link lengths typically on the order of a few tens of kilometers to a few hundred kilometers. Table 3.1 lists the achieved long term instability of a few selected existing fiber links.
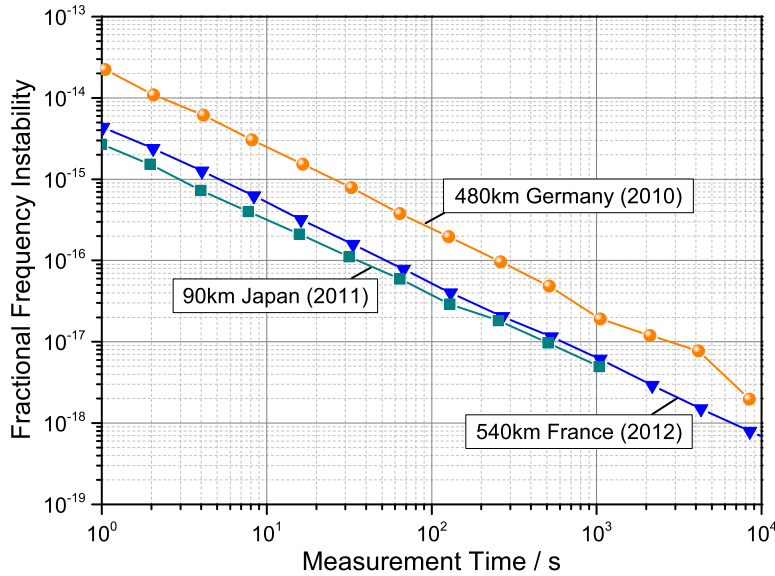
FIGURE 3.5: Literature values of the fractional frequency instability after transferring an optical carrier through different fiber links [9, 10, 108].

In the mean time, a whole variety of different techniques have been employed as an alternative or an addition to the methods described in the next chapter. Instead of delivering an optical frequency to a remote location, a two-way optical phase comparison can be performed [109]. This method also allows the comparison of distant frequency standards but in contrast to the methods discussed in this work, no stable frequency is delivered to a remote location. Another interesting approach that is worth mentioning attempts to transfer a stable frequency to multiple remote locations simultaneously [110]. Here, a branching fiber network is used and the stabilization of the fiber link transfer is done at the remote end of the link instead of at the local end. A clear advantage of this technique is that in case of a malfunction of one of the link stabilization systems, all the other segments remain unaffected. This advantage comes at the cost of higher optical losses compared to the conventional technique. Delivering a stable frequency to more than one location can also be done by extracting a portion of the transferred signal at any point between the local and the remote end [111, 112]. The signals traveling in the forward and in the backward direction between the two ends of the stabilized link can be used to derive a correction signal to extract a stable optical frequency. This way, many places along the actual fiber link can be served with an optical reference frequency. This approach comprises only one single fiber link stabilization control loop which reduces the complexity of the system. The extraction of the signal, however, introduces additional optical losses that have to be compensated.

## 3.6    Requirements for optical clock comparisons and other applications

Many applications rely on accurate timing and frequency synchronizations. For instance, mobile broadband internet access uses synchronized base stations that require frequency

accuracies below $10^{-8}$ or timing accuracies of about 1.5 $\mu$s to handle the rapidly growing demands. The electrical power grid also needs accurate timing of ideally 100 ns or better for fault detection. The highest requirements on accurate frequency synchronization are set by atomic clock comparisons. As discussed in Chapter 2, the comparison of microwave frequency standards requires a frequency accuracy of better than $10^{-15}$. Advanced satellite technology allows a frequency accuracy of slightly below this requirement (see Chapter 6). The ultimate demands in terms of frequency transfer accuracy, however, are dictated by the performance of optical clocks (see Section 2.4), raising the required accuracy to currently about $10^{-18}$. Up to date, only the transfer of optical frequencies via fiber links has demonstrated performances satisfying those needs for long distances.

# Chapter 4

# Optical Fiber Links between MPQ and PTB

## 4.1 Introduction

The glass fibers used for the dissemination of the optical frequency are provided by the communication network corporation GasLINE GmbH in a collaboration with the German Science Network (DFN). Besides the Max Planck Institute of Quantum Optics (MPQ) and the Physikalisch-Technische Bundesanstalt (PTB) between which the links discussed in this work are operated, the Institute of Quantum Optics (IQ) at the University of Hanover, the Max Planck Institute for the Science of Light and Menlo Systems GmbH are further contributors. The establishment of the two fiber links began in 2007 by the construction and installation of a number of amplifier systems along the fiber route. Both MPQ and PTB began to establish short sections of the link while successively increasing its length to eventually meet in the middle between the two institutes. Frequency transmission between MPQ and PTB was successfully demonstrated for the first time in 2009. The establishment of the fiber links and initial investigations were subject to an earlier PhD thesis [113].

The fibers are buried at least one meter below the surface of the earth but they make short excursions to the surface at certain distribution and regeneration stations. The isolated and quiet environment of the fibers is favorable as acoustic noise and temperature variations are strongly reduced (see Section 3.4.5). Figure 4.1 shows the route of the 920 km long fibers that run in parallel in the same cable duct, spanning a large part of Germany.

The ITU-T G.652 specified fibers [114] have a core refractive index of $n = 1.4681$ and an optical attenuation of $\alpha \leq 0.23$ dB/km at 1550 nm. The total one-way attenuation of the 920 km link therefore adds up to about 210 dB. The fibers are accessible approximately every 90 km via telecommunication stations and via computing centers in Garching and at the Universities of Erlangen and Leipzig. Each of the nine stations are equipped with two EDFAs (see Section 3.4.4) for signal regeneration. The gain of those amplifiers has
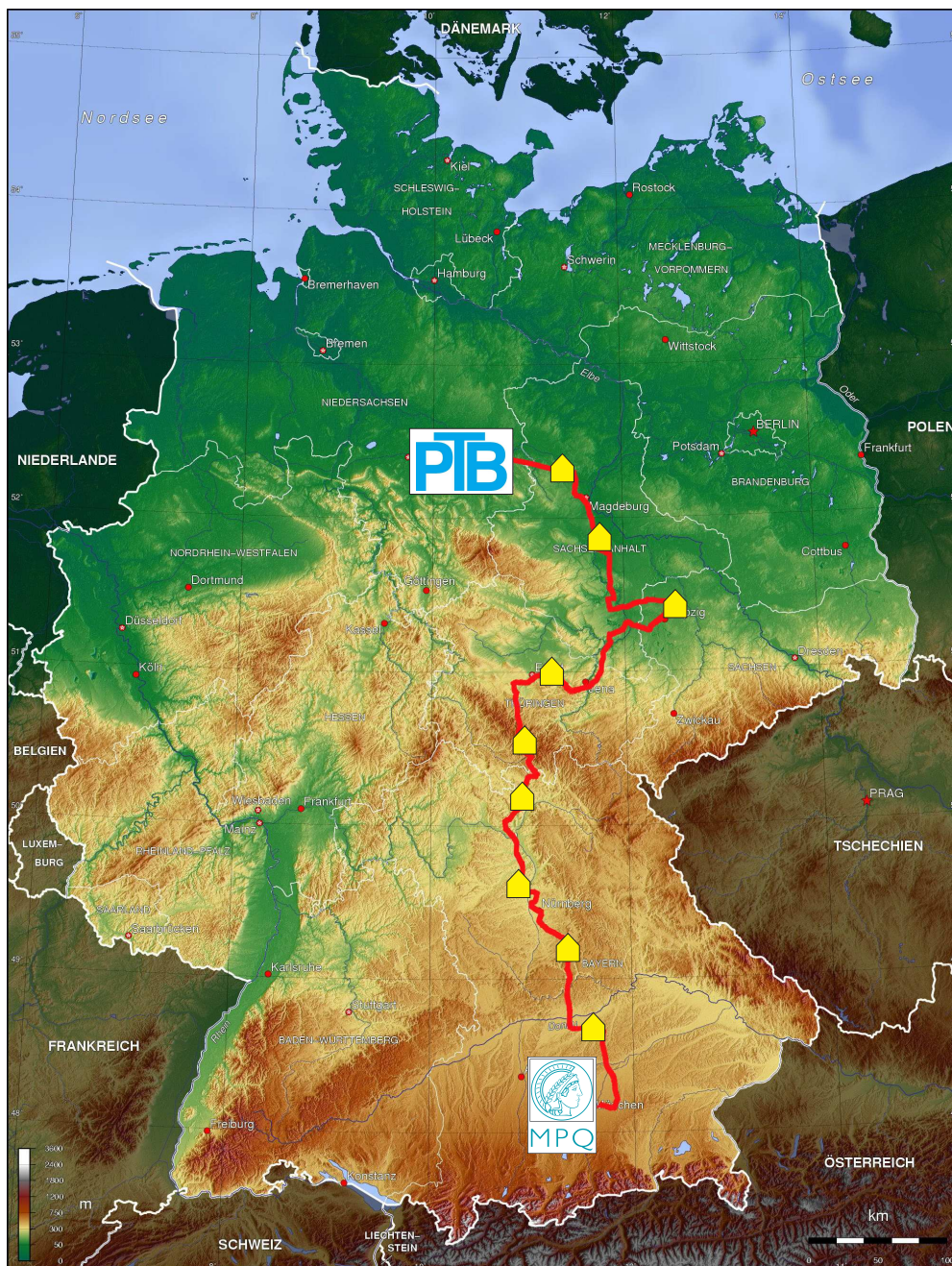
FIGURE 4.1: Map of Germany with the path of the two 920 km fiber links between MPQ and PTB. The yellow houses indicate the nine amplifier stations equidistantly distributed along the link with a spacing of roughly 90 km. Each station houses two separate amplifiers; one for each fiber.

to be kept below $\approx$ 20 dB as Rayleigh scattering [115] and stray reflections cause self-lasing that in turn leads to sudden dropouts of the signal resulting in a loss of coherence. Additionally, nonlinear effects like stimulated Brillouin scattering limit the maximum optical power that can be launched into the fiber. The threshold of this effect depends on multiple parameters like the fiber type, the laser wavelength and the linewidth of the optical signal. For the setup used here the threshold and therefore the maximum injectable power is about 6 mW [113]. As a consequence, the EDFAs are installed every

$\approx 90$ km. The gain provided by the EDFAs is not quite sufficient to compensate for the fiber induced attenuation for which reason two FBAs located at MPQ and PTB are used for additional signal amplification. Thereby, the fully operational 920 km link involves eleven amplifiers at eleven different locations.

The fibers carry exclusively the light sent from MPQ and PTB. No additional channels in the ITU grid are used for internet data traffic from third parties. Dedicated fibers like this are often denoted as *dark fibers* as compared to a *dark channel*, where only a channel in the ITU grid is used for the frequency transfer in addition to other channels carrying internet data traffic. A dark fiber has the significant advantage of being free of any optical isolators often used in telecommunication amplifier systems for data transmission. This is important since the active stabilization of the frequency transfer requires bi-directionality as discussed in Section 3.4.6.

As the amplifiers are distributed along the entire link, a means of remote control to monitor and surveil the EDFAs is a prerequisite for operating the fiber link. Due to the absence of internet reception in most of the amplifier stations, an optical remote control is established. Here, in addition to the "science signal" at 1542 nm, a "communication signal" at 1310 nm is sent through the same fiber. The 1310 nm signal is amplitude modulated (on-off keying) with signals based on the RS-232 protocol. A wavelength division multiplexer (WDM) in the EDFA separates the two wavelength and a micro controller processes the RS-232 signals after the conversion to an electrical signal. That way, the status of the EDFA including its temperature and gain can be monitored and altered. During the course of the experiments, the fine adjustment of the EDFA gain turned out to have a crucial impact which eventually allowed the coherent frequency transfer over many hours.

In this chapter, the frequency transfer via the 920 km fiber links between MPQ and PTB is characterized in detail. The results indicate a limitation due to temperature fluctuations in the MPQ laboratory which is overcome subsequently. An 1840 km fiber link is set up in a loop configuration and the transfer of an optical frequency over this link is investigated as well.

## 4.2   Characterization of the subsystems

As explained in Section 3.4, the apparatus used for the optical frequency transfer can be subdivided into different components. In order to achieve a stable and accurate frequency transfer, it has to be verified that all of these components meet the required performance. In the following, these components are characterized in detail and the limitations imposed by them are pointed out.

### 4.2.1   Transfer laser

The fiber link stabilization (see Section 3.4.6) relies on the heterodyne beat between the sent light and the round-trip light. As described in Section 3.4.6.1, the noise that
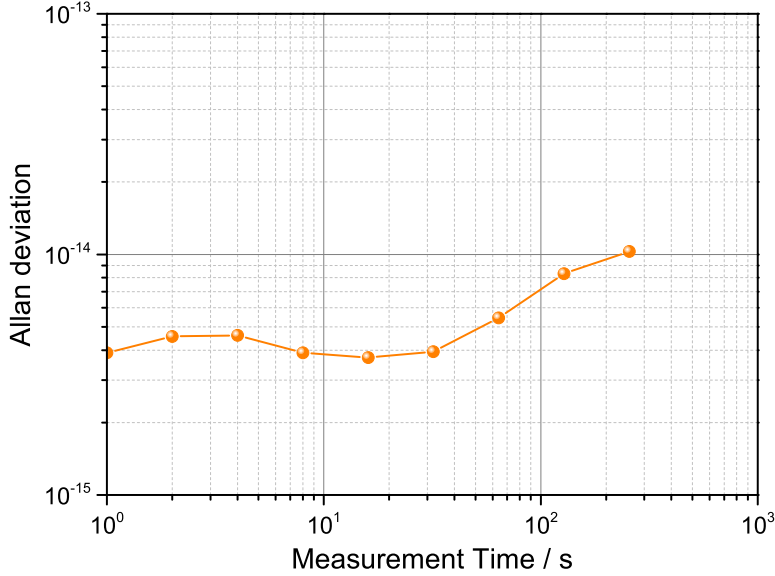
FIGURE 4.2: Frequency instability of the beat note between the cavity stabilized transfer lasers. Courtesy of K. Predehl [113].

this heterodyne beat contains has to originate entirely from the fiber link transfer. For this reason, the noise of the transfer laser has to be well below that of the fiber link itself within the control bandwidth of the fiber link stabilization. Transfer laser noise at frequencies outside the control bandwidth is less problematic since the link stabilization is not able to mistakenly correct for this noise.

The two cw transfer lasers used in this work are both near-infrared distributed feedback fiber lasers (Koheras AdujstiK) operating at a wavelength of 1542 nm. They deliver up to 100 mW of power and exhibit a free-running linewidth of about 5 kHz (FWHM). To reduce the laser phase noise, the transfer lasers are locked to optical cavities that consist of high reflecting mirrors which are optically contacted to a ULE spacer. The finesse of the cavity has been determined to $\mathcal{F} = 250,000$ and $\mathcal{F} = 330,000$ for the systems used here, respectively. Approximately 100 $\mu$W of optical power are coupled into each cavity. The stabilization of the laser to the cavity is achieved by a Pound-Drever-Hall (PDH) lock [116, 117] which features an acousto-optic modulator (AOM) in the laser output for the frequency stabilization. As the AOM has a limited dynamic range, a piezo-electric transducer (PZT) is used for controlling the laser cavity length, thereby keeping the AOM frequency centered. The cavities of both systems are temperature stabilized and kept in high vacuum ($p \approx 10^{-9}$ mbar). Additionally, they rest on active vibration isolation platforms to reduces the influence of building vibrations.

The characterization of the transfer laser systems was done by generating a beat between the two cavity stabilized lasers directly when both systems were operated at the same location prior to the actual frequency transfer experiments. The instability of the measured beat frequency after subtraction of a third-order drift is shown in Figure 4.2. The linewidth of the beat note was measured to 2 Hz. Under the assumption of equal performances and a Lorentzian line shape, the linewidth of the individual lasers is estimated to 1.5 Hz [113]. The coherence length, $L_c$, of this transfer laser can be calculated
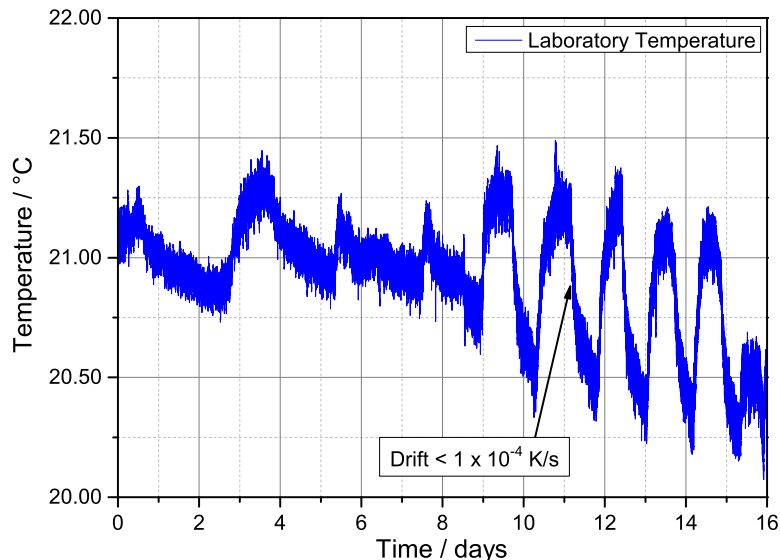
FIGURE 4.3: Air temperature fluctuations of the MPQ laboratory. Stable temperature conditions as well as periods with strong oscillations that are caused by the air condition can be observed.

to be on the order of 64,000 km (see Section 3.4.6.1) which is significantly longer than all the fiber links investigated in this work.

## 4.2.2 Interferometer for fiber noise detection

The detection of the fiber induced phase noise is accomplished by comparing the sent light with the round-trip light as mentioned above in a setup that is similar to a Michelson interferometer (Figure 3.4). Like in every interferometer the light in the reference arm is compared to the light in the measurement arm, which in this case is the actual fiber link. It is crucial to isolate the reference arm well from the laboratory environment as any perturbations on the light in this arm will be interpreted as noise arising in the measurement arm. Figure 4.3 shows typical fluctuations of the air temperature in the MPQ laboratory over the course of 16 days. Periods of stable temperature with only minor variations as well as strong oscillations with high drifts of up to $1 \times 10^{-4}$ K/s can be observed. Note, that temperature drifts, i.e. the change in temperature with time, is the critical parameter rather than absolute temperature variations. The noise floor of the interferometer is strongly related to temperature drifts acting on the reference arm. Therefore, the performance that can be achieved depends on the current environmental conditions.

### 4.2.2.1 Passively isolated interferometer housing

In a first attempt, an aluminum housing for the interferometer is constructed in order to isolate the reference arm from the rest of the laboratory. This housing is meant to suppress the strong oscillations seen in Figure 4.3 in order to decrease its effect on the interferometer. To determine the effectiveness of this passive isolation, the interferometer
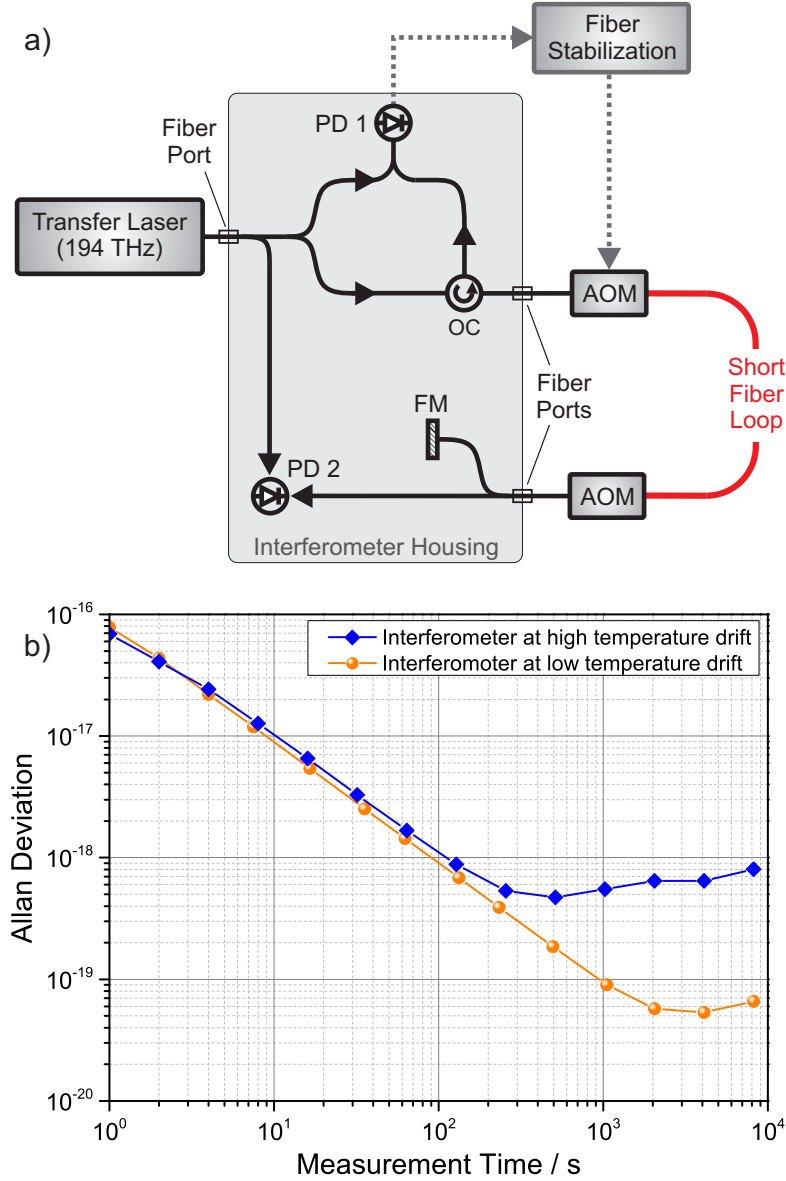
FIGURE 4.4: a) Setup used to determine the noise floor of the interferometer. OC: Optical circulator, FM: Faraday mirror, PD 1: Inloop photo diode, PD 2: Out-of-loop photo diode. b) Fractional frequency instability expressed as the ADEV and measured with a Π-type counter indicating the noise floor of the interferometer used for the fiber link noise detection and stabilization. Strong temperature fluctuations of the laboratory environment may increase the noise floor up to $5 \times 10^{-19}$. In periods with high temperature stability the noise floor can be as low as $5 \times 10^{-20}$.

noise floor is determined by replacing the fiber link with a short, $\approx 50$ cm long fiber (see Figure 4.4 a)). The out-of-loop beat signal on PD 2 is counted in order to characterize the noise floor of the whole interferometer including the electronics used for the fiber stabilization. It can be seen that the interferometer supports an instability of about $5 \times 10^{-20}$ for measurement times of 2000 s and above if the environmental temperature fluctuations are low (see first 8 hours in Figure 4.3). In case of strong temperature fluctuations, however, the noise floor increases by about one order of magnitude.
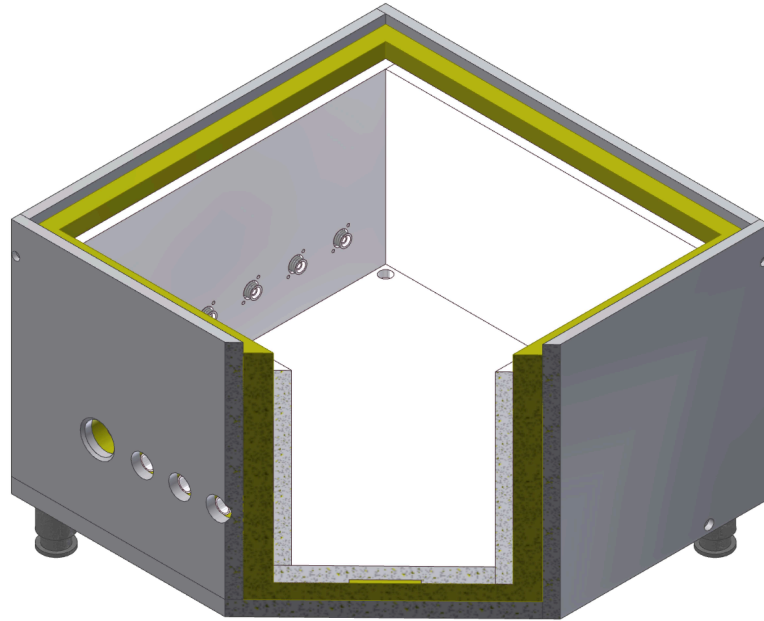
FIGURE 4.5: Redesigned and temperature stabilized interferometer housing. Inner and outer box are separated by a 10 mm layer of isolating foam. The inner box is actively stabilized to a temperature of $\approx 23$ °C. Various fiber ports and BNC connectors allow to exchange optical and RF beat signals between the inside and outside. Dimensions: $270 \times 270 \times 150$ mm$^3$

#### 4.2.2.2 Actively temperature stabilized interferometer housing

To reduce the instability floor even at the presence of strong laboratory temperature drifts better isolation and subsequently lower temperature fluctuations inside the interferometer housing is required. The initially used passive housing is redesigned entirely to provide a better passive isolation and additionally, the interferometer housing is actively temperature stabilized in order to minimize the effect of room temperature fluctuations on the interferometer.

Figure 4.5 shows the redesigned housing of the interferometer at MPQ. It consists of an inner and an outer box which are separated by a 10 mm layer of isolating foam. The inner box is actively stabilized to a temperature of $\approx 23$ °C by means of a heating foil, which is about three degrees above room temperature. Optical signals are transported in and out of the box via fiber ports. The photo diodes that generate the beat signals are kept inside the box and the RF beat signals are fed through BNC ports to the outside.

The interferometer housing has to suppress the laboratory air temperature fluctuations shown in Figure 4.3 to a level that can be determined with the help of Equation 3.3. Assuming a length of 60 cm for the reference arm of the interferometer and a desired temperature induced fractional frequency shift of $< 1 \times 10^{-19}$, any residual temperature drift has to be suppressed to below $4 \times 10^{-6}$ K/s.

In Figure 4.6 the temperature inside the interferometer housing is shown which has been measured at the same time as the laboratory air temperature of Figure 4.3. It can be seen that the interferometer temperature tracks the ambient temperature to some
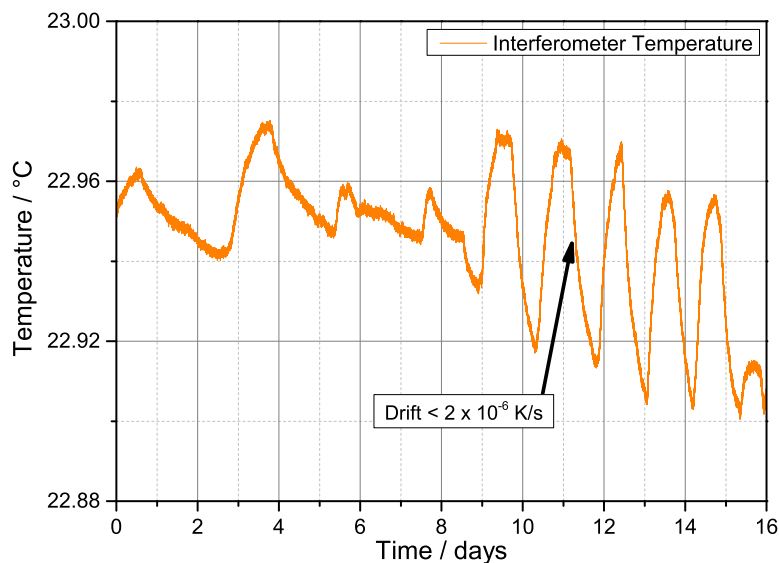
FIGURE 4.6: Temperature fluctuations inside the interferometer housing. The re-designed housing provides a suppression factor of $\approx 50$.

extent. The fluctuations, however, are well suppressed to $< 2 \times 10^{-6}$ K/s which indicates a suppression factor of $\approx 50$.

According to Equation 3.3 the observed temperature drift should support an interferometer noise floor of below $5 \times 10^{-20}$. Figure 4.7 shows the measured noise floor expressed as the modADEV which has been determined in the same way as described above (see Section 4.2.2.1) but by using a $\Lambda$-type counter. A flicker floor is reached after 500 s at a level of $7 \times 10^{-21}$, thus indicating that the measured temperature drift inside the interferometer housing does not act at this magnitude on the whole 60 cm of the



FIGURE 4.7: Fractional frequency instability indicating the redesigned actively temperature stabilized interferometer noise floor measured with a $\Lambda$-type frequency counter and expressed as the modADEV.

FIGURE 4.8: Schematic of the electronics used for the fiber noise cancellation and the characterization of the frequency transfer. A digital phase detector is used to derive an error signal between the he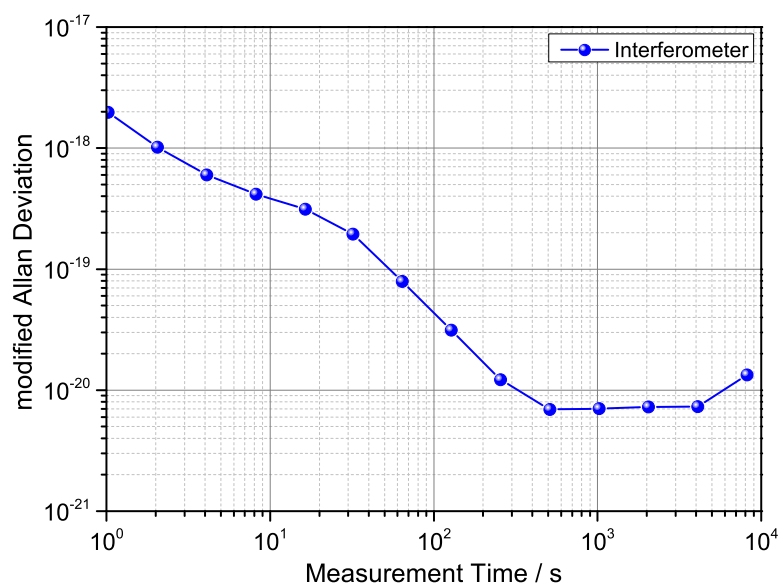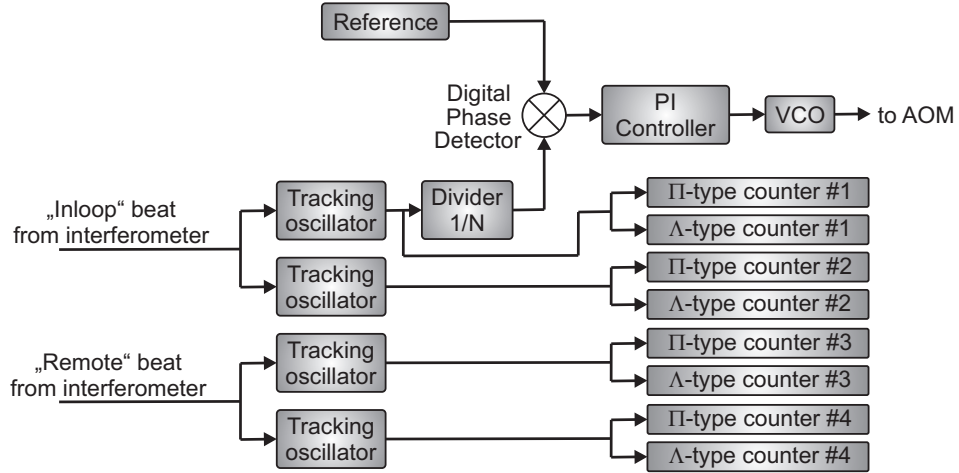terodyne beat signal and a stable reference. A proportional-integral (PI) controller generates a control signal that is fed into a voltage-controlled oscillator (VCO) which steers an acousto-optic modulator (AOM). Both, the inloop beat (PD 1 in Figure 4.4) and the remote beat (PD 2 in Figure 4.4) are tracked twice and each signal is counted with a Π- as well as a Λ-type counter.

interferometer reference arm. As the measured noise floor is well below the targeted level of performance for the fiber link frequency transfer the redesigned interferometer should not constitute a limitation.

## 4.2.3 Locking electronics and frequency counters

The fiber stabilization contains various electronic components as, for instance, a phase detector, a PI-controller, a VCO etc. as illustrated in Figure 4.8. Those components can also constitute a limitation and therefore need to be characterized independently. Instead of generating an optical beat, the VCO that usually controls the AOM frequency is now locked to a stable reference frequency, thereby eliminating all optical parts of the setup.

The locked VCO frequency is counted against the frequency reference with the help of a frequency counter. A perfect lock and noise free electronics would make the VCO frequency identical to the frequency reference and the frequency counter output should represent the noise floor of the counter itself. The true frequency counter noise floor, however, can be determined by directly counting the counters frequency reference against itself. Both, the instability of the electronics as well as that of the frequency counter (Π-type) alone is shown in Figure 4.9. It can be seen that the instability of the electronics is about $1.5 \times 10^{-17}$ in 1 s and averages down to below $10^{-21}$. This (Π-type) frequency counter has a resolution of 1 mHz and an instability of about $2 \times 10^{-18}$ in 1 s. It reaches a floor of $1.5 \times 10^{-22}$ which determines the ultimate limit for this particular counter.
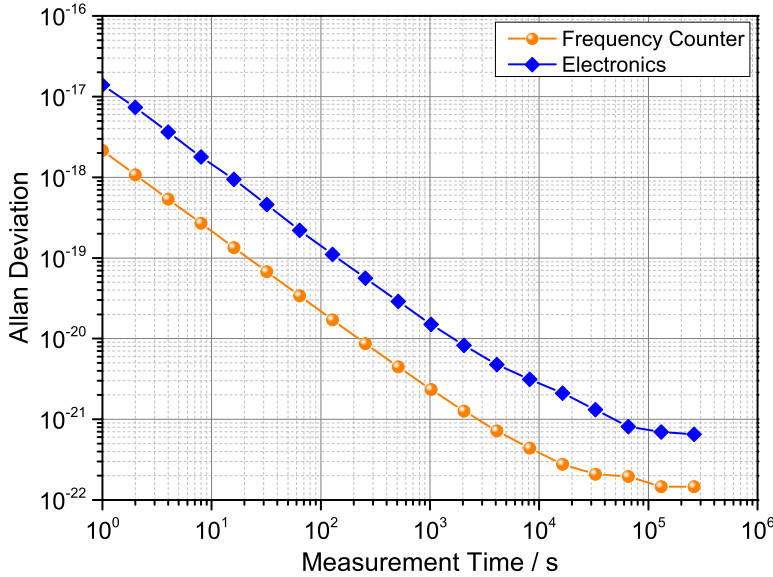
FIGURE 4.9: Fractional frequency instability of the electronics used for the fiber link stabilization and the frequency counter itself (Π-type).

### 4.2.4    Polarization mode dispersion

The effect of light with different polarizations traveling at different velocities in fibers is known as polarization mode dispersion (PMD) which is caused by variations of the refractive index of the fiber due to mechanical stress or uncertainties in the manufacturing process. This effect leads to birefringence and therefore to variations in the propagation delay which in turn can limit the achievable frequency transfer performance. An exact calculation of the PMD effects is complicated due to the statistic nature of this process. However, a simple estimate of the phase noise caused by PMD is given in [8]. The PMD causes a differential group delay (DGD), $\tau_{DGD}$, [118] that depends on the fiber type and the fiber length. The PMD coefficient that describes the strength of this effect is 0.1 ps/$\sqrt{km}$ for SMF-28 fiber that is used here. For a link length of 920 km the DGD calculates to $\tau_{DGD} = 3$ ps. It can be shown that the effect of PMD exceeds the delay-unsuppressed fiber noise (see Section 3.4.6) only at Fourier frequencies

$$f < \frac{\sqrt{3}\,\tau_{DGD}}{4\pi\tau_{delay}^2}. \tag{4.1}$$

The one-way propagation delay of the 920 km fiber link is $\tau_{delay} = 4.5$ ms, resulting in $f < 20$ nHz which is on the order of years. Therefore, the PMD does not constitute any limitation on the experiments described in this work.

## 4.3    Two 920 km fiber links between MPQ and PTB

At the time when the characterization of the fiber links between MPQ and PTB began only a hand full of links of up to 480 km had been investigated [8, 9, 119, 120]. Most of
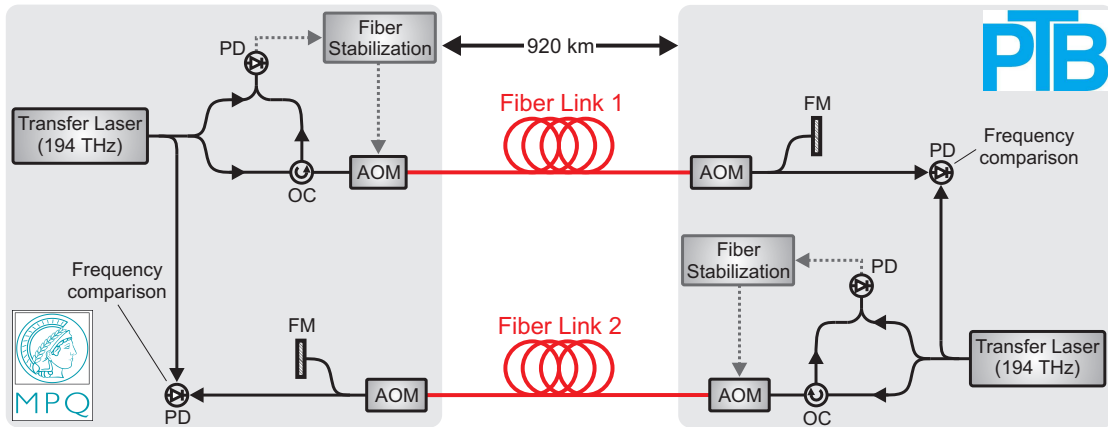
FIGURE 4.10: Experimental setup for the characterization of the two 920 km fiber links. The light of a transfer laser at MPQ is sent through one of the fibers to PTB. Simultaneously, light from a transfer laser at PTB is sent to MPQ via the second fiber. Comparisons between the transferred frequency and the local frequency are performed at both sites. AOM: acousto-optic modulator, PD: photo diode, OC: optical circulator, FM: Faraday mirror

those fiber links were set up in a loop configuration where sender and receiver are located in the same laboratory to conveniently characterize the frequency transfer. In contrast to that, the fiber links between MPQ and PTB are used to transfer a frequency from one local to a remote site as is the case, for example, for a comparison of two distant clocks. The experiments discussed in this chapter are performed by using the passively isolated interferometer of Section 4.2.2.1.

### 4.3.1 Transmission scheme

In order to characterize the frequency transfer between MPQ and PTB, two largely identical but independent setups are constructed which are schematically shown in Figure 4.10. The light of a transfer laser at MPQ is sent to PTB through one of the fibers. The stabilization of the transfer is done at the sender side, i.e. at MPQ, as described in Section 3.4.6. Simultaneously, the light of another transfer laser at PTB is sent to MPQ via the second fiber. In this anti-parallel configuration, comparisons between the local and the transferred frequency are performed at both sites. Due to the redundant setup and the simultaneous transfer, noise, for example from the transfer lasers, that is present in both systems is common mode and drops out in the difference between the two comparisons.

In contrast to cascading multiple fiber links where each section is stabilized individually [120], each 920 km link is stabilized in a single span. This approach yields a simpler setup, as no intermediate repeaters or stable lasers have to be installed and operated along the link. The critical hardware for the stabilization is located at the sender site of the link, which makes it easier to maintain. As discussed in Section 3.4.6, those advantages come at the cost of a severely reduced control bandwidth for the fiber-induced noise suppression, due to the propagation delay of the light in the fibers. In the case of the 920 km links the round-trip time for the signal is close to 9 ms, limiting the
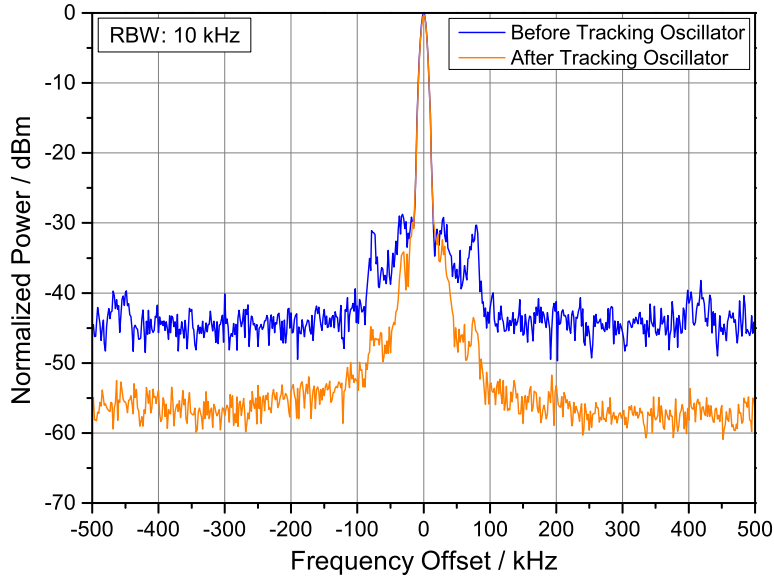
FIGURE 4.11: Heterodyne beat signal between the sent and the round-trip light of the 920 km fiber link. This signal is used for the stabilization of the fiber link transfer. A tracking oscillator clears the noisy signal and removes amplitude fluctuations that the signal is subject to. The sidebands around 31 kHz and 77 kHz, respectively, are of unknown origin.

control bandwidth to $\approx 55$ Hz. Noise components arising at higher frequencies cannot be compensated by the stabilization system and remain in the transferred signal.

As an example, the beat note used for the fiber stabilization of the 920 km link is shown in Figure 4.11 before and after the tracking oscillator. The signal-to-noise ratio of more than 40 dB in a 10 kHz resolution bandwidth is sufficient for achieving a stable phase lock over timescales of hours.

The two fibers are running in parallel in the same cable duct. Previous experiments revealed very similar noise characteristics of the two fibers [113]. The two identical setups allow for a widely redundant investigation of the link systematics.

## 4.3.2   Free-running fiber link

A low inherent fiber noise is important in particular for long-haul fiber links that suffer from a strongly reduced control bandwidth for the noise cancellation due to the propagation delay of the light in the fiber (see Section 3.4.6). The fiber links investigated in this work are mostly installed in a well isolated environment at least one meter below the surface of the earth due to which both thermal as well as acoustic noise are suppressed to a large extent. The link, however, also passes through three computing centers in Garching, Erlangen and Leipzig in a poorly controlled and noisy environment. Even though the fiber noise detection does not allow for a spatial localization of the noise sources, it seems reasonable to believe that most of the fiber induced noise originates from those computing centers. Nevertheless, the passive isolation of the fibers still allows
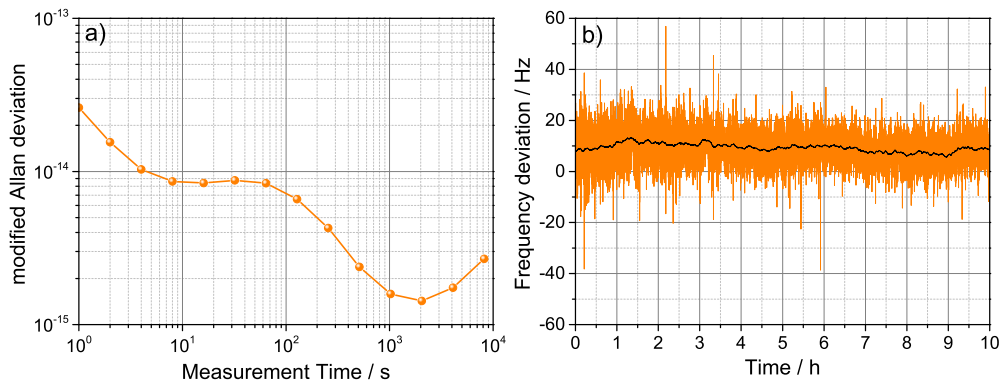
FIGURE 4.12: a) Frequency instability of one of the free-running 920 km fiber links. b) Corresponding time series measured with a Λ-type frequency counter with a gate time of 1 s. A fiber induced frequency shift of $\approx$ 10 Hz is clearly visible.

for short-term instabilities of a few parts in $10^{14}$ at 1 s (see Figure 4.12). Residual fiber noise, however, leads to a flicker floor of $> 10^{-15}$ on long time scales.

The frequency instability shown in Figure 4.12 has been observed several times during the course of this work with little variation. A direct correlation between the instability and the weather or the season could, however, not be performed due to the lack of precise weather data along the link. In the right plot in Figure 4.12 a time series of the round-trip signal of the free-running fiber link is shown. The fiber link causes a frequency shift of about +10 Hz compared to the injected frequency which again is a very typical value. The sign of this shift has been found to change occasionally so that this shift is probably caused by slow temperature variations along the link. The observed values are in good agreement with the estimations discussed in Section 3.4.5.

### 4.3.3 Desynchronization of remote frequency counters

The transfer lasers exhibit a slow frequency drift that results from imperfect temperature stabilization and/or from the aging of the reference cavity spacer material that the lasers are locked to (see Section 3.4.2). The typical drift rate of the lasers are on the order of 50 to 100 mHz/s even for perfect temperature control. For the laser at PTB, however, drift rates as high as 300 mHz/s are observed as well due to a malfunction of the temperature stabilization.

The experiments discussed here require the measurement of this drifting frequency at two different locations (MPQ and PTB) simultaneously. Every frequency counter has a measurement window that defines when a measurement begins and when it ends. Even if the frequency counters are set to the same measurement duration, i.e. gate time $\tau = 1$ s, the measurement windows can still show an offset in time with respect to each other if no means of synchronization between the counters is applied. The maximum timing offset $\Delta t$ is half the gate time which in this case is 0.5 s. As a result of a possible timing offset, the frequency counters count a slightly different frequency as the signal drifts
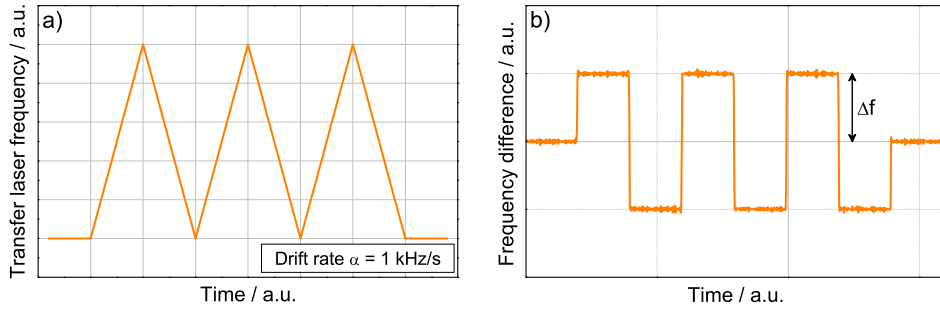
FIGURE 4.13: Determination of the timing offset between two remote frequency counters. a) Strong but well defined artificially induced laser drift that is measured with both counters at MPQ and PTB. b) Any timing offset between the two counters results in a difference between the two counted frequencies that can be used to determine the timing offset of the counters.

during the time $\Delta t$. For a signal with drift rate $\alpha$, the difference of the two counted frequencies is

$$\Delta f = \alpha \cdot \Delta t. \tag{4.2}$$

To avoid this problem, the measurement windows of the counters need to be synchronized. During the course of this work, we first used counters which did not provide the ability to synchronize them. Those counters were upgraded at a later time to provide the synchronization option. All experiments discussed in this chapter are performed using unsynchronized counters (K + K Messtechnik GmbH, Models FXM and FXE [26]). To still be able to perform the measurements needed for the characterization of the fiber link, the timing offset $\Delta t$ has to be determined. This is achieved by applying a strong artificial but well known frequency modulation with rate $\alpha$ to one of the transfer laser signals. This triangular modulation is shown in Figure 4.13 a). In accordance to Equation 4.2 the timing offset can be determined by measuring the resulting frequency shift $\Delta f$ (see Figure 4.13 b).

The accuracy of the timing offset determination is estimated to be 0.1 ms for the experiments discussed here. The knowledge about the timing offset allows us to correct the data subsequently after the drift rate of the transfer lasers has been determined. The drift rate is measured for every single data point so that a specific correction term is attributed to every point. Without this correction, a drift rate of 100 mHz/s and an observed timing offset of 0.25 s causes a systematic frequency shift of about $1 \times 10^{-16}$. The correction decreases the effect of the timing offset so that any contribution from it should be smaller than $1 \times 10^{-19}$. The effect of the timing offset correction can be seen in Figure 4.14. The upper graph shows the frequency difference between the two transfer lasers from which the drift rate is determined. In the lower graph the transferred frequency between MPQ and PTB are binned into 1000 s long intervals. The orange diamonds indicate the transferred frequency without the timing offset correction. A correlation between the drift rate, i.e. the slope of the graph in Figure 4.14 a), and the
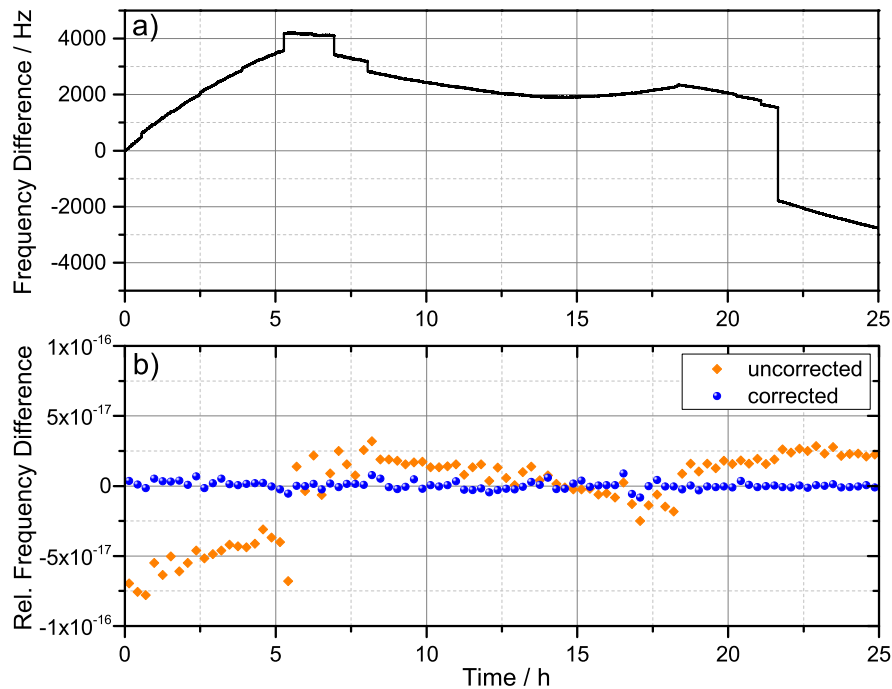
FIGURE 4.14: Effect of the frequency counter timing offset correction. a) Frequency difference between the two drifting transfer lasers to determine the current drift rate. Steps are due to missing data points. b) Relative frequency difference of the transferred frequencies before and after correction. Data has been binned to 1000 s intervals.

shift in the transferred frequency can clearly be seen. The blue points in the lower graph show the transferred frequency after the correction for the timing offset is applied.

The timing offset remains constant as long as the frequency counters are connected to power. However, power outages throughout the measurements caused significant variations of the timing offset. As a result, the timing offset is determined at the beginning of each measurement.

Alternatively to the determination of the timing offset $\Delta t$, Equation 4.2 suggests to cancel the drift rate $\alpha$ of the transfer lasers. This can be achieved with the help of an AOM behind the cavity stabilized transfer laser. We use a software PI control loop to effectively cancel the drift of this laser (see Appendix A). As a result, the long term stability of the transfer laser could be improved significantly and a fractional frequency instability of below $2 \times 10^{-14}$ is achieved for averaging times of up to $10^4$ s. A similar locking scheme is developed at PTB where a slave laser is stabilized to a cavity stabilized master laser and a hydrogen maser [121]. This way, the short term stability of the master laser is combined with the long term stability of the hydrogen maser. The achieved frequency instability is below $5 \times 10^{-15}$ for averaging times of up to $10^4$s. Although with both approaches the transfer laser drift is effectively canceled to a large extent, the determination of the timing offset proved to be simpler and allowed us to use the data that had already been taken before the realization of the drift cancellation systems. Consequently, all experiments described here are performed with drifting transfer lasers.

| Criterium | Threshold |
|---|---|
| Difference of redundantly counted $f_{Beat,F1}$ at PTB | $< 0.2$ Hz |
| Difference of redundantly counted $f_{Beat,F2}$ at MPQ | $< 0.2$ Hz |
| Difference of both $f_{Beat,F1}$ and its nominal frequency at PTB | $< 1$ Hz |
| Difference of both $f_{Beat,F2}$ and its nominal frequency at MPQ | $< 1$ Hz |

TABLE 4.1: Validation criteria for the 920 km fiber link to identify loss of phase coherent events. All data points that exceed at least one of the threshold values are discarded.

### 4.3.4  Data acquisition and validation criteria

The characterization of the frequency transfer via the fiber links is done by comparing the sent and the transmitted frequency. For that, a heterodyne beat at PTB is generated between the transferred light from MPQ and the local laser at PTB. In the same way, a heterodyne beat at MPQ is generated between the transferred light from PTB and the local laser at MPQ (see Figure 4.10). The difference between those signals reveals the performance of the two 920 km fiber links. This approach is equivalent to creating a virtual loop in which the laser frequencies cancel while the noise of the two fiber links adds up. At both sites, PTB and MPQ, Π- as well as Λ-type frequency counters are used simultaneously to record the beat frequencies.

At the targeted level of accuracy redundant counting is required in order to detect loss of phase coherence events (cycle-slips) and to prevent them from entering the data analysis [122]. A reliable cycle-slip detection is absolutely crucial for the characterization of the fiber link frequency transfer as most of the applied analysis techniques rely on the phase coherence of the signals. In a previous study [113] it had been found that only Λ-type frequency counters are able to identify cycle-slips on the required level of confidence. As discussed in Section 2.2.3.2, Λ-type frequency counters perform an averaging of the countered frequency that leads to a strong suppression of white phase noise which in turn allows for the detection of cycle-slips. Hence, Λ-counters are able to uncover cycle-slips that are hidden in data obtained with non-averaging Π-type counters. Each of the signals used for the cycle-slip detection are counted twice at MPQ and twice at PTB. Table 4.1 lists the validation criteria for a frequency counter gate time of 1 s that are used to separate valid from invalid data points. The beat note, $f_{Beat}$, that is generated by heterodyning the sent light and the round-trip light and which is used for the fiber link stabilization is redundantly counted at PTB for fiber $F1$ and at MPQ for fiber $F2$. $f_{Beat,F1}$ and $f_{Beat,F2}$ both have certain nominal frequencies that are given by the AOM frequencies in the link path (see Figure 4.10). When the link stabilization is active and working properly the two beat frequencies should be identical to their nominal frequencies within some uncertainty. A greater deviation of the beat frequencies from their nominal values indicates a malfunction of the fiber link stabilization.

The criteria are chosen so that a slight variation of them does not affect the result of whether a data point is considered to be valid or invalid significantly. All data points that pass these criteria are treated as valid and make it to the subsequent data analysis. The rate with which cycle-slips occur can be kept below 0.01% under optimized conditions,
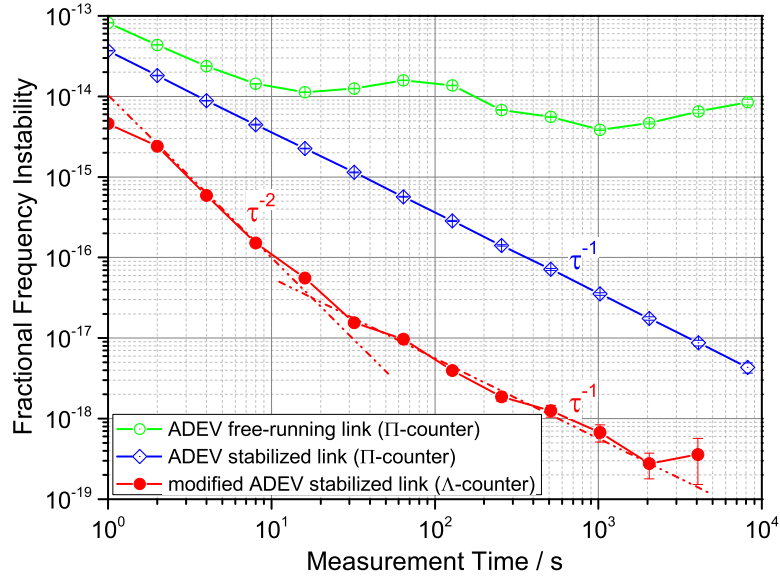
FIGURE 4.15: Fractional frequency instability of the free-running 920 km fiber link (open circles) and the stabilized fiber link (diamonds) derived from a non-averaging ($\Pi$-type) frequency counter expressed as the ADEV. To distinguish between white phase, flicker phase and other noise types, averaging (overlapping $\Lambda$-type) frequency counters are used from which the modADEV is derived (filled circles).

resulting in only a few invalid data points per day. Continuous tracking of the signal phase over several hours is demonstrated in the 920 km fiber link system. The cycle-slip rate is strongly correlated with the signal-to-noise ratio of the heterodyne beat signals (see Figure 4.11). Occasional variations of the polarization state of the light emitted by the transfer lasers cause the signal-to-noise ratio to drop significantly below 20 dB so that a reliable tracking and counting is not possible anymore. In this case a manual readjustment of the polarization state is required in order to recover the signal-to-noise ratio of the beat signals.

### 4.3.5 Results

The recorded data streams of the two transferred frequencies at MPQ and PTB first have to be temporally overlapped. For this, we synchronize the time of the computers that are used for the data recording to the same time server. A time stamp that is written in the data files helps to synchronize the data from MPQ and PTB. Additionally, we purposefully cause a number of easy-to-recognize spikes in the data at the beginning of each measurement. These spikes are used for the synchronization so that we do not have to rely on the accuracy of the computer time. After the synchronization, the measured transferred frequencies are subtracted. From the resulting signal we calculate the instability of the transferred frequency which is shown in Figure 4.15. The instability of the stabilized 920 km link expressed as the Allan deviation (ADEV) is obtained from data recorded with a $\Pi$-type counter and results to $3.8 \times 10^{-14}$ in 1 s. The slope of this curve is proportional to $\tau^{-1}$ as expected for a phase-locked signal that is dominated by white or flicker phase noise (see Section 2.2.1).

Unfortunately, the 35,000 s long data set used for the calculation of the ADEV does not allow us to state the instability floor of the fiber link as an instability of only $4 \times 10^{-18}$ is reached after $10^4$ s. To take advantage of the strong noise suppression and to distinguish between white and flicker phase noise, we use data from a $\Lambda$-type counter to calculate the modified Allan deviation (modADEV). The residual frequency instability is $5 \times 10^{-15}$ in 1 s and averages as $\approx \tau^{-3/2}$ until 30 s after which the slope flattens to be proportional to $\tau^{-1}$. The instability of today's best optical clocks is surpassed after $\approx 20$ s [17] and an instability of below $1 \times 10^{-18}$ is reached after only $\approx 700$ s. This means, that in a remote comparison of two distant optical clocks, the noise of the fiber link itself becomes negligible within seconds. The instability floor of the whole frequency transfer system seems to be at about $3 \times 10^{-19}$.

The dependency of the modADEV from the measurement time is expected to be proportional to $\tau^{-2}$ as will be discussed in detail in Chapter 5. We attribute the deviation from the $\tau^{-2}$ slope to noise that is added by the correction process for the frequency counter timing offset (see Section 4.3.3). The long term behavior including the noise floor can be explained by an insufficient isolation of the interferometer at MPQ used for the Doppler noise cancellation (see Section 4.2.2.1).

The instability analysis described above does not reveal potential systematic shifts of the transmitted frequency that could be introduced through fiber noise during the link transfer. In addition to the frequency instability, the accuracy of the transmitted signal has to be verified. This is done by comparing the transferred frequency with the sent frequency over a total period of three days. The result of this comparison is shown in Figure 4.16 where we measure the frequency with $\Lambda$-type counters set to a gate time of 1 s (orange data points, left axis). The gaps are due to cycle-slips as, for instance, the
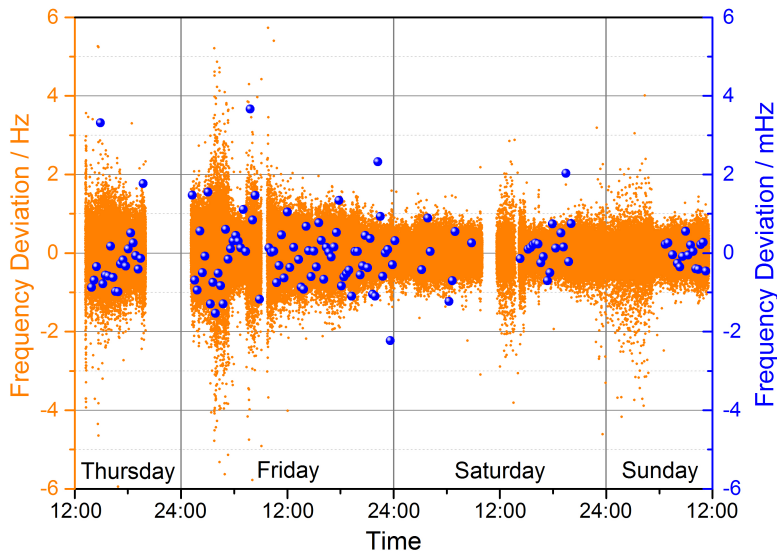


FIGURE 4.16: Comparison between the sent and the transmitted frequency over the 920 km fiber link measured with a $\Lambda$-type frequency counter set to a gate time of 1 s (orange data points, left axis). Phase coherent intervals are binned into 1000 s long sequences by applying an unweighted average (blue data points, right axis, enlarged scale).

fiber link stabilization did not work properly. Regions of higher noise can be linked to poor signal-to-noise ratios of one of the heterodyne beat notes. The normal distribution of the data suggests that we apply common statistics which leads to an arithmetic mean of $(-0.4 \pm 2.5) \times 10^{-18}$. It can be seen that the mean frequency is purely statistically limited [11].

If a frequency signal is dominated by white phase noise and coherently measured over a certain period of time, the uncertainty with which the mean frequency of this signal can be determined decreases with the number of data points $N$ [123] rather than with $\sqrt{N}$ as is the case for other noise types or incoherent signals. To take advantage of this fact, we binned all phase coherent data subsets with a length of 1000 s by applying a non-weighted average which is equal to calculating the arithmetic mean. The resulting 135 data points are shown in Figure 4.16 as blue dots, right axis. The bin size of 1000 s was chosen as the best tradeoff between the total number of resulting data points and reduced statistical uncertainty. We again use common statistics for the 1000 s data points and determine an arithmetic mean of $(-0.7 \pm 3.7) \times 10^{-19}$.

These results demonstrate that a 194 THz carrier can be transferred via a 920 km fiber link with an instability and an accuracy of $\approx 4 \times 10^{-19}$. Comparing this number with the performance of the most stable and accurate optical clocks to date (Section 2.4) reveals that the fiber link frequency transfer performance exceeds the requirements by about one order of magnitude. These measurements were conducted in 2011 and the results were published in *Science* [11] and partially discussed in a preceding PhD thesis [113].

## 4.4 An 1840 km looped optical fiber link

The anti-parallel configuration of the two 920 km fiber links discussed in the previous chapter clearly demonstrate the high performance achievable when transferring a frequency from one location to a remote site. Even though this anti-parallel configuration represents the more realistic case of a remote clock comparison, it is more typical to characterize a fiber link when it is set up in a loop configuration. The beauty of a loop configuration is that sender and receiver are located in the same laboratory. This simplifies the characterization as all measurements can be performed at one single location. Consequently, there is no need to synchronize remote frequency counters (Section 4.3.3) and potential systematic effects due to any residual timing offsets simply disappear. On the other hand, however, common mode noise such as, for example, the drift of the transfer laser is rejected in a loop configuration which is not the case if a frequency is transferred between different locations.

The research on optical frequency standards is promoted in an increasing number of precision metrology institutes and a long term goal of the optical metrology community is to connect all of the major precision measurement laboratories across Europe by fiber links. Within Europe, the average distance that those laboratories are separated by is $\approx 1000$ km. Some sites, however, are located up to 2500 km apart from each other. To
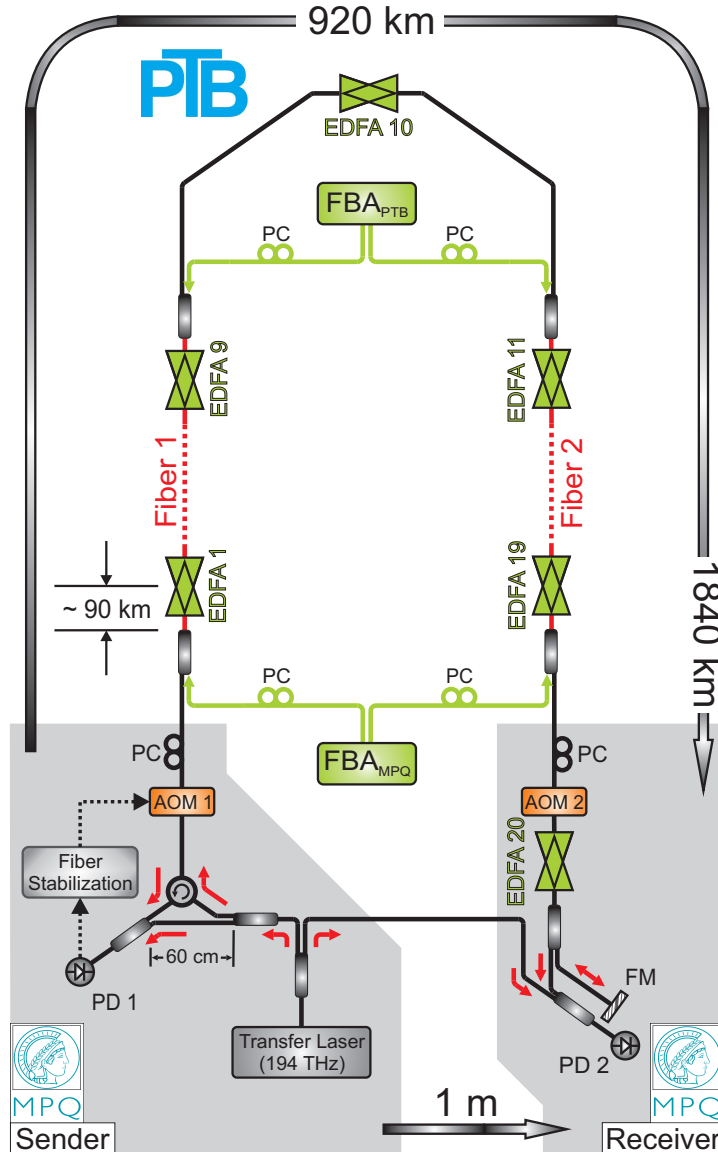
FIGURE 4.17: Schematic of the optical fiber link. The light of a cw transfer laser is launched into one of the fibers at MPQ. After an 1840 km loop the light arrives back at MPQ where a fraction of it is retro-reflected. The round-trip light is used to derive an error signal for the fiber stabilization with AOM 1 as the actuator. EDFA: erbium-doped fiber amplifier, FBA: fiber Brillouin amplifier, AOM: acousto-optic modulator, PC: polarization controller, FM: Faraday mirror, PD: photo diode.

connect even those remote laboratories, stable and accurate frequency transfer over such long distances has to be achieved.

## 4.4.1  Transmission scheme

The two 920 km fiber links that connect MPQ and PTB are combined to form an 1840 km fiber link. The experimental setup is sketched in Figure 4.17. We connect the two fiber ends at PTB, so that sender and receiver are located in the same laboratory at MPQ. The whole link includes 20 fiber amplifiers (EDFA) at eleven different locations

| Criterium | Threshold |
|---|---|
| Difference of redundantly counted $f_{Beat}$ at MPQ | $< 0.2$ Hz |
| Difference of both $f_{Beat}$ and its nominal frequency at MPQ | $< 5$ Hz |

TABLE 4.2: Validation criteria for the 1840 km fiber link to identify loss of phase coherent events. All data points that exceeded at least one of the threshold values are discarded.

and two fiber Brillouin amplifiers (FBA) to compensate for more than 420 dB of optical attenuation introduced by the fibers. The fiber link stabilization is done in an analogous manner to the 920 km fiber links by reflecting a portion of the transferred light at the fiber exit back to the sender. When the retro-reflected light eventually reaches its origin it has been amplified 40 times by EDFAs and four times by FBAs. We determine the link performance by characterizing an RF beat signal that contains the relevant out-of-loop information. It is generated by heterodyning the non-reflected portion of the transferred light and the sent light (PD 2 in Figure 4.17).

In analogy to the 920 km links, we stabilize the 1840 km link in a single span. The propagation delay of the round-trip light is about 18 ms, limiting the bandwidth of the fiber stabilization control loop to $\approx 27$ Hz. Due to the increased link length, fiber-induced Doppler shifts of up to 20 Hz are frequently observed (see Figure 4.12). In this experiment, we use the redesigned actively temperature stabilized interferometer (see Section 4.2.2.2) to avoid the limitation of the previously used interferometer.

We adopt the validation criteria introduced in Section 4.3.4 for the 920 km links to the higher noise level in this longer link. As no data are taken at PTB and the two 920 km links are connected to form one single 1840 km link, the cycle-slip detection simplifies to the criteria listed in Table 4.2. These values are given for a gate time of 1 s using a $\Lambda$-type frequency counter. We are able to keep the cycle-slip rate below 0.1% on average.

### 4.4.2 Results

The beat note generated by heterodyning the transferred light after the 1840 km fiber link with the sent light on PD 2 in Figure 4.17 is counted with a $\Pi$- and with a $\Lambda$-type frequency counter simultaneously. In contrast to previous measurements where the characterization was mainly focused on the long term performance, here we analyze the short term instability as well by counting the beat frequency with a gate time of 1 ms. Additionally, we perform phase noise measurements of the transferred frequency allowing for an extended noise analysis.

Figure 4.18 shows the frequency instability achieved for the transferred frequency after the 1840 km fiber link. As expected, the instability of the free-running link is about a factor of two higher compared to the free-running 920 km link, indicating that the inherent fiber noise rises linear with fiber link length. When the link transfer is stabilized the frequency instability increases up to an averaging time of $\approx 20$ ms as the signal is subject to phase noise, that cannot be compensated for by the fiber stabilization
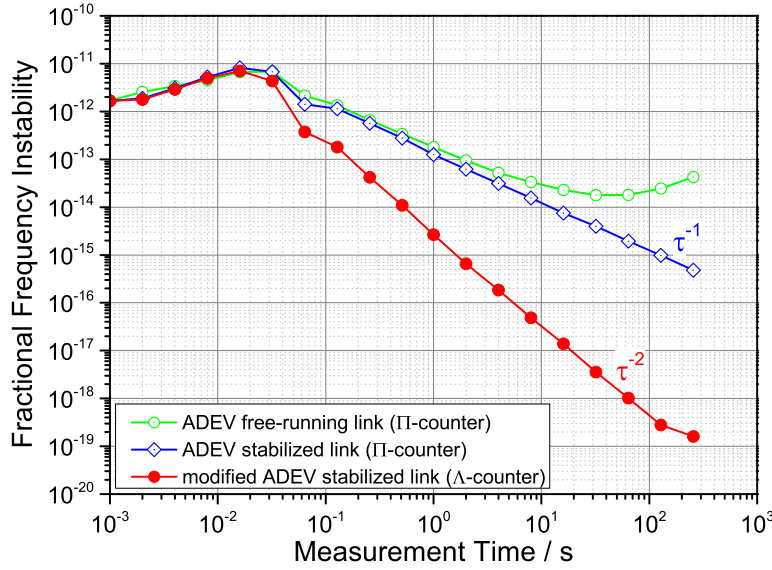
FIGURE 4.18: Fractional frequency instability of the 1840 km free-running fiber link (open circles) and the stabilized link (open squares) derived from a non-averaging Π-type frequency counter and expressed as the ADEV. Averaging Λ-type frequency counters are used to derive the instability expressed as the modADEV (filled circles). The transferred frequency is subject to phase noise at measurement times of up to 20 ms that cannot be compensated for by the noise cancellation control loop due to the propagation delay of the signal in the fiber.

control loop due to the large propagation delay in the fiber. When we measure the transferred frequency with a non-averaging Π-type frequency counter, we calculate the ADEV and observe an instability of $1.3 \times 10^{-13}$ in 1 s. The instability averages down as $\tau^{-1}$, as expected for a signal that is dominated by white or flicker phase noise (see Section 2.2.1). Additionally, we use Λ-type counters to calculate the instability of the transferred frequency expressed as the modADEV. The residual instability is $2.7 \times 10^{-15}$ in 1 s and it averages down as $\tau^{-2}$. The reason for this fast averaging lies in the spectral noise distribution of the fiber link and will be discussed in detail in Chapter 5.

After 100 s, the instability reaches $4 \times 10^{-19}$, which surpasses the requirements for an optical clock comparison today by about one order of magnitude [17]. The length of coherent data does not allow us to measure a clear flicker floor. However, to estimate the level at which a flicker floor might be present, we take three possible contributions into account: (1) undetected cycle slips, (2) the noise of the transfer laser, and (3) the noise floor of the interferometer. The latter one is determined to be slightly below $1 \times 10^{-20}$ (Figure 4.7). The estimated contributions of the transfer laser reveals an upper limits of about $1 \times 10^{-20}$ with the setup used in this experiment. The estimation of the influence of undetected cycle-slips is difficult but may be as high as several parts in $10^{20}$.

In analogy to the characterization of the 920 km link, the accuracy of the frequency transfer for the 1840 km link needs to be verified independently as the instability analysis described above does not reveal possible systematic shifts. We measure the transferred frequency with a Λ-type frequency counter set to a gate time of 1 s over the period of three days. A comparison with the sent frequency is shown in Figure 4.19 as orange
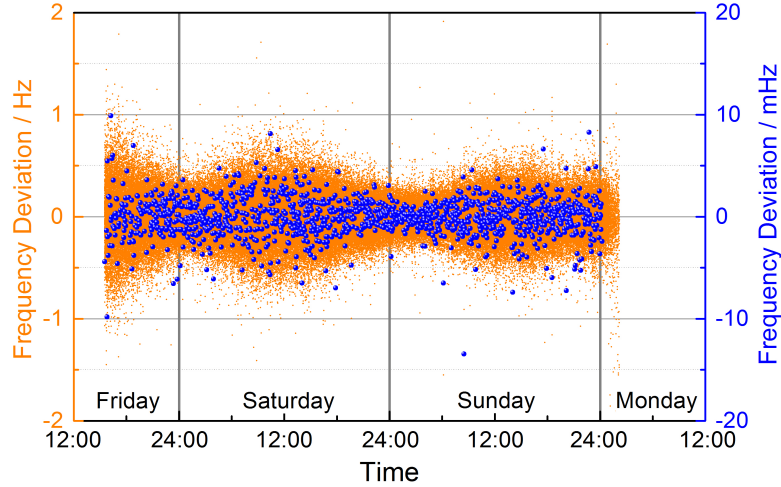
FIGURE 4.19: Three-day frequency comparison between sent and transferred frequency after the 1840 km fiber link. Data are taken with a $\Lambda$-type frequency counter with a gate time of 1 s (orange data points, left axis). The arithmetic means of all cycle-slip free 100 s intervals are computed (blue dots, right axis, enlarged scale).

data points, left axis. Human activity causes a slight time dependence of the fiber link performance. It can nicely be seen that the transferred frequency experiences higher noise during the day and less noise in the night. The statistically limited arithmetic mean of the 1 s data points is calculated to $(-1.4 \pm 2.5) \times 10^{-18}$.

To take advantage of the fast averaging for white phase noise dominated signals [123], we bin all phase coherent data subsets with a length of 100 s by applying a non-weighted average ($\Pi$-type evaluation). The resulting 1367 data points are shown in Figure 4.19 as blue dots, right axis. The bin size is reduced in comparison to the 920 km fiber link analysis due to the higher cycle-slip rate which limits the length of phase coherent data sets. The standard deviation of the 100 s data points is $1 \times 10^{-17}$ which is a factor of 100 smaller than the modADEV at $\tau = 1$ s as expected for this $\Pi$-type evaluation. We determine the arithmetic mean of all 100 s data points to $(-0.1 \pm 2.6) \times 10^{-19}$. In absolute values, these results demonstrate that a 194 THz carrier can be transmitted over 1840 km of fiber with an uncertainty of 50 $\mu$Hz.

Complementary to the time-domain approach, a widespread frequency domain characterization of phase instability is the power spectral density (PSD) of phase fluctuations $S_\phi(f) = |\tilde{\phi}(2\pi f)|^2$ with the Fourier transform normalized to the measurement time of the phase $\phi(t)$ between the sent and transferred optical waves. We measure the phase noise by feeding the heterodyne beat at the exit of the fiber link (PD 2 in Figure 4.17) together with a stable frequency reference in a phase detector. The voltage fluctuations at the phase detector output are then measured with an FFT-analyzer to obtain the phase fluctuations $S_\phi(f)$. We determine the phase noise PSD for the stabilized fiber link and for the free-running link where no noise cancellation is applied (see Figure 4.20). The free-running link features a distinct broad maximum around 15 Hz which has been observed on other links as well [9, 119], above which the noise rolls off quickly. This maximum is attributed to building and ground vibrations which was also found by [124]. The Doppler cancellation system suppresses the noise within its control bandwidth, i.e.
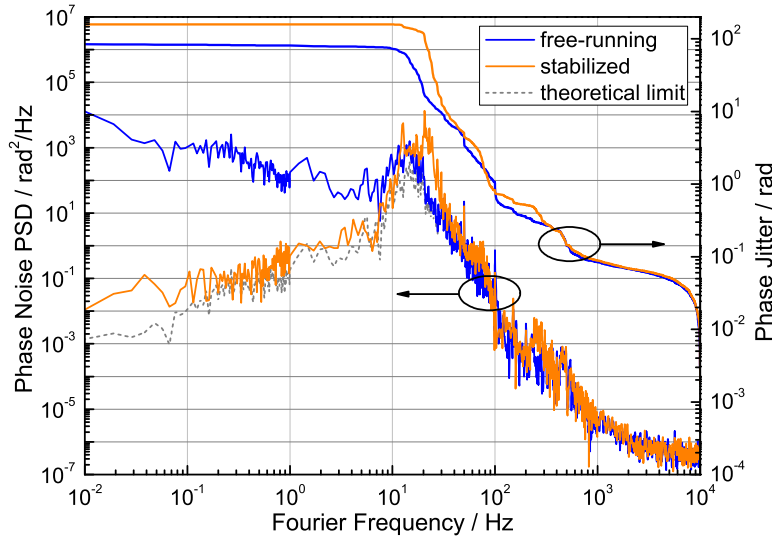
FIGURE 4.20: Phase noise power spectral density $S_\phi(f)$ of the free-running (blue line) and the stabilized (orange line) 1840 km link. The servo bump around 27 Hz is in agreement with the bandwidth limit due to the propagation delay. Also shown is the Doppler noise suppression limit [8] (dashed gray line). The phase jitter is calculated by integration of the PSD from high to low frequencies.

below 27 Hz. From Figure 4.20 it can be seen that the measured noise suppression is close to the theoretical limit for delay-limited noise suppression, derived in [8]. With the Doppler cancellation system active the noise increases with Fourier frequency up to $f \approx 20$ Hz. The integration of the phase noise data reveals the ADEV and modADEV in accordance to Equation 2.10 and Equation 2.11 as will be discussed in Section 4.4.3. The total integrated phase jitter is about 80 rad and 160 rad for the free-running and the stabilized link, respectively. The noise of the stabilized link is higher due to the effect of the servo bump which degrades the short term stability of the transferred frequency. Despite these large phase fluctuations, continuous tracking and counting of the phase is accomplished by using prescalers, tracking oscillators and digital phase detectors as discussed in Section 4.2.3. The standard PI controller used for the fiber stabilization is not optimized for the large signal delay of $\approx 18$ ms. A specially designed loop filter [125] could reduce the influence of the servo bump and thus decrease the overall phase noise of the stabilized link. First experiments with an all-digital control loop that is optimized for the properties of our fiber links reveal promising results. The experiments discussed in this section were conducted in 2012 and the results were published in *Physical Review Letters* [13].

### 4.4.3   Instability of the 1840 km fiber link from phase noise

According to Equation 2.10 and Equation 2.11, there is an integral relation between the measured phase noise PSD and the frequency instability. As a verification that the calculated instability (modADEV) of the stabilized 1840 km link which exhibits the $\tau^{-2}$ dependency does indeed represent the correct properties of the transferred frequency, the instability can be calculated from the phase noise data shown in Figure 4.20. We
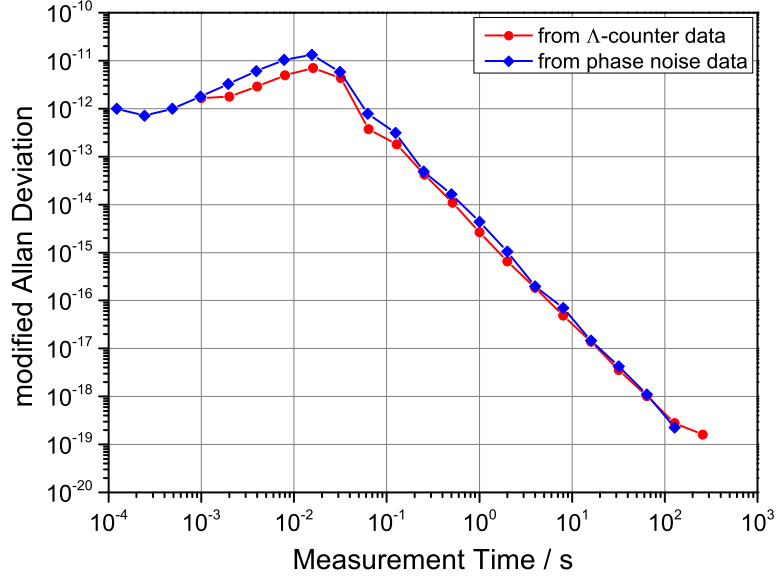
FIGURE 4.21: Fractional frequency instability of the 1840 km fiber link calculated from frequency counter data (red dots) and from phase noise data (blue diamonds). An identical result is obtained despite the use of completely independent measurement devices and techniques.

use Equation 2.11 together with Equation 2.8 to reveal the modADEV. The result is compared with the modADEV calculated from the frequency counter data and shown in Figure 4.21. It can nicely be seen that both of these completely independent methods lead to the same result. The slight variations between the curves can simply be explained by performance variations of the fiber link transfer during the day (see Figure 4.19) as these measurements were performed at different times.

### 4.4.4 Frequency instability scaling law

During the past years, a number of different fiber links have been investigated in our collaboration. According to [106], the (short term) fractional frequency instability $\sigma_y$ of the transferred frequency $\nu_0$ can be expressed as

$$\sigma_y \approx \nu_0^{-1} \sqrt{\frac{8}{3} h} \ \tau_{delay} \ \tau^{-3/2} \tag{4.3}$$

where $h$ defines the magnitude of the fiber noise, $\tau_{delay}$ the one-way propagation time and $\tau$ the frequency counter gate time. Under the assumption of spatially uniform noise distribution, $h$ and $\tau_{delay}$ are both proportional to the fiber link length $L$. As a result, the instability of the transferred frequency $\sigma_y$ scales with $L^{3/2}$.

The first fiber link characterized in our collaboration consisted of a fiber loop from PTB to the University of Hanover and back to PTB with a total length of 146 km [119]. A fractional frequency instability of the transferred frequency of $3 \times 10^{-15}$ in 1 s was achieved. By taking this result as a reference to calculate the value of $h$, Equation 4.3
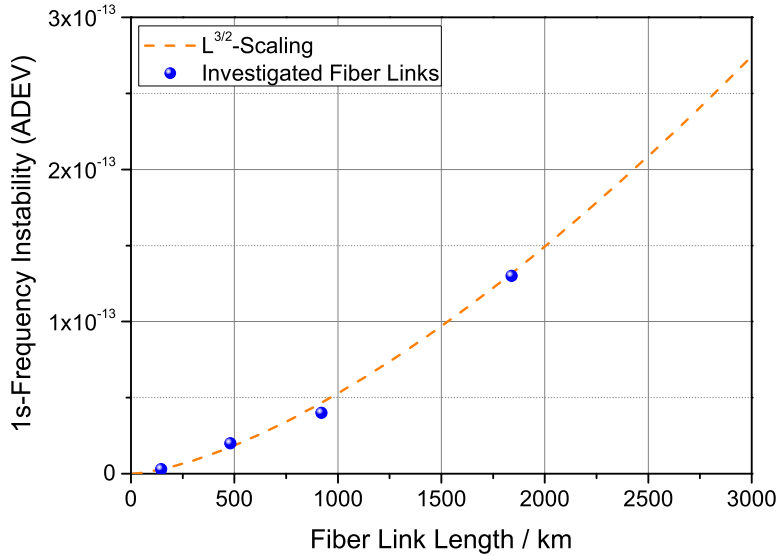
FIGURE 4.22: 1-s frequency instability derived from data measured with a Π-type frequency counter and expressed as the ADEV for fiber links that have been investigated in our group [9, 11, 13, 119]. The achievable instability scales with the fiber link length as $L^{3/2}$ as expected from [106].

allows us to predict the achievable frequency instability for longer fiber links if a single-span stabilization is used. This prediction is shown as a dashed line in Figure 4.22. For a 480 km link, the predicted 1-s frequency instability is $\approx 1 \times 10^{-14}$ and the actually achieved instability is $2 \times 10^{-14}$ [9]. The achieved instability in the 920 km link is $3.8 \times 10^{-14}$ [11] (prediction: $4.6 \times 10^{-14}$) and in the 1840 km link the achieved instability is $1.3 \times 10^{-13}$ [13] (prediction: $1.3 \times 10^{-13}$).

The $L^{3/2}$ scaling technically only holds under the assumption, that the fiber-induced noise is distributed equally over the entire fiber length and that the total noise scales linearly with increasing link length. The results demonstrate that the scaling is still valid for link lengths of up to $\approx 2000$ km even though entirely different fiber links were investigated. Figure 4.22 also illustrates the evolution of achievable frequency instabilities for longer fiber links. As it can be seen, even with a fiber link that would span all across Europe highly stable frequency transfer could still be achieved, provided that the fiber noise is on the same order of magnitude compared to the links investigated in this work.

## 4.5   Discussion

The long-haul fiber links that are characterized in detail here all show superior performances which are many orders of magnitude better compared to alternative techniques (see Section 3.3). A fractional frequency instability of $5 \times 10^{-15}$ in 1 s (modADEV) is achieved after transferring an optical frequency over two 920 km fiber links that are set up in an anti-parallel configuration. The instability averages to less than $10^{-18}$ after

FIGURE 4.23: Fractional frequency instability of well established satellite based frequency dissemination techniques in comparison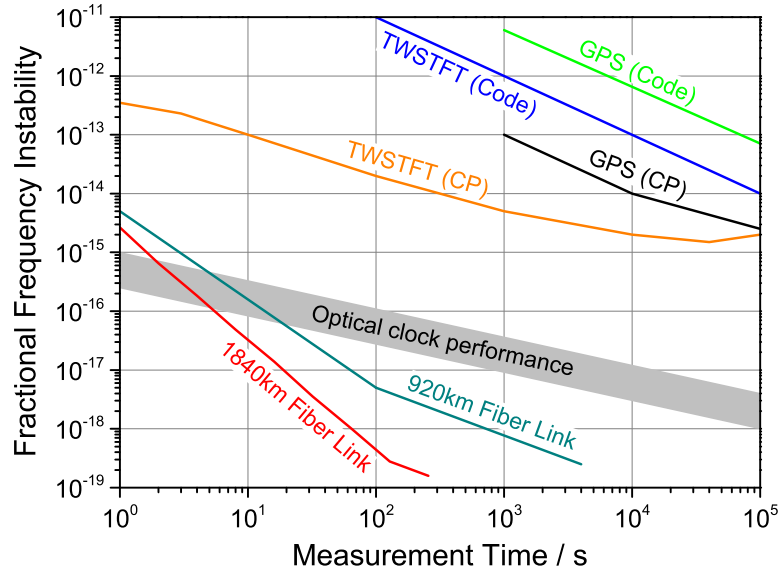 with the results obtained for the fiber link frequency transfer analyzed in this work. The instability contribution of the fiber link becomes negligible in an optical clock comparison within seconds.

$\approx 700$ s. The accuracy of the transferred frequency is determined to have an uncertainty of below $4 \times 10^{-19}$ after the 920 km link.

An improved setup and a simpler measurement scheme in which no frequency counters had to be synchronized allows us to improve the aforementioned results even though the fiber link length is increased by a factor of two. A fractional frequency instability of $3 \times 10^{-15}$ in 1 s (modADEV) can be demonstrated after transferring an optical frequency over an 1840 km fiber link. Here, an instability of below $10^{-18}$ is reached in only $\approx 70$ s of averaging. Any deviation between the sent and transferred frequency can be constrained to less than $3 \times 10^{-19}$. Obviously, a looped fiber link does not represent a realistic case when two remote frequency standards are supposed to be compared. In such a setup, common-mode noise in the laboratory is suppressed to a large degree which would not be the case for two remote laboratories. However, as the fiber-induced noise scales as expected, the achieved frequency instability level is still realistic even if the fiber link would stretch out over a geographical distance of 1840 km.

At the level of performance demonstrated here, a reliable cycle-slip detection is absolutely crucial. Finding the appropriate validation criteria requires some knowledge about the signals and the fine adjustment of the criteria might involve some trial-and-error as no strict rules for choosing these criteria exist. As discussed above, standard $\Pi$-type counters are inadequate to detect cycle-slips that are present in the data. The redundant counting scheme with two $\Lambda$-type counters applied here on the other hand obviously allows the characterization at the lower $10^{-19}$ level. However, pushing the instability and accuracy of the transferred frequency to significantly lower values might require more advanced techniques as, for example, using three redundant counters.

Every amplifier, whether RF or optical, inevitably adds a certain amount of noise to the signal. Our experiments demonstrate, however, that carefully designed low-noise optical amplifiers allow us to amplify signals with a power of a few tens of microwatts dozens of times without adding a substantial amount of noise. The signal-to-noise ratio of the heterodyne beat notes is on the order of 40 dB in a 10 kHz resolution bandwidth even after the signal is amplified 40 times by EDFAs.

Figure 4.23 shows the frequency instability achievable with the commonly used frequency dissemination techniques based on satellites which have been discussed in Section 3.3 together with the results obtained in this work by transferring an optical frequency over fiber links. The comparison between those techniques clearly illustrates the outstanding performance of the fiber link technology. Additionally, it solves the issue of remote optical clock comparisons for today's and even for the next generation of state-of-the-art optical frequency standards. The instability contribution of the fiber link transfer itself becomes negligible within seconds thanks to the low inherent fiber noise and the fast averaging.

In the experiments on the 1840 km link, the frequency is sent from MPQ to PTB whereby a difference in height above the geoid of the earth of more than 400 m is bridged. According to general relativity, the transferred frequency experiences an upshift of about $4.4 \times 10^{-14}$ on the way from MPQ to PTB which reverses on the way back. As the transferred frequency after the 1840 km link matches the sent frequency on a level of a few $10^{-19}$, a possible irregularity in the gravitational redshift between the transition from a lower to a higher gravitational potential and vice versa can be constrained to be lower than this value.

The ability to bridge almost 2000 km with a fiber link allows one to connect all the major precision measurement laboratories within Europe with the infrastructure, that means the glass fibers, being mostly already in place. Besides clock comparisons, the transfer of highly stable optical signals also enables a variety of novel, potentially groundbreaking experiments from tests of fundamental physics to high-resolution spectroscopy and relativistic geodesy.

### 4.5.1   Limitations of fiber based optical frequency transfer

The results presented in this chapter are extremely promising and clearly demonstrate that, according to the current knowledge, fiber links are by far the best approach for the dissemination of stable optical frequencies over long distances. As the performance of optical clocks is rapidly improving, it is worthwhile to discuss the limitations of fiber based optical frequency transfer.

As mentioned above, the propagation delay imposes a fundamental limit for the effectiveness of the noise cancellation. Scaling a fiber link to longer lengths not only leads to an increase in fiber noise but additionally reduces the bandwidth of the noise cancellation control loop. One way to overcome this limitation is to divide a fiber link into multiple sections where each of them is stabilized individually [120]. The gain of control

bandwidth, however, comes at the cost of a more complex and expensive setup as additional stabilization systems need to be operated along the fiber link. Also intermediate oscillators could by operated along the link to clean the signals from most of the residual noise so that a significantly better (short-term) frequency stability could be achieved.

The analog PI controller used here is in no way adopted to the noise properties or the long signal delay of the fiber links. A digital PLL on the other hand offers great flexibility and filter functions that are very difficult or impossible to realize with an analog controller. We performed initial experiments with such a digital control loop and achieved significantly lower short-term instabilities. Hence, optimizing the noise cancellation system without applying any changes to the fiber link itself might lead to a substantial improvement in the frequency transfer performance.

Another concern when increasing the link length is the signal-to-noise ratio of the heterodyne beat signals, especially the one used for the link stabilization. The higher losses associated with longer links call for more amplifiers where each of them adds a certain amount of noise, spreading the signal power away from the carrier and thereby lowering the achievable signal-to-noise ratio [126]. Instead of using EDFAs, other kinds of amplifiers might be advantageous as for instance fiber Brillouin amplifiers. Here, the amplifier gain is concentrated over a much smaller spectral bandwidth which increases the efficiency and allows one to bridge distances of more than 250 km with a single amplifier [9]. As a result, longer fiber links can be operated with the same or less amount of optical amplifiers.

# Chapter 5

# Extended Analysis of Noise Types

In Section 2.2.1 the five most common noise types present in typical electronic and optical systems were discussed and the response of the ADEV as well as the modADEV was given in Figure 2.2 as well as in Table 2.1. In this chapter, we extend the list of noise types in order to correctly describe the noise properties of our fiber link system. Simulations with different phase noise spectra reveal an, up to now, unconsidered response of the modADEV that leads to an unprecedented fast averaging towards low frequency instabilities. Additionally, we derive and discuss analytical solutions for those noise spectra.

## 5.1    Noise in time and frequency domain

If a frequency signal is counted with a frequency counter and the instability is expressed as, for example, the ADEV or modADEV, the slope of the resulting instability curve gives hints to the underlying noise type that the signal is dominated by (see Figure 2.2). Since in this case the frequency instability is given as a function of time, this analysis can be considered as the time domain representation of noise or stability. The frequency domain characterization of the phase instability is the power spectral density (PSD) of phase fluctuations $S_\phi(f)$. This analysis reveals the full frequency information of the noise present in the system as the name implies. The ADEV is a useful measure for the instability of a signal as it allows one to compare different oscillators operating at various frequencies in a particularly easy way. Since the ADEV is the integral of the PSD, single noise components that are easily recognized in the PSD are harder to identify in the ADEV. Therefore, both the ADEV as well as the spectral analysis are important tools for the noise characterization of an oscillator with their own advantages and drawbacks.

The relation between time and frequency domain is given by Equation 2.10 and Equation 2.11 which allow us to calculate the frequency instability $\sigma_y(\tau)$ and mod $\sigma_y(\tau)$, respectively, from the measured phase fluctuations $S_\phi(f)$. Since frequency measurements nowadays are performed straightforwardly while the determination of the PSD can be significantly more complex, it would be advantageous to calculate $S_\phi(f)$ from the

frequency counter data. The determination of $S_\phi(f)$ from $\sigma_y(\tau)$ or mod $\sigma_y(\tau)$, however, is possible only in simple cases where the frequency dependence of $S_\phi(f)$ is well known [127]. In the literature, the phase noise PSD is usually parametrized as [24, 25]

$$S_\phi(f) = \sum_{\alpha=-2}^{2} h_\alpha f^{\alpha-2} \tag{5.1}$$

with the coefficients $h_\alpha$ as a measure of the corresponding noise level. This means that phase noise that falls off with frequency as $f^{-4}, f^{-3}, \dots$ or frequency independent noise
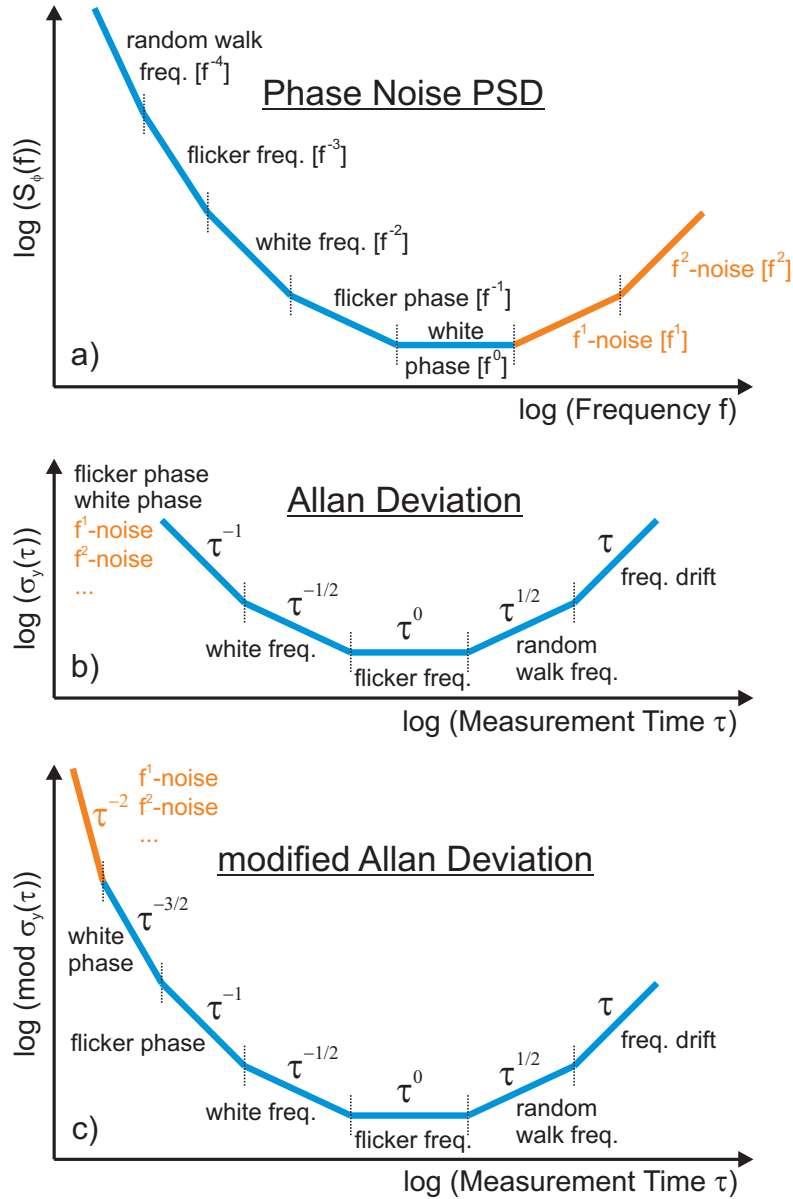


FIGURE 5.1: a) Parametrization of the phase noise PSD for different noise types according to Equation 5.1. b) and c) the response of the ADEV and the modADEV to those noise types, respectively.

($f^0$) is covered by this model. Figure 5.1 illustrates the relation between the PSD and the frequency instability in which all noise types of Equation 5.1 are shown in blue.

## 5.2 Response of the (modified) Allan deviation to higher order noise types

The spectral noise distribution of the 1840 km link shown in Figure 4.20 with the broad maximum around 15 Hz is a typical feature of underground fiber links [108, 113, 128, 129]. Besides slight variations in the shape of the PSD that are expected for different links, the magnitude mostly scales with fiber link length. For low frequencies, the PSD of
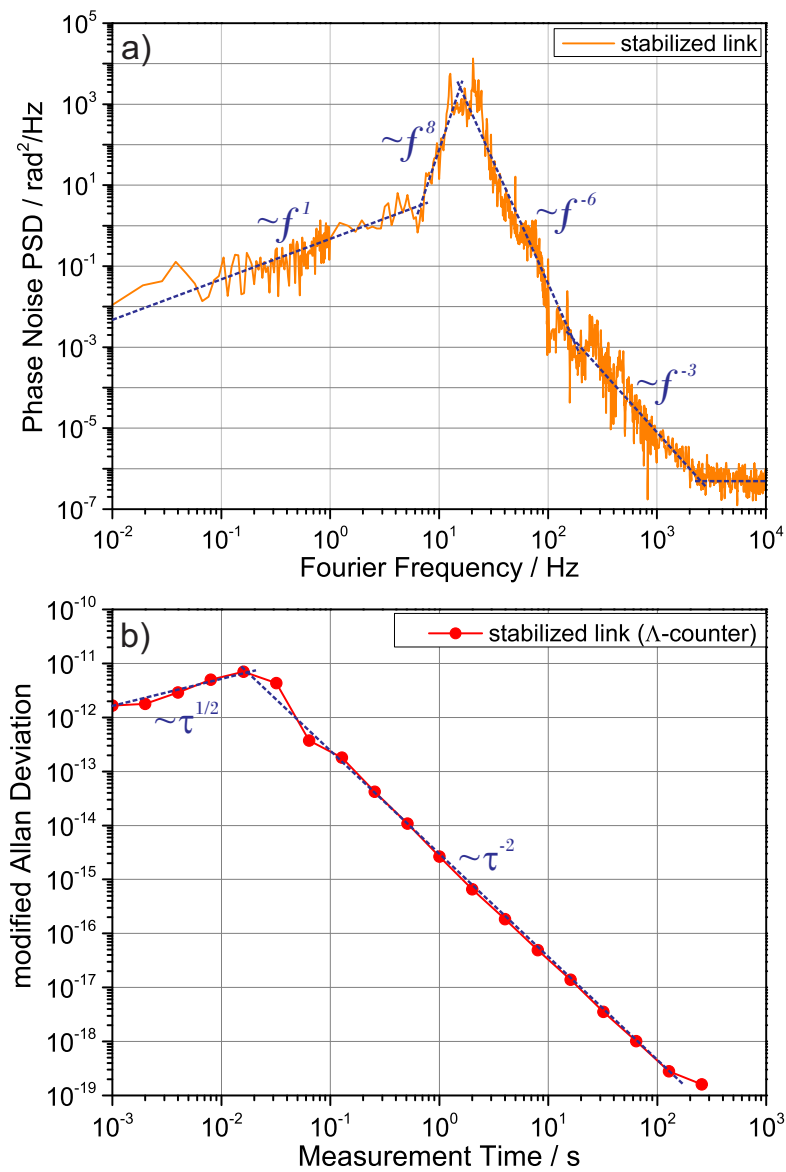


FIGURE 5.2: a) Frequency dependency of the phase noise PSD of the stabilized 1840 km fiber link. b) Corresponding frequency instability measured with a Λ-type frequency counter and expressed as the modADEV.

the free-running link exhibits a $\approx f^{-1}$ dependency. According to feedback theory, the phase noise cancellation control loop suppresses the noise within the control bandwidth proportional to $f^2$. Consequently, the residual phase noise of the stabilized link features a $f^1$ dependency within the bandwidth of the control loop as can be seen in Figure 5.2.

Such a spectrum, however, is not covered by the standard parametrization given in Equation 5.1. One way to determine the response of the ADEV and modADEV to a spectrum proportional to $f^1$, $f^2$ or higher orders, is to simply generate a phase noise PSD with such a spectrum and use Equation 2.10 and Equation 2.11 to calculate the frequency instability from it. The calculations performed with those artificial spectra revealed that the ADEV shows a dependency from the measurement time as $\tau^{-1}$ which is identical to the response to flicker phase and white phase noise as can be seen in Figure 5.1 b). In contrast to that, the modADEV which has a dependency of $\tau^{-1}$ for flicker phase noise and $\tau^{-3/2}$ for white phase noise shows a $\tau^{-2}$ dependency to a phase noise spectrum of $f^1$, $f^2$ or higher orders. This relation is sketched in Figure 5.1 c) in which the higher order noise types are shown in orange.

Figure 5.2 illustrates the effect of the higher order noise terms on the frequency instability of our fiber link. The measured phase noise increases with frequency between 0.01 and $\approx 25$ Hz with $f^1$ and $f^8$. In the modADEV, this should lead to a $\tau^{-2}$ dependency for measurement times between 0.04 and 100 s which is indeed observed. Beyond 25 Hz, the phase noise rolls off quickly with $f^{-3} \ldots f^{-6}$. According to theory (Figure 5.1 c)) this indicates random walk or flicker frequency noise which has a dependency of $\tau^0 \ldots \tau^{1/2}$ in the modADEV. Again, the same behavior is observed in the instability analysis.

The five common noise types that are given by Equation 5.1 as well as higher order noise types which are characterized by their individual $S_\phi(f)$ can be inserted in Equation 2.10 and Equation 2.11 to derive analytical solutions for the ADEV and modADEV. Those solutions are summarized in Table 5.1 as an expansion to Table 2.1. Here, the variances $\sigma_y^2(\tau)$ and mod $\sigma_y^2(\tau)$ are given so that taking the square root allows the comparison with Figure 5.1 and Figure 5.2. It can nicely be seen that the $\tau$ dependency of the ADEV is the same for flicker phase noise, white phase noise and all higher order noise types. The modADEV on the other hand can distinguish between flicker phase noise, white phase noise and higher order noise types. However, also the limits of the modADEV become obvious as there is no distinction between $f^1$-noise and all higher order noise types. Yet another kind of algorithm would be desired to be able to differentiate between those noise types.

The analysis of the modADEV to higher order noise types which are discussed in detail here helps to understand the noise properties of our fiber links. The analytical solutions for various noise types given in Table 5.1 and the remarkable agreement of the two instability curves in Figure 4.21 support the correctness of our analysis. In the results of the 920 km links the $\tau^{-2}$ dependency could not be seen as clearly as in the 1840 km link analysis. The reason for this is that the correction for the timing offset of the frequency counters required the determination of the drift rate of the two transfer lasers against each other for every data point. The noise of this signal, however, led to an over- or underestimation of the real drift rate which resulted in an imperfect correction

| Noise Type | $S_y(f)$ | $S_\phi(f)$ | $\sigma_y^2(\tau)$ | mod $\sigma_y^2(\tau)$ |
|---|---|---|---|---|
| Random walk freq. | $h_{-2}f^{-2}$ | $\nu_0^2 h_{-2} f^{-4}$ | $\frac{2\pi^2 h_{-2}}{3}\tau$ | $\frac{11\pi^2 h_{-2}}{20}\tau$ |
| Flicker frequency | $h_{-1}f^{-1}$ | $\nu_0^2 h_{-1} f^{-3}$ | $2\ln(2)h_{-1}$ | $2\ln(1.59)h_{-1}$ |
| White frequency | $h_0 f^0$ | $\nu_0^2 h_0 f^{-2}$ | $\frac{h_0}{2}\tau^{-1}$ | $\frac{h_0}{4}\tau^{-1}$ |
| Flicker phase | $h_1 f^1$ | $\nu_0^2 h_1 f^{-1}$ | $\frac{(3.12+3\ln(\pi f_h \tau))h_1}{4\pi^2}\tau^{-2}$ | $\frac{3\ln(9.48)h_1}{8\pi^2}\tau^{-2}$ |
| White phase | $h_2 f^2$ | $\nu_0^2 h_2 f^0$ | $\frac{3 f_h h_2}{4\pi^2}\tau^{-2}$ | $\frac{3 h_2}{8\pi^2}\tau^{-3}$ |
| $f^1$-noise | $h_3 f^3$ | $\nu_0^2 h_3 f^1$ | $\frac{3 f_h^2 h_3}{8\pi^2}\tau^{-2}$ | $\frac{(9.64+10\ln(\pi f_h \tau))h_3}{16\pi^4}\tau^{-4}$ |
| $f^2$-noise | $h_4 f^4$ | $\nu_0^2 h_4 f^2$ | $\frac{f_h^3 h_4}{4\pi^2}\tau^{-2}$ | $\frac{10 f_h h_4}{16\pi^4}\tau^{-4}$ |
| $f^3$-noise | $h_5 f^5$ | $\nu_0^2 h_5 f^3$ | $\frac{3 f_h^4 h_5}{16\pi^2}\tau^{-2}$ | $\frac{10 f_h^2 h_5}{32}\tau^{-4}$ |
| $f^4$-noise | $h_6 f^6$ | $\nu_0^2 h_6 f^4$ | $\frac{3 f_h^5 h_6}{20\pi^2}\tau^{-2}$ | $\frac{10 f_h^3 h_6}{48\pi^4}\tau^{-4}$ |

TABLE 5.1: The five most common noise types present in many systems plus so far unconsidered noise types observed in the fiber link system. The corresponding frequency dependence of the power spectral densities together with the response of the Allan variance and the modified Allan variance. $f_h$: cutoff frequency that determines the measurement bandwidth. Small oscillating terms are ignored.

and therefore to the observed instability curve. The $\tau^{-2}$ dependency strongly suggests the use of the modADEV as not only more noise types can be identified unambiguously but additionally and more importantly, the noise contribution of the fiber link transfer becomes negligible after very short measurement times.

In summary, the spectral noise distribution of the free-running fiber link in combination with the limited noise suppression bandwidth results in the unique shape of the phase noise PSD of the stabilized link which is the reason for the fast averaging in the modADEV. A different, more effective loop filter for the noise cancellation or a larger control bandwidth capable of suppressing the broad 15 Hz noise might result in, for example, white phase noise within the control bandwidth. In this case, an averaging proportional to $\tau^{-3/2}$ would be expected in the modADEV but the instability would in total be lower than the one measured here.

# Chapter 6

# GPS Carrier-Phase Link Characterization using the 920 km Fiber Link

The transfer of stable frequencies via fiber links that is discussed in this work is still a novel technology. From today's point of view, the first fiber link connections between European countries will go in operation within the next few years and it is expected that this technology becomes a standard for international clock comparisons at least on distances up to a few thousand kilometers. Similarly, fiber link networks might be established in some parts of Asia and North America for the same purpose. However, intercontinental frequency transfer by fiber links as, for instance, between Europe and North America is still a long way off due to the technological challenges.

Until then, some of the satellite based frequency dissemination techniques discussed in Section 3.3 will still be used extensively. The international timescale UTC, for example, relies entirely on those techniques. Without the assistance of satellites no international timescale would exist simply due to the absence of a means for remote clock comparisons. Among these satellite techniques, the one based on global navigation satellite systems (GNSS) is most commonly used. The reason for that is that such a system is set up straight forwardly and in addition it is very cost efficient as only receiving equipment is required. Therefore, it is worth to investigate the performance of such a link in greater detail. In this chapter, the frequency transfer capability of a GPS carrier-phase link is analyzed by the help of one of the 920 km fiber links discussed in Section 4.3.

## 6.1   State-of-the-Art

In the context of frequency transfer via navigation satellites the wording can be a bit misleading as there is no information directly transferred from one location to another by the satellite. The satellite only provides a common reference for the locations on the ground. If two clocks at two locations are to be compared, each site first measures

the difference between the local clock and the frequency reference from the satellite. Afterwards the data files are exchanged and the difference between the clocks can be calculated whereby the satellite's reference drops out.

In order to take advantage of the more precise carrier-phase measurements, knowledge of the satellite's ephemeris and clocks is necessary. This data is provided by the International GNSS Service (IGS) which is a voluntary federation of over 200 institutes worldwide that span a network of GNSS reference stations [130]. IGS provides precise corrections for the satellites' flight paths and clock errors that are applied to the measurement data in a post-processing step. Precise Point Positioning (PPP) is such a post-processing method which was originally developed for precise positioning applications with accuracies of up to a few centimeters [131]. Today, PPP is considered to be the most stable method for time and frequency comparisons. Different software packages for the PPP method have been developed out of which the NRCan-PPP software from the geodetic institute Natural Resources Canada [132] is the most widespread one. All investigations described here are done by processing the relevant data with the NRCan software package.

Performance evaluations of various GPS carrier-phase links have been performed on baselines of typically a few thousand kilometers using different receiving equipment [7, 81, 86, 133]. Those evaluations were done by comparing remote frequency standards over the GPS link. Typically, hydrogen masers are chosen for this task as their low short term instability (see Figure 2.6) is clearly below that of the GPS link so that the measured performance can securely be attributed to the GPS transfer itself. Active hydrogen masers, however, reach a flicker floor in the frequency instability of $\approx 1 \times 10^{-15}$ after $10^4$ s ... 1 day. Therefore, the frequency standards contributing in the GPS link characterization limit the achievable performance on long time scales. Consequently, GPS carrier-phase links have been shown to support a frequency instability and accuracy of a few parts in $10^{15}$. Recently, two satellite links, namely a GPS carrier-phase and a TWSTFT link have been operated simultaneously to compare two hydrogen masers over a baseline of about 9,000 km [87]. In this study it was shown that a GPS carrier-phase link supports a frequency instability of about $3 \times 10^{-16}$ after 4 days.

The obvious way of characterizing a GPS link below this level involves better frequency standards such as optical clocks. Optical clocks, however, still need a substantial amount of attention during operation, making multi-day comparisons challenging. Here, the fiber link discussed in Section 4.3 enables us to circumvent the mentioned limitation.

## 6.2   Experimental setup

Having two precision measurement laboratories each equipped with active hydrogen masers and connected by a GPS carrier-phase link as well as by a fiber link constitutes a unique opportunity to unambiguously characterize the performance achievable with a GPS frequency transfer link. By comparing the two hydrogen masers via both the GPS and the fiber link simultaneously, the difference between the two comparisons
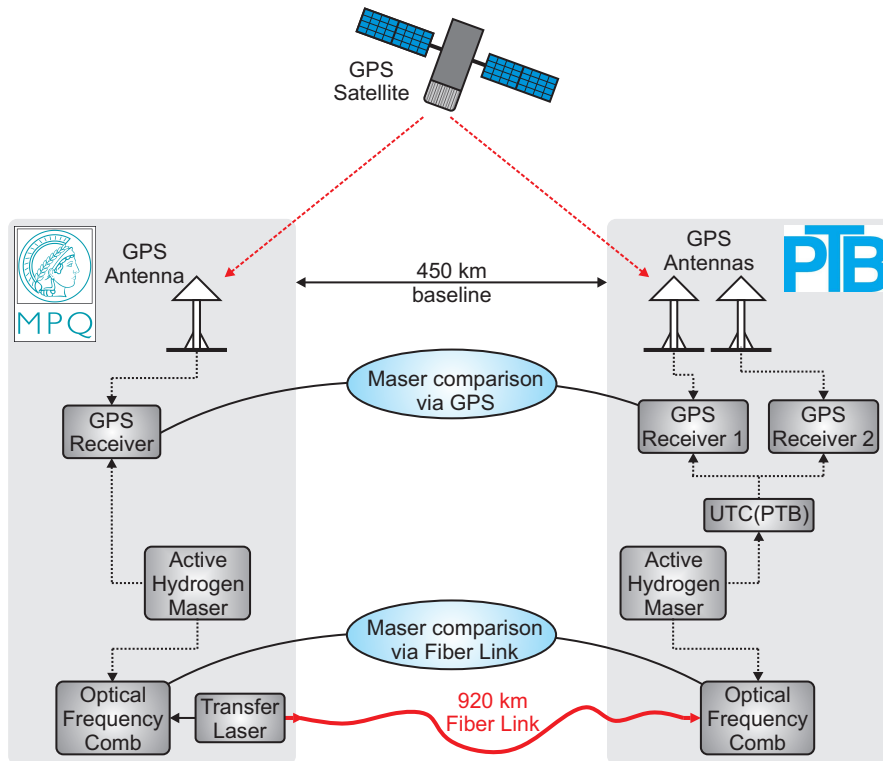
FIGURE 6.1: Experimental setup for the characterization of the GPS carrier-phase link. Two hydrogen masers are compared via one of the 920 km fiber links described in Section 4.3 and via a GPS link simultaneously. At each site, an optical frequency comb is locked to the local maser. The fiber link stabilization is done at MPQ and the maser comparison via fiber link is accomplished by measuring the transfer laser frequency against the optical frequency combs. The maser comparison via GPS is performed by measuring the maser frequency against the GPS signal. See text for details.

can be calculated in which the contribution from the masers drops out. The superior performance of the fiber link enables the full characterization the GPS carrier-phase link.

### 6.2.1 Transmission scheme

In Figure 6.1 the experimental setup for the GPS carrier-phase link characterization is shown. The two locations, MPQ and PTB, are separated by a total distance of about 450 km (line of sight). At MPQ, an active hydrogen maser is operated with a specified performance shown in Figure 2.6. The repetition rate of an optical frequency comb (Menlo Systems GmbH) is locked to the hydrogen maser. The light of a transfer laser is sent through the fiber link from MPQ to PTB while measuring its frequency via the frequency comb at the same time. The fiber link stabilization is done at MPQ in the same way as described in Section 3.4.6. Additionally, the MPQ maser signal is fed into a GPS receiver (Septentrio PolaRx2e) to determine the frequency difference between the maser and the GPS signal.

At PTB, a similar setup is employed and the frequency of the incoming light from MPQ is measured with a frequency comb (Menlo Systems GmbH). The repetition rate of the

comb at PTB is locked to the local maser. Instead of measuring the maser frequency directly against the GPS signal, it is measured against PTB's representation of UTC, which is another hydrogen maser steered by a cesium fountain clock [134]. UTC(PTB) is fed into two different GPS receivers (both Ashtech Z-XII3T) to measure the frequency difference between UTC(PTB) and the GPS signal. From the difference between the maser versus UTC(PTB) and UTC(PTB) versus the GPS signal, the difference between the maser and GPS is calculated.

We determine the difference of the two masers via the fiber link from the measurements of the transfer laser against the combs as the combs represent the frequency of the masers. Simultaneously, the GPS receivers measure the maser frequencies against the GPS signal so that these data can be used to calculate the maser difference via the GPS link. Finally, the difference between these two maser comparisons can be calculated, which results in the so called *double difference*. In this double difference the contributions of the masers drop out so that the result represents the difference of the two frequency transfer links. As the noise of the fiber link is at least four orders of magnitude below that of the GPS link, the double difference reveals the true GPS link performance.

### 6.2.2   Data acquisition and validation criteria

Instead of determining the performance of the fiber link as has been the main task of all previous experiments throughout this work, here we use the excellent performance of the fiber link as a tool for the GPS link characterization. Same as previously, the issue to measure time varying frequencies at remote locations again applies here. However, the difficulties experienced before (see Section 4.3.3) are prevented by the use of frequency counters that can be synchronized externally as mentioned in Section 4.3.3. This is done by adjusting the measurement window of the counters ($\Lambda$-type, K + K Messtechnik GmbH) to a PPS signal from a GPS receiver. To verify the synchronization of the counters we apply a step function to the AOM at MPQ that is usually used for the fiber induced noise cancellation. We measure the heterodyne beat frequency of the sent and the round-trip light with a gate time of 1 ms. Due to this frequency step, the outgoing light from MPQ gets shifted up by 100 kHz as can be seen in Figure 6.2. After a propagation time of $\approx$ 9 ms the returning light experiences a second shift in the same direction. The sent light reaches PTB after a propagation time of 4.5 ms where the step is also measured with a gate time of 1 ms. The two counters are synchronized if the frequency step at PTB is precisely in between the two steps measured at MPQ. It can be seen that the two frequency counters are synchronized to better than 1 ms which is more than sufficient for the current application. The PPS signal from the GPS receiver has a specified accuracy of a few nanoseconds and we expect that the counter synchronization accuracy can at least be as good as a few microseconds.

To detect cycle-slips, we again apply redundant counting for the optical part of the system. Here, however, we exclusively use $\Lambda$-type frequency counters. The counters are set to a gate time of 1 s, in analogy to previous experiments. In contrast to the experiments on the 920 km fiber link described in Section 4.3, here we only operate one fiber link from MPQ to PTB. Therefore, the validation criteria are altered with respect to
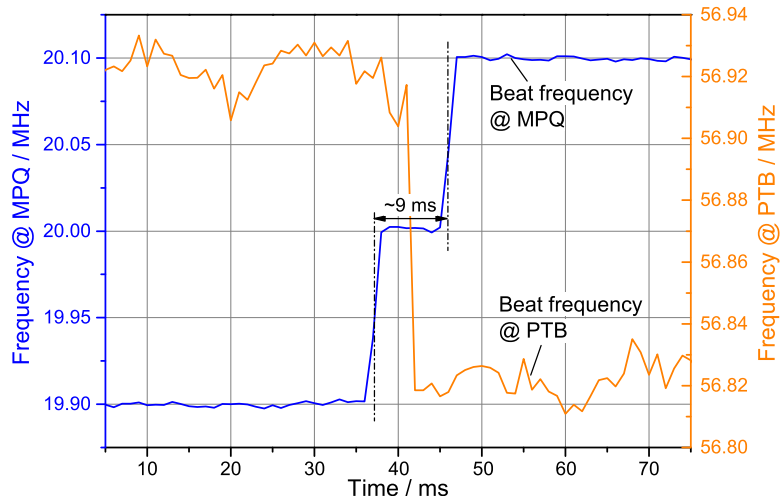
FIGURE 6.2: Verification of the synchronization of the two frequency counters operated at MPQ and PTB. A step function is applied to the AOM at MPQ that shifts the frequency of the light by 100 kHz. This frequency step is measured at MPQ and PTB simultaneously to determine the synchronization of the two frequency counters. See text for details.

the previous experiments. Instead of setting a fixed threshold for the difference between the redundantly counted signals, a variable threshold is used that is adopted to the noise of the individual signals. The median absolute deviation (MAD) that is defined as

$$\text{MAD} = \text{median}_i(\mid X_i - \text{median}_j(X_j) \mid) \tag{6.1}$$

for a data set with values $X_1 \ldots X_n$. The MAD is calculated for each of the counted signals and the criteria listed in Table 6.1 are used. A beat, $f_{Comb-TL}^{MPQ}$, between the transfer laser and the frequency comb at MPQ is generated and counted twice. Additionally, a beat, $f_{Comb-TL}^{PTB}$, between the transferred light from MPQ and the frequency comb at PTB is generated which is again counted twice. To monitor the two frequency combs itself, both repetition rates $f_{rep}^{PTB}$ and $f_{rep}^{MPQ}$ as well as both offset frequencies $f_{ceo}^{PTB}$ and $f_{ceo}^{MPQ}$ are counted.

The threshold of $8 \times \text{MAD}$ is a robust value in the sense that varying this threshold does not change the amount of detected cycle-slips significantly. To surveil the fiber links functionality additional cycle-slip criteria are introduced. The transferred light is heterodyned against two ultra-stable lasers at PTB. If the fiber induced noise cancellation is deactivated, these heterodyne beats show a 1-s instability of about $1 \times 10^{-14}$. When the noise cancellation control loop is active on the other hand, the 1-s instability decreases to about $9 \times 10^{-16}$ so that a clear distinction between those two cases can be made. The 1-s ADEV is calculated from 30 adjacent data points. We now introduce a threshold for the short-term instability to identify whether the fiber link stabilization is working properly. If the 1-s ADEV of the beat signal of the transferred light against both ultra-stable lasers exceeds $3 \times 10^{-15}$, the 30 s interval is marked as invalid. Again, we choose this threshold due to the robustness over the resulting number of invalid data points. An alternative cycle-slip analysis which uses criteria similar to the ones listed in

| Criterium | Threshold |
|---|---|
| Difference of redundantly counted $f_{Comb-TL}^{MPQ}$ at MPQ | $< 8 \times$ MAD |
| Difference of redundantly counted $f_{Comb-TL}^{PTB}$ at PTB | $< 8 \times$ MAD |
| Difference of $f_{rep}^{PTB}$ and its nominal value at PTB | $< 8 \times$ MAD |
| Difference of $f_{rep}^{MPQ}$ and its nominal value at MPQ | $< 8 \times$ MAD |
| Difference of $f_{ceo}^{PTB}$ and its nominal value at PTB | $< 8 \times$ MAD |
| Difference of $f_{ceo}^{MPQ}$ and its nominal value at MPQ | $< 8 \times$ MAD |

TABLE 6.1: Validation criteria for the 920 km fiber link from MPQ to PTB and for the frequency combs to identify loss of phase coherent events. All data points that exceeded at least one of the threshold values are discarded.

Table 4.1 is conducted independently and leads to very similar results compared to the criteria mentioned above.

In the GPS part of the system, the data acquisition is done by the GPS receivers which directly deliver the phase difference between the maser and the GPS signal. The sample rate is chosen to 30 s at MPQ and PTB. The data from the receivers are processed with NRCan-PPP as mentioned above. Here, ephemeris and clock corrections are applied with the help of IGS products where the most precise corrections (final products [135]) with a sample interval of 30 s are used.

In order to synchronize the fiber link data files from MPQ and PTB, we use the modulation shown in Figure 6.2. Before each measurement, we synchronize the time of the computers used for the data recording to the same time server in analogy to previous experiments. To synchronize the fiber link and the GPS link data, we rely on the accuracy of the time stamps that are derived from the computer times.

Due to the different sampling intervals of the fiber and GPS link data, the combination of both data sets requires some treatment of the fiber link data beforehand. The most intuitive approach is to average 30 fiber link data points to equalize the sampling intervals. However, one single cycle-slip in the fiber link data would lead to a rejection of the remaining 29 data points within the corresponding GPS data window. As the difference of the two masers measured over the fiber link shows an instability of $\approx 1 \times 10^{-13}$ in 1 s (see Figure 2.6), it is sufficient to select and average a minimum of 10 fiber link data points within one 30 s GPS data window. In the worst case, all 10 fiber link data points will be incoherent due to cycle-slips which results in an instability of $1 \times 10^{-13}/\sqrt{10} \approx 3 \times 10^{-14}$. The difference of the masers measured over the GPS link, however, has an instability of $\approx 3 \times 10^{-13}$ in 30 s. Therefore, the instability of the $\geq$ 10-s averaged fiber link data points will always be at least one order of magnitude below that of the GPS link data points. After applying a non-weighted average to the fiber link data we subtract the fiber link from the GPS link data which reveals the GPS link performance without the contributions from the masers.
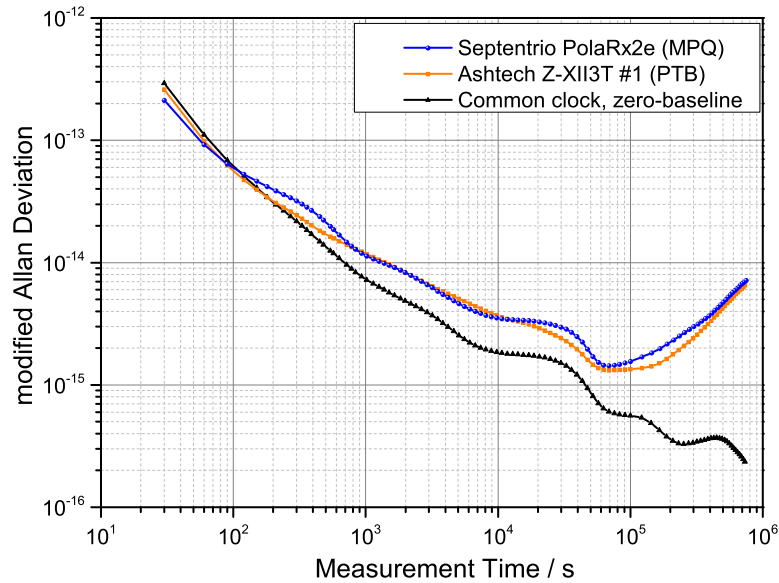
FIGURE 6.3: Fractional frequency instability of the difference between a hydrogen maser and the GPS signal. At PTB, two GPS receivers are operated simultaneously that show very similar performances while at MPQ only one receiver is used. The common clock zero-baseline configuration is used to determine the instability limit of the present system. See text for details. Courtesy of J. Leute.

## 6.3 Results

As discussed in Section 3.3, GNSS based frequency dissemination techniques are limited by various effects causing path length fluctuations between the satellites and the clocks on the ground. The incoming signals broadcasted by the satellites are processed by special GPS receivers that use sophisticated electronics and algorithms to calculate the frequency difference between the received signals and the local frequency standard. At MPQ, only one receiver is used while at PTB, two GPS receivers are operated at the same time. Since both PTB receivers are connected to the same hydrogen maser as a common clock they can be used to determine the ultimate instability limit of the present system. Although both receivers are located in the same laboratory, they are equipped with individual GPS antennas. As the same maser is fed into the two receivers whose antennas are separated by a distance of only a few meters on the roof of the PTB building, this part of the setup can be seen as a zero-baseline comparison of one maser to itself. The noise arising in the transfer between the satellites and the receivers as well as in the receivers themselves determines the noise floor of the system used here. The performance of the receivers at MPQ and one of the receivers at PTB is shown in Figure 6.3 together with the instability floor determined in the common clock zero-baseline configuration. Both PTB receivers show very similar performances and the Ashtech Z-XII3T #1 receiver is the one that is used in the remainder of this chapter.

At timescales of roughly half a day and above the frequency instability is expected to be limited by the performance of the masers. To eliminate this contribution, the GPS link as well as the fiber link between MPQ and PTB are operated continuously over the course of about four weeks. The result is shown in Figure 6.4. As the instability

| Measured signal | Arithmetic mean | Statistical uncertainty |
|---|---|---|
| Maser difference via fiber link | $4.595 \times 10^{-13}$ | $4.2 \times 10^{-17}$ |
| Maser difference via GPS link | $4.597 \times 10^{-13}$ | $9.2 \times 10^{-16}$ |
| Double difference | $1.9 \times 10^{-16}$ | $9.2 \times 10^{-16}$ |

TABLE 6.2: Results of the maser difference measured via the fiber and via the GPS link together with the results of the double difference. All results are calculated from 30 s data.

contribution of the fiber link is below that of the masers on all relevant timescales (see Figure 4.15), the data obtained with the fiber link directly represent the difference of the two masers without any contribution of the fiber link transfer itself. The data obtained with the GPS link, on the other hand, contains both contributions from the masers on long timescales and noise from the GPS link on shorter timescales.

The arithmetic mean and the statistical uncertainty of the maser difference measured via the fiber link and via the GPS link are shown in Table 6.2. The results are obtained from a total of 71,375 data points that were measured with a sampling interval of 30 s. We calculate the double difference by subtracting the two data sets of Figure 6.4 in order to eliminate the contributions of the masers. The uncertainty of the double difference is limited by the GPS link data. In analogy to the evaluation procedure introduced in Section 4.3.5 and Section 4.4.2 where coherent data subsets were generated, here we bin 10 GPS data points by applying a non-weighted average. Within this new 300 s long GPS data window, we select and average a minimum of 100 fiber link data points. From here, we calculate the double difference which reveals an arithmetic mean of $(2.1 \pm 5.9) \times 10^{-16}$. As will be discussed below, the frequency instability of the double
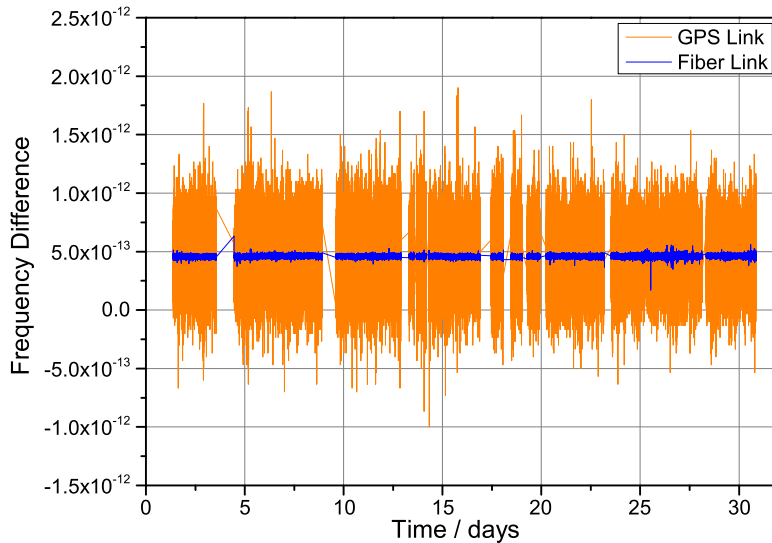


FIGURE 6.4: Frequency difference of the two hydrogen masers at MPQ and PTB measured over the GPS carrier-phase link and over the fiber link, respectively. The masers have a mean frequency difference of about $4.6 \times 10^{-13}$ with respect to each other. The occasion gaps in the data are due to a malfunction of one of the frequency comb systems.
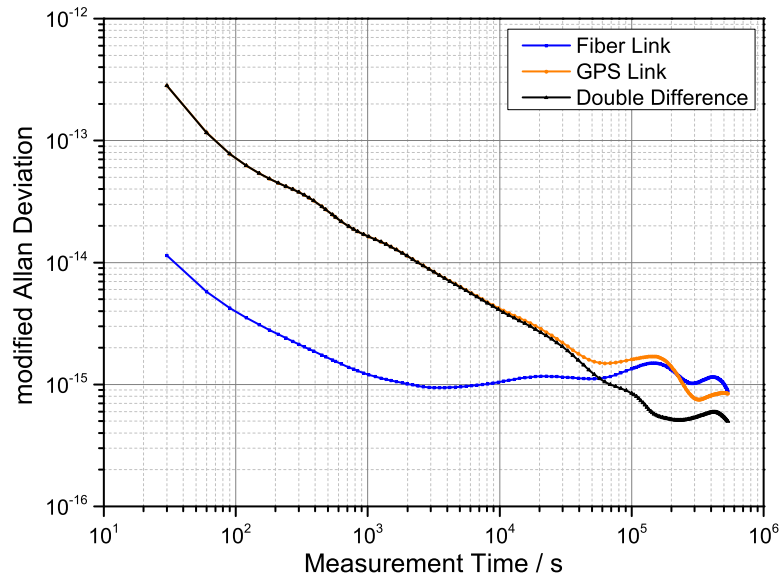
FIGURE 6.5: Frequency instability of the maser difference measured over the fiber link and over the GPS link, respectively. The double difference reveals the true GPS link performance without any contributions from the masers.

difference reaches a flicker floor at a level of about $5 \times 10^{-16}$ so that the application of standard statistics at this level may not be valid anymore.

The frequency instability of the maser difference can be calculated and is shown in Figure 6.5. After about 100,000 s of measurement time the instabilities of the maser difference measured via the GPS link and via the fiber link coincide, indicating a limitation due to the masers on a level of a few parts in $10^{15}$ as expected for active hydrogen masers. The double difference is not affected by any maser noise and thereby reflects the true GPS link performance. The instability of the double difference averages down to $5 \times 10^{-16}$ in 200,000 s at which level it reaches a floor. The reason for this floor cannot be determined unambiguously due to the complexity of the GPS system. Several effects degrade the positioning accuracy which a GPS link is based on. Table 6.3 lists the most important effects. Corrections to all of these effects have to be applied to reach the required accuracy for an atomic clock comparison. Obviously, the corrections themselves have a limited accuracy which in the end may lead to the instability floor that we observe here.

As the microwave signals from the satellites pass through the atmosphere it seems conceivable that the performance of the GPS link might be affected by the influence of the sun. The ionosphere, for example, experiences the biggest changes during sunrise and sunset when neutral atoms are ionized due to the sun's radiation and when the ions and electrons recombine after sunset, respectively. During the course of the measurement, sunrise occurred between 6:00 am and 7:00 am while sunset was between 7:45 pm and 8:30 pm. We separate the measurement data into day time (6 am to 6 pm) and night time (6 pm to 6 am) so that in both parts either sunrise or sunset is included. Figure 6.6 shows the frequency instability of the double difference for the day and for the night time. The difference between the two instabilities is a factor of 1.6 at maximum which

| Effect | Description |
| --- | --- |
| Sagnac effect | Path length variations between satellite and ground stations due to the rotation of the earth |
| Relativistic effects | Frequency shifts due to motion of the satellite and gravitational potential of the earth |
| Satellite clock offsets | Clock synchronism errors to GNSS reference time scale |
| Atmospheric delays | Path length changes between satellite and ground stations due to refractive index variations in ionosphere and troposphere |
| Phase wind-up | Changes in carrier-phase due to satellite rotation |
| Side displacement | Deformation of the earth and forces on the satellite due to sun and moon |
| Solid earth tides | Deformations of the solid earth due to gravitational attraction of sun and moon |
| Rotational deformation due to polar motion | Variations of the earth's spin axis |
| Ocean loading | Load of the ocean tides on the underlying crust |
| Satellite antenna offsets | Offset between the satellites center of mass and the antenna's phase center |

TABLE 6.3: Effects that cause variations in the positioning accuracy of a ground location. Corrections to all of these effects have to be applied if frequency standards are being compared via a GPS link.

indicates that the GPS link performance varies only slightly over the course of a day. Further analyses in which we include sunrise *and* sunset into either the day time or the night time reveals no significant difference from the data shown in Figure 6.6.

## 6.4   Discussion

The superior performance of the fiber link between MPQ and PTB is used to characterize a GPS carrier-phase frequency transfer link. The main challenge of an unambiguous characterization is the noise of the contributing frequency standards which limits the achievable instability and accuracy of a GPS carrier-phase link at a level of a few parts in $10^{15}$ and below. Here we compare two hydrogen masers located at MPQ and PTB over a GPS link and over the fiber link simultaneously. In the difference between the two comparisons the noise from the masers drops out, resulting in the combined performance of the two links. As the fiber link is at least four orders of magnitude more stable than the GPS link (see Figure 4.23), the results solely reflect the instability and accuracy of the GPS link.

It can be shown that a GPS carrier-phase link supports an instability of $5 \times 10^{-16}$ and an accuracy of at least $6 \times 10^{-16}$ thereby supporting the results presented in [87]. In particular, these results extend the findings of previous work obtained by comparing
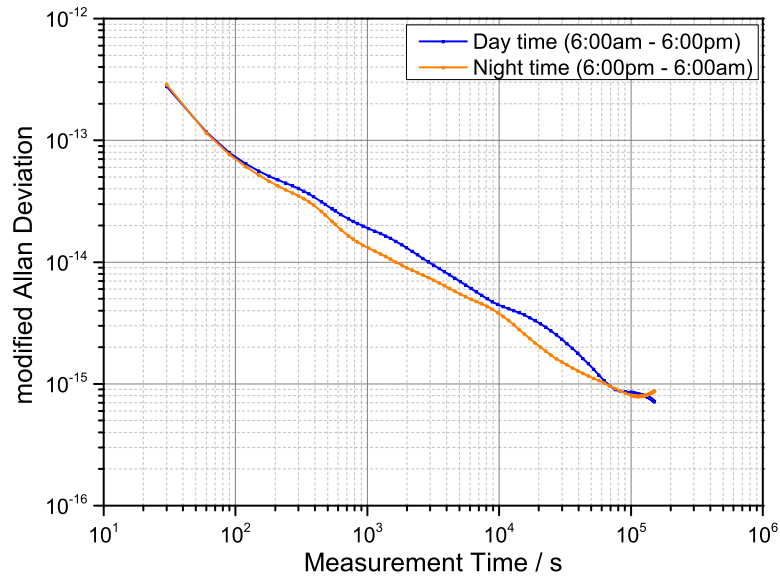
FIGURE 6.6: Frequency instability of the double difference for the day time from 6:00am to 6:00pm and for the night time from 6:00pm to 6:00am.

hydrogen masers over GPS links of different baselines [7, 78, 86] on long timescales. Figure 6.7 shows a comparison of the results discussed in this chapter with previous results in the literature while concentrating on short to medium baselines. In 2011, masers at MPQ and PTB have been compared [78] over a GPS carrier-phase link in a similar way but without the use of the fiber link. On timescales up to about 20,000 s both comparisons lead to the same results. On longer timescales, however, the drift of the masers cause an increase in the frequency instability thereby preventing an unambiguous GPS link characterization if no fiber link is used.
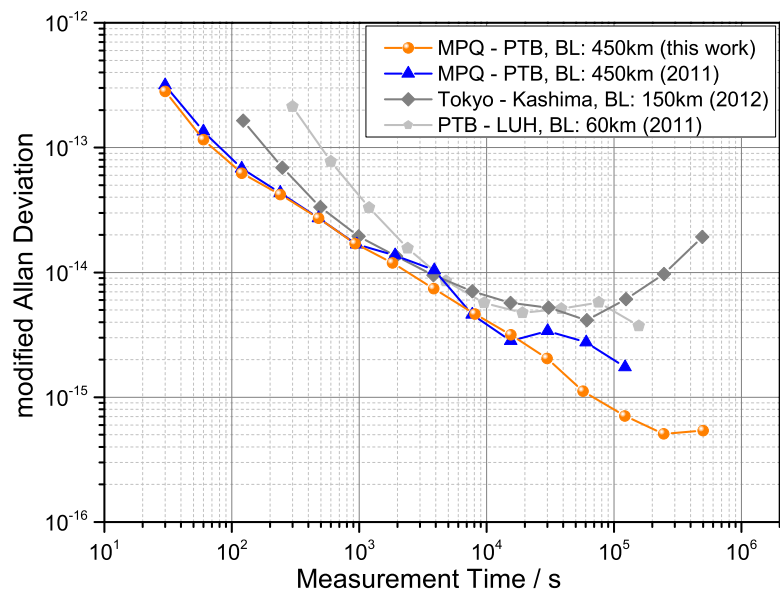


FIGURE 6.7: Literature values of frequency instabilities obtained by comparing active hydrogen masers on short to medium baseline (BL) GPS carrier-phase links [78, 86].

The separate analysis of day and night time reveals no significant influence on the performance of the GPS link. Sunrise and sunset cause the biggest ionospheric changes that might affect the performance of GPS link. However, excluding the periods of sunrise and sunset from the data does not lead to any significant changes in the frequency instability of the GPS link.

A comparison of the results achieved in GPS link characterization experiments conducted by different research groups proves to be difficult due to the use of different hardware on various baselines. Nevertheless, the results achieved here demonstrate that a GPS carrier-phase link does support a performance sufficient for the comparison of most microwave frequency standards (see Section 2.3) which could hardly be demonstrated up to date. As a large number of microwave clocks are routinely compared via GPS links, the results achieved here give hope that those comparisons are not limited by the performance of the frequency transfer link even though the demonstrated performance is inadequate for the comparison of the best cesium fountain clocks. The fact, that all three investigated receivers show very similar noise performances implies that the achieved performance might not be limited by the receivers themselves but are rather caused by, for example, inaccurate correction models. Even though the fiber link is used as a reference for the GPS link here, this can also be seen from the other side. By doing so, the experiment described here also provides an independent verification of a fiber link with a true remote end at a level of a few parts in $10^{16}$ in contrast to the often constructed fiber link loops.

# Chapter 7

# Summary & Outlook

The long-haul fiber links that span across Germany and which were characterized in detail in this work provide a testbed for a future European fiber link network. The distance of 1840 km demonstrated here is sufficient to connect all of the major precision measurement laboratories within Europe to benefit from the recent advances in fiber frequency transfer.

Throughout this work, single-span stabilization schemes have been employed exclusively, which means that the entire fiber link has been stabilized from the local to the remote end in one step. A fundamental limit of the fiber noise cancellation is the propagation delay of the light in the fiber. As a result, the achievable frequency instability grows with increasing fiber link length. Given the speed with which optical clocks improved in the last decade, it is possible that the frequency stability achievable with long distance single-span fiber links might not be sufficient some time in the future. In this case, the fiber link could be split into multiple sections where each section has its own fiber noise cancellation system [120]. This would circumvent the mentioned delay limit and would allow one to achieve higher frequency stabilities. Additionally, concatenating fiber links could allow for the construction of links with even longer lengths which might be required for intercontinental fiber connections.

During the course of this work, no real optical clock comparison could be performed as MPQ does not operate such a clock and no portable one exist yet. First mobile optical frequency standards are expected to go in operation in the near future and a comparison of such a device to a stationary clock at a remote location would be an exciting project. With real clocks being involved, a few more things have to be taken into consideration. First of all, the local optical clock has to be connected to a frequency comb in order to transfer the properties of the clock laser to the transfer laser. The transfer laser can be locked to the comb in order to cancel its drift or alternatively, one can measure the beat frequency of the transfer laser against the frequency comb without actively locking it. At the remote location, the transferred light can be measured against the second comb to which the remote clock is connected. If the transfer laser is not locked to the local frequency comb, it is still subject to a slow drift induced by the optical reference cavity. Same as discussed in Section 4.3.3, it is crucial to be able to either

synchronize the remote frequency counters or to correct for a possible counter timing offset. It is desired that the influence of the counter timing offset does not affect the clock comparison even on their ultimate instability level. Therefore, the impact of the counter timing offset has to below a level of $\approx 1 \times 10^{-19}$. Assuming a typical drift rate of 100 mHz/s at a frequency of 194 THz, the counter synchronization offset has to be smaller than 200 $\mu$s. We could show that the accuracy with which the synchronization offset between the counters can be determined can be below a microsecond if a strong triangular modulation of 100 kHz/s is applied [136]. No such correction is required, however, if frequency counters are used that can be actively synchronized as has been the case in the experiments discussed in Chapter 6.

A great advantage of this technique is that the existing telecommunication infrastructure can be used, to which most of the relevant laboratories are already connected. As only a narrow optical bandwidth is required for the frequency dissemination, those existing fibers can be used even if they carry internet traffic since many channels in the ITU grid are typically unused [108]. However, the costs for the access to those fibers can often be a political or financial problem which hinders the establishment of new fiber links.

The fiber link technology still is a very novel approach for atomic clock comparisons. Although an increasing number of research groups are attempting to establish fiber links in various European and Asian countries, the traditional satellite links remain the most prominent technique for the distribution of stable frequencies. Especially for intercontinental clock comparisons where oceans constitute major obstacles for fiber links the satellite based systems are expected to be the main method for the foreseeable future. For this reason, there is still active research on improving those links [87]. One of such satellite links has been investigated in this work in order to characterize the performance achievable on a short to medium range baseline. It was found that the stability and accuracy is sufficient for the comparison of most microwave clocks. However, the performance is about three orders of magnitude worse compared to that of the fiber links.

In Germany, additional optical fiber links are currently under construction (see Figure 7.1). The experiments on the 920 km and the 1840 km link, respectively, between MPQ and PTB proved that frequency transfer with outstanding performance can be achieved. One major goal, however, are international comparisons of frequency standards. One of the first international fiber links for this purpose will connect PTB with the French institute for Système de Références Temps-Espace (SYRTE) in Paris. Additionally, the future fiber links allow MPQ to get remotely access to atomic frequency references not only from PTB but also from SYRTE in order to continue performing high precision experiments like the spectroscopy of hydrogen [137]. Therefore, a portable atomic clock that has been used for those experiments in the past is not required.

Besides international clock comparisons, a whole variety of experiments requiring stable reference frequencies or timing signals can benefit from this technology as well. Besides pure frequency metrology, particle accelerator facilities [138, 139] and large scale antenna arrays for astronomical observations [140, 141] demand accurate time and frequency distribution systems. NASA's Deep Space Network is an antenna array used for spacecraft
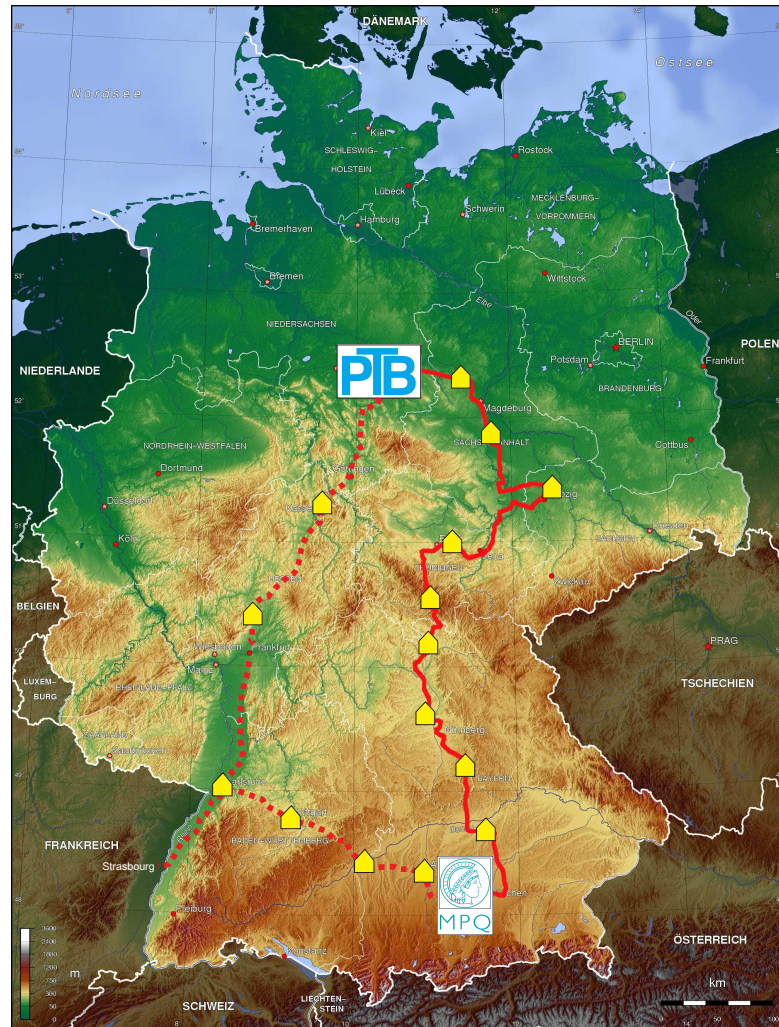
FIGURE 7.1: Map of Germany with the path of the two 920 km fiber links (solid red line) and the future links that are currently under construction (dashed red lines). The boarder between Germany and France will be crossed near Strasbourg, France.

communication and navigation. The remote antenna locations need to be synchronized by stable frequency signals [142] so that the advances described in this work may be used to increase the synchronization accuracy. Recently it has been proposed that a network of atomic clocks could be used for the detection of dark matter [143]. A stable configuration of dark matter, which is often referred to as a topological defect, may propagate through such a network with a certain velocity. Such a topological defect would lead to a time discrepancy of two initially synchronized clocks so that a large fiber link network could help to search for dark matter objects.

Fiber links have become an intense field of research not only in Germany but in several European countries. Figure 7.2 shows a map of Europe with fiber links that are already in existence as well as future links that are currently under construction or will be established in the near future. Note, however, that not all of the existing links have been characterized for ultra-stable frequency transfer yet.

Since 1967 cesium atomic clocks constitute the base for the unit of time. With the optical

FIGURE 7.2: Map of Europe with existing fiber links (red) and future fiber links (white).

clocks now clearly outperforming their microwave counterparts a redefinition of time seems reasonable. The fiber link technology allows us to perform remote comparisons of distant optical clocks without significant loss of accuracy. Therefore, the establishment of a European fiber link network lays the foundation of an upcoming redefinition of the SI-second.

# Appendix A

# ULE Cavity Drift Cancellation

The cw transfer laser is a commercial distributed feedback fiber laser operating at a wavelength of 1542 nm and exhibiting a free-running linewidth of about 5 kHz (FWHM). The phase noise of this laser is reduced by locking it to a high-finesse reference cavity made from an ultra-low expansion (ULE) glass spacer via the Pound-Drever-Hall (PDH) locking technique [116, 117]. The PDH lock reduces the linewidth of the transfer laser to about 1.5 Hz. More detailed information about the transfer laser system can be found in [113].

As the ULE cavity provides a reference for the transfer laser, it has to be well isolated from external perturbations. Temperature stabilization is employed together with vibration isolation equipment to decouple the cavity from the environment. This way, cavity length variations due to temperature fluctuations can be controlled to a high degree. However, even if temperature related effects are suppressed to a negligible level, the cavity length still changes slowly due to the aging of the ULE spacer material. This
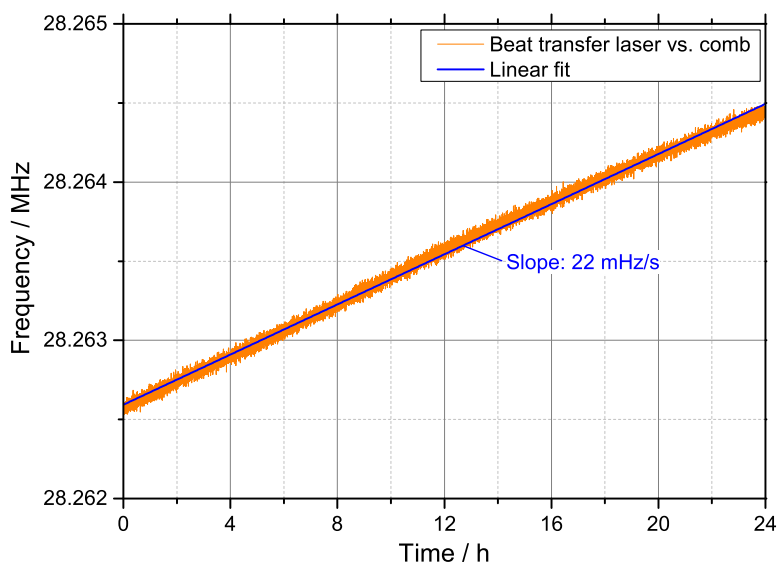


FIGURE A.1: Drift of the cavity stabilized transfer laser at MPQ measured against a frequency comb. A drift rate of $\approx$ 20 mHz/s is typically observed.
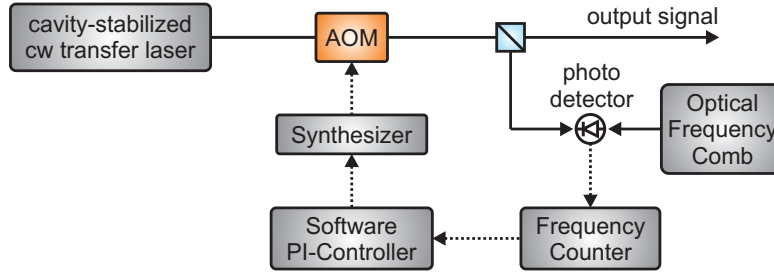
FIGURE A.2: Schematic of the experimental setup to cancel the ULE cavity induced frequency drift. An acousto-optic modulator (AOM) is used to shift the laser frequency slowly in the opposite direction compared to the cavity. A software PI control loop is used to deliver a drift-reduced output signal.

effect turns into a drift of the frequency of the transfer laser that is locked to the cavity. In the setup used at MPQ a linear drift of typically 20 mHz/s is observed as shown in Figure A.1.

In some cases, this drift can constitute a limiting factor for solving an experimental problem so that a cancellation of it is desirable. A system for canceling this inevitable frequency drift has been set up and is schematically shown in Figure A.2. An acousto-optic modulator (AOM) is used as a frequency shifter in a proportional-integral (PI) control loop and placed after the ULE cavity stabilized transfer laser. A heterodyne beat against an optical frequency comb is counted with a frequency counter (HP, Model: 53131A) and reveals the drift of the cw laser. Due to the stability of the frequency comb, the beat note has a standard deviation of about 50 Hz when measured with a gate time of 1 s. In order to determine the comparably small drift of the cw laser, 600 individual frequency measurements are performed and a linear fit of the data reveals the rate and


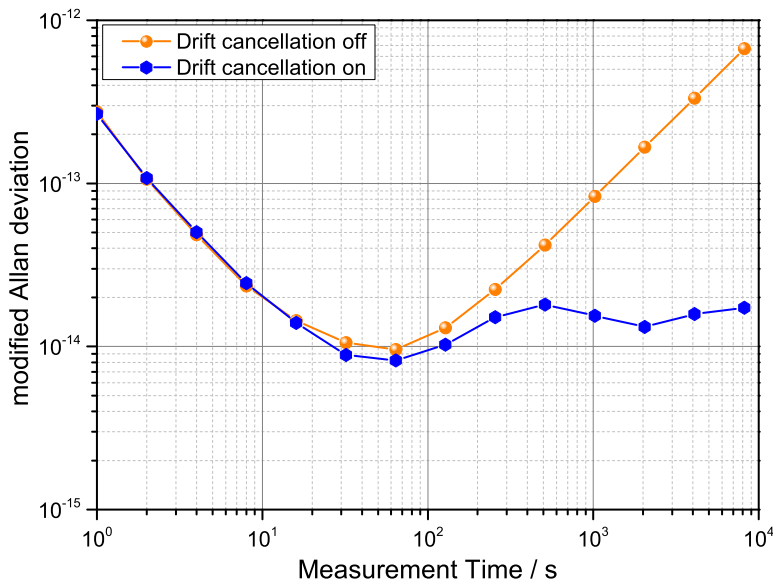
FIGURE A.3: Fractional frequency instability of the beat signal of the cavity stabilized cw laser against the frequency comb measured with a Π-type frequency counter. The short term instability is set by the frequency comb. For time scales longer than a few hundred seconds, the drift cancellation reduces the instability significantly.

the sign of the drift. The result equals the momentary drift rate. For the following 10 min it is assumed that the rate does not change significantly. An average over those 600 data points is used as a nominal value for the software PI control loop. In the next 10 min, the controller steers a frequency synthesizer (Agilent, Model: 33521A) once every second with a rate equal to the determined drift rate of the cw laser but with the opposite sign. Simultaneously, the current beat frequency is measured continuously and those new values are then used for the determination of the drift rate for the following 10 min.

The low short term stability of the hydrogen maser to which the comb is locked limits the accuracy with which the drift rate can be measured. A meaningful determination of the drift rate reduces the speed of the whole control loop. For this reason, only medium and long term drifts can be canceled out. The effect of the drift cancellation loop can be seen in Figure A.3 which shows the instability of the beat note between the cw laser and the frequency comb. On short time scales, the instability is limited by the comb that in turn is stabilized to a hydrogen maser. Only after a few hundred seconds the cancellation of the drift becomes noticeable. On long time scales, the effect is significant and the instability of the cw laser can be kept below $2 \times 10^{-14}$.

# Bibliography

[1] S. W. Thompson and P. G. Tait, *Treatise on natural philosophy.* Cambridge University Press, 1879, vol. 1. [Online]. Available: http://books.google.de/books?id=X4QTK9mkTaAC

[2] J. P. Gordon, H. J. Zeiger, and C. H. Townes, "The maser - New type of microwave amplifier, frequency standard, and spectrometer," *Phys. Rev.*, vol. 99, pp. 1264–1274, Aug 1955. [Online]. Available: http://link.aps.org/doi/10.1103/PhysRev.99.1264

[3] H. Schnatz, B. Lipphardt, J. Helmcke, F. Riehle, and G. Zinner, "First phase-coherent frequency measurement of visible radiation," *Phys. Rev. Lett.*, vol. 76, pp. 18–21, Jan 1996. [Online]. Available: http://link.aps.org/doi/10.1103/PhysRevLett.76.18

[4] J. Ye and S. Cundiff, *Femtosecond Optical Frequency Comb: Principle, Operation and Applications.* Springer, 2006. [Online]. Available: http://books.google.de/books?id=Myd2VdEUm-0C

[5] H. Dehmelt, "Monoion oscillator as potential ultimate laser frequency standard," *IEEE Transactions on Instrumentation and Measurement*, vol. IM-31, no. 2, pp. 83–87, 1982.

[6] P. Gill, "When should we change the definition of the second?" *Philosophical Transactions of the Royal Society A: Mathematical, Physical and Engineering Sciences*, vol. 369, no. 1953, pp. 4109–4130, 2011.

[7] A. Bauch, J. Achkar, S. Bize, D. Calonico, R. Dach, R. Hlavać, L. Lorini, T. Parker, G. Petit, D. Piester, K. Szymaniec, and P. Uhrich, "Comparison between frequency standards in Europe and the USA at the $10^{-15}$ uncertainty level," *Metrologia*, vol. 43, no. 1, p. 109, 2006. [Online]. Available: http://stacks.iop.org/0026-1394/43/i=1/a=016

[8] P. A. Williams, W. C. Swann, and N. R. Newbury, "High-stability transfer of an optical frequency over long fiber-optic links," *J. Opt. Soc. Am. B*, vol. 25, no. 8, pp. 1284–1293, Aug 2008. [Online]. Available: http://josab.osa.org/abstract.cfm?URI=josab-25-8-1284

[9] O. Terra, G. Grosche, and H. Schnatz, "Brillouin amplification in phase coherent transfer of optical frequencies over 480 km fiber," *Opt. Express*,

vol. 18, no. 15, pp. 16102–16111, Jul 2010. [Online]. Available: http://www.opticsexpress.org/abstract.cfm?URI=oe-18-15-16102

[10] M. Fujieda, M. Kumagai, S. Nagano, A. Yamaguchi, H. Hachisu, and T. Ido, "All-optical link for direct comparison of distant optical clocks," *Opt. Express*, vol. 19, no. 17, pp. 16498–16507, Aug 2011. [Online]. Available: http://www.opticsexpress.org/abstract.cfm?URI=oe-19-17-16498

[11] K. Predehl, G. Grosche, S. M. F. Raupach, S. Droste, O. Terra, J. Alnis, T. Legero, T. W. Hänsch, T. Udem, R. Holzwarth, and H. Schnatz, "A 920-kilometer optical fiber link for frequency metrology at the 19th decimal place," *Science*, vol. 336, no. 6080, pp. 441–444, 2012. [Online]. Available: http://www.sciencemag.org/content/336/6080/441.abstract

[12] O. Lopez, A. Kanj, P.-E. Pottie, D. Rovera, J. Achkar, C. Chardonnet, A. Amy-Klein, and G. Santarelli, "Simultaneous remote transfer of accurate timing and optical frequency over a public fiber network," *Applied Physics B*, vol. 110, no. 1, pp. 3–6, 2013. [Online]. Available: http://dx.doi.org/10.1007/s00340-012-5241-0

[13] S. Droste, F. Ozimek, T. Udem, K. Predehl, T. W. Hänsch, H. Schnatz, G. Grosche, and R. Holzwarth, "Optical-frequency transfer over a single-span 1840 km fiber link," *Phys. Rev. Lett.*, vol. 111, p. 110801, Sep 2013. [Online]. Available: http://link.aps.org/doi/10.1103/PhysRevLett.111.110801

[14] C. W. Chou, D. B. Hume, T. Rosenband, and D. J. Wineland, "Optical clocks and relativity," *Science*, vol. 329, no. 5999, pp. 1630–1633, 2010. [Online]. Available: http://www.sciencemag.org/content/329/5999/1630.abstract

[15] T. Rosenband, D. B. Hume, P. O. Schmidt, C. W. Chou, A. Brusch, L. Lorini, W. H. Oskay, R. E. Drullinger, T. M. Fortier, J. E. Stalnaker, S. A. Diddams, W. C. Swann, N. R. Newbury, W. M. Itano, D. J. Wineland, and J. C. Bergquist, "Frequency ratio of $Al^+$ and $Hg^+$ single-ion optical clocks; metrology at the 17th decimal place," *Science*, vol. 319, no. 5871, pp. 1808–1812, 2008. [Online]. Available: http://www.sciencemag.org/content/319/5871/1808.abstract

[16] C. G. Parthey, A. Matveev, J. Alnis, B. Bernhardt, A. Beyer, R. Holzwarth, A. Maistrou, R. Pohl, K. Predehl, T. Udem, T. Wilken, N. Kolachevsky, M. Abgrall, D. Rovera, C. Salomon, P. Laurent, and T. W. Hänsch, "Improved measurement of the hydrogen $1S - 2S$ transition frequency," *Phys. Rev. Lett.*, vol. 107, p. 203001, Nov 2011. [Online]. Available: http://link.aps.org/doi/10.1103/PhysRevLett.107.203001

[17] I. Ushijima, M. Takamoto, M. Das, T. Ohkubo, and H. Katori, "Cryogenic optical lattice clocks with a relative frequency difference of $1 \times 10^{-18}$," *arXiv:1405.4071 [physics.atom-ph]*, 2014. [Online]. Available: http://arxiv.org/abs/1405.4071

[18] F. Riehle, *Frequency Standards - Basics and Applications.* Wiley-VCH Verlag GmbH, Weinheim, 2004.

[19] D. Allan, "Statistics of atomic frequency standards," *Proc. IEEE*, vol. 54, pp. 221–230, 1966.

[20] W. Riley, "Handbook of frequency stability," *NIST Special Publication 1065*, 2008.

[21] E. Rubiola, "On the measurement of frequency and of its sample variance with high-resolution counters," *Review of Scientific Instruments*, vol. 76, no. 5, pp. 054 703 –054 703–6, 2005.

[22] D. Allan and J. Barnes, "A modified Allan variance with increased oscillator characterization ability," in *Thirty Fifth Annual Frequency Control Symposium. 1981*, 1981, pp. 470 – 475.

[23] S. Dawkins, J. McFerran, and A. Luiten, "Considerations on the measurement of the stability of oscillators with frequency counters," *Ultrasonics, Ferroelectrics and Frequency Control, IEEE Transactions on*, vol. 54, no. 5, pp. 918 –925, may 2007.

[24] J. A. Barnes, A. R. Chi, L. S. Cutler, D. J. Healey, D. B. Leeson, T. E. McGunigal, J. A. Mullen, W. L. Smith, R. L. Sydnor, R. F. C. Vessot, and G. M. R. Winkler, "Characterization of frequency stability," *IEEE Transactions on Instrumentation and Measurement*, vol. IM-20, no. 2, pp. 105 –120, may 1971.

[25] J. Rutman and F. Walls, "Characterization of frequency stability in precision frequency sources," *Proceedings of the IEEE*, vol. 79, no. 7, pp. 952 –960, jul 1991.

[26] G. Kramer and W. Klische, "Multi-channel synchronous digital phase recorder," in *Frequency Control Symposium and PDA Exhibition, 2001. Proceedings of the 2001 IEEE International*, 2001, pp. 144 –151.

[27] S. Johansson, "New frequency counting principle improves resolution," in *Proceedings of the 2005 IEEE International Frequency Control Symposium and Exposition*, 2005.

[28] *Datasheet Symmetricom 5071A*. [Online]. Available: http://www.symmetricom.com

[29] W. Demtröder, *Laser Spectroscopy: Basic Concepts and Instrumentation*. Springer-Verlag, 2003.

[30] A. Bauch, "Caesium atomic clocks: Function, performance and applications," *Measurement Science and Technology*, vol. 14, no. 8, p. 1159, 2003. [Online]. Available: http://stacks.iop.org/0957-0233/14/i=8/a=301

[31] T. Hänsch and A. Schawlow, "Cooling of gases by laser radiation," *Optics Communications*, vol. 13, no. 1, pp. 68 – 69, 1975. [Online]. Available: http://www.sciencedirect.com/science/article/pii/0030401875901595

[32] K. Gibble and S. Chu, "Laser-cooled Cs frequency standard and a measurement of the frequency shift due to ultracold collisions," *Phys. Rev. Lett.*, vol. 70, pp. 1771–1774, Mar 1993. [Online]. Available: http://link.aps.org/doi/10.1103/PhysRevLett.70.1771

[33] R. Wynands and S. Weyers, "Atomic fountain clocks," *Metrologia*, vol. 42, no. 3, p. S64, 2005. [Online]. Available: http://stacks.iop.org/0026-1394/42/i=3/a=S08

[34] M. A. Lombardi, T. P. Heavner, and S. R. Jefferts, "NIST primary frequency standards and the realization of the SI second," *NCSL International Measure*, 2007.

[35] R. Li, K. Gibble, and K. Szymaniec, "Improved accuracy of the NPL-CsF2 primary frequency standard: Evaluation of distributed cavity phase and microwave lensing frequency shifts," *Metrologia*, vol. 48, no. 5, p. 283, 2011. [Online]. Available: http://stacks.iop.org/0026-1394/48/i=5/a=007

[36] G. Santarelli, P. Laurent, P. Lemonde, A. Clairon, A. G. Mann, S. Chang, A. N. Luiten, and C. Salomon, "Quantum projection noise in an atomic fountain: A high stability cesium frequency standard," *Phys. Rev. Lett.*, vol. 82, pp. 4619–4622, Jun 1999. [Online]. Available: http://link.aps.org/doi/10.1103/PhysRevLett.82.4619

[37] L. Lorini, N. Ashby, A. Brusch, S. Diddams, R. Drullinger, E. Eason, T. Fortier, P. Hastings, T. Heavner, D. Hume, W. Itano, S. Jefferts, N. Newbury, T. Parker, T. Rosenband, J. Stalnaker, W. Swann, D. Wineland, , and J. Bergquist, "Recent atomic clock comparisons at NIST," *Eur. Phys. J. Special Topics*, vol. 163, pp. 19–35, 2008.

[38] J. Camparo, "The rubidium atomic clock and basic research," *Physics Today*, vol. 60, no. 11, pp. 33–39, 2007. [Online]. Available: http://dx.doi.org/10.1063/1.2812121

[39] S. Peil, J. L. Hanssen, T. B. Swanson, J. Taylor, and C. R. Ekstrom, "Evaluation of long term performance of continuously running atomic fountains," *arXiv:1406.1376 [physics.atom-ph]*, 2014. [Online]. Available: http://arxiv.org/abs/1406.1376

[40] A. Giles, A. Mann, S. Jones, D. Blair, and M. Buckingham, "A very high stability sapphire loaded superconducting cavity oscillator," *Physica B: Condensed Matter*, vol. 165–166, Part 1, pp. 145 – 146, 1990, Proceedings of the 19th International Conference on Low Temperature Physics. [Online]. Available: http://www.sciencedirect.com/science/article/pii/S0921452690809226

[41] J. Hartnett and N. Nand, "Ultra-low vibration pulse-tube cryocooler stabilized cryogenic sapphire oscillator with $10^{-16}$ fractional frequency stability," *IEEE Transactions on Microwave Theory and Techniques*, vol. 10, p. 420, 2010.

[42] Y. Y. Jiang, A. D. Ludlow, N. D. Lemke, R. W. Fox, J. A. Sherman, L.-S. Ma, and C. W. Oates, "Making optical atomic clocks more stable with $10^{-16}$-level laser stabilization," *Nat. Photon.*, vol. 5, no. 3, pp. 158–161, Mar. 2011. [Online]. Available: http://dx.doi.org/10.1038/nphoton.2010.313

[43] R. Holzwarth, T. Udem, T. W. Hänsch, J. C. Knight, W. J. Wadsworth, and P. S. J. Russell, "Optical frequency synthesizer for precision spectroscopy," *Phys. Rev. Lett.*, vol. 85, pp. 2264–2267, Sep 2000. [Online]. Available: http://link.aps.org/doi/10.1103/PhysRevLett.85.2264

[44] T. M. Fortier, M. S. Kirchner, F. Quinlan, J. Taylor, J. C. Bergquist, T. Rosenband, N. Lemke, A. Ludlow, Y. Jiang, C. W. Oates, and S. A. Diddams, "Generation of ultrastable microwaves via optical frequency division," *Nature Photonics*, vol. 5, no. 7, pp. 425–429, Jul. 2011. [Online]. Available: http://dx.doi.org/10.1038/nphoton.2011.121

[45] A. Haboucha, W. Zhang, T. Li, M. Lours, A. N. Luiten, Y. L. Coq, and G. Santarelli, "Optical-fiber pulse rate multiplier for ultralow phase-noise signal generation," *Opt. Lett.*, vol. 36, no. 18, pp. 3654–3656, Sep 2011. [Online]. Available: http://ol.osa.org/abstract.cfm?URI=ol-36-18-3654

[46] J. Alnis, A. Matveev, N. Kolachevsky, T. Udem, and T. W. Hänsch, "Subhertz linewidth diode lasers by stabilization to vibrationally and thermally compensated ultralow-expansion glass Fabry-Pérot cavities," *Physical Review A*, vol. 77, 2008.

[47] H. Katori, "Optical lattice clocks and quantum metrology," *Nature Photonics*, vol. 5, no. 4, pp. 203–210, Apr. 2011. [Online]. Available: http://dx.doi.org/10.1038/nphoton.2011.45

[48] D. J. Wineland and W. M. Itano, "Laser cooling of atoms," *Phys. Rev. A*, vol. 20, pp. 1521–1540, Oct 1979. [Online]. Available: http://link.aps.org/doi/10.1103/PhysRevA.20.1521

[49] W. Neuhauser, M. Hohenstatt, P. Toschek, and H. Dehmelt, "Optical-sideband cooling of visible atom cloud confined in parabolic well," *Phys. Rev. Lett.*, vol. 41, pp. 233–236, Jul 1978. [Online]. Available: http://link.aps.org/doi/10.1103/PhysRevLett.41.233

[50] V. Chebotayev, V. Goldort, V. Klementyev, M. Nikitin, B. Timchenko, and V. Zakharyash, "Development of an optical time scale," *Applied Physics B*, vol. 29, no. 1, pp. 63–65, 1982. [Online]. Available: http://dx.doi.org/10.1007/BF00694370

[51] C. O. Weiss, G. Kramer, B. Lipphardt, and E. Garcia, "Frequency measurement of a $CH_4$ hyperfine line at 88 THz/'Optical clock'," *IEEE Journal of Quantum Electronics*, vol. 24, no. 10, pp. 1970–1972, 1988.

[52] M. Takamoto, F.-L. Hong, R. Higashi, and H. Katori, "An optical lattice clock," *Nature*, vol. 435, no. 7040, pp. 321–324, May 2005. [Online]. Available: http://dx.doi.org/10.1038/nature03541

[53] J. Hartnett, N. Nand, C. Wang, and J.-M. Le Floch, "Cryogenic sapphire oscillator using a low-vibration design pulse-tube cryocooler: First results," *IEEE Transactions on Ultrasonics, Ferroelectrics and Frequency Control*, vol. 57, no. 5, pp. 1034–1038, 2010.

[54] C. W. Chou, D. B. Hume, J. C. J. Koelemeij, D. J. Wineland, and T. Rosenband, "Frequency comparison of two high-accuracy $Al^+$ optical clocks," *Phys. Rev. Lett.*, vol. 104, p. 070802, Feb 2010. [Online]. Available: http://link.aps.org/doi/10.1103/PhysRevLett.104.070802

[55] N. Huntemann, M. Okhapkin, B. Lipphardt, S. Weyers, C. Tamm, and E. Peik, "High-accuracy optical clock based on the octupole transition in $^{171}Yb^{+}$," *Phys. Rev. Lett.*, vol. 108, p. 090801, Feb 2012. [Online]. Available: http://link.aps.org/doi/10.1103/PhysRevLett.108.090801

[56] P. O. Schmidt, T. Rosenband, C. Langer, W. M. Itano, J. C. Bergquist, and D. J. Wineland, "Spectroscopy using quantum logic," *Science*, vol. 309, no. 5735, pp. 749–752, 2005. [Online]. Available: http://www.sciencemag.org/content/309/5735/749.abstract

[57] N. D. Lemke, A. D. Ludlow, Z. W. Barber, T. M. Fortier, S. A. Diddams, Y. Jiang, S. R. Jefferts, T. P. Heavner, T. E. Parker, and C. W. Oates, "Spin-1/2 optical lattice clock," *Phys. Rev. Lett.*, vol. 103, Aug 2009. [Online]. Available: http://link.aps.org/doi/10.1103/PhysRevLett.103.063001

[58] W.-H. Tseng, "A survey of time transfer via a bidirectional fiber link for precise calibration services," *NCSL International Measure J. Meas. Sci.*, vol. 8, pp. 70–77, 2013.

[59] J. Terrien, "News from the international bureau of weights and measures," *Metrologia*, vol. 4, no. 1, p. 41, 1968. [Online]. Available: http://stacks.iop.org/0026-1394/4/i=1/a=006

[60] L. Galleani and P. Tavella, "Time and the Kalman filter," *Control Systems, IEEE*, vol. 30, no. 2, pp. 44–65, 2010.

[61] [Online]. Available: http://www.bipm.org/en/scientific/tai/ftp_server/introduction.html

[62] [Online]. Available: http://www.iag-aig.org

[63] T. A. Herring, J. L. Davis, and I. I. Shapiro, "Geodesy by radio interferometry: The application of kalman filtering to the analysis of very long baseline interferometry data," *Journal of Geophysical Research: Solid Earth*, vol. 95, no. B8, pp. 12 561–12 581, 1990. [Online]. Available: http://dx.doi.org/10.1029/JB095iB08p12561

[64] R. Rummel, G. Balmino, J. Johannessen, P. Visser, and P. Woodworth, "Dedicated gravity field missions—principles and aims," *Journal of Geodynamics*, vol. 33, no. 1–2, pp. 3 – 20, 2002, earth's Gravity and Magnetic Fields from Space. [Online]. Available: http://www.sciencedirect.com/science/article/pii/S0264370701000503

[65] A. Antognini, F. Nez, K. Schuhmann, F. D. Amaro, F. Biraben, J. M. R. Cardoso, D. S. Covita, A. Dax, S. Dhawan, M. Diepold, L. M. P. Fernandes, A. Giesen, A. L. Gouvea, T. Graf, T. W. Hänsch, P. Indelicato, L. Julien, C.-Y. Kao, P. Knowles, F. Kottmann, E.-O. Le Bigot, Y.-W. Liu, J. A. M. Lopes, L. Ludhova, C. M. B. Monteiro, F. Mulhauser, T. Nebel, P. Rabinowitz, J. M. F. dos Santos, L. A. Schaller, C. Schwob, D. Taqqu, J. F. C. A. Veloso, J. Vogelsang, and R. Pohl, "Proton structure from the measurement of 2s-2p transition frequencies of muonic hydrogen," *Science*, vol. 339, no. 6118, pp. 417–420, 2013. [Online]. Available: http://www.sciencemag.org/content/339/6118/417.abstract

[66] J.-P. Uzan, "The fundamental constants and their variation: Observational and theoretical status," *Rev. Mod. Phys.*, vol. 75, pp. 403–455, Apr 2003. [Online]. Available: http://link.aps.org/doi/10.1103/RevModPhys.75.403

[67] J. K. Webb, V. V. Flambaum, C. W. Churchill, M. J. Drinkwater, and J. D. Barrow, "Search for time variation of the fine structure constant," *Phys. Rev. Lett.*, vol. 82, pp. 884–887, Feb 1999. [Online]. Available: http://link.aps.org/doi/10.1103/PhysRevLett.82.884

[68] T. M. Fortier, N. Ashby, J. C. Bergquist, M. J. Delaney, S. A. Diddams, T. P. Heavner, L. Hollberg, W. M. Itano, S. R. Jefferts, K. Kim, F. Levi, L. Lorini, W. H. Oskay, T. E. Parker, J. Shirley, and J. E. Stalnaker, "Precision atomic spectroscopy for improved limits on variation of the fine structure constant and local position invariance," *Phys. Rev. Lett.*, vol. 98, p. 070801, Feb 2007. [Online]. Available: http://link.aps.org/doi/10.1103/PhysRevLett.98.070801

[69] E. Peik, "Fundamental constants and units and the search for temporal variations," *Nuclear Physics B - Proceedings Supplements*, vol. 203–204, no. 0, pp. 18 – 32, 2010. [Online]. Available: http://www.sciencedirect.com/science/article/pii/S0920563210001866

[70] J. Alfaro, H. A. Morales-Técotl, and L. F. Urrutia, "Loop quantum gravity and light propagation," *Phys. Rev. D*, vol. 65, p. 103509, Apr 2002. [Online]. Available: http://link.aps.org/doi/10.1103/PhysRevD.65.103509

[71] R. F. C. Vessot, M. W. Levine, E. M. Mattison, E. L. Blomberg, T. E. Hoffman, G. U. Nystrom, B. F. Farrel, R. Decher, P. B. Eby, C. R. Baugher, J. W. Watts, D. L. Teuber, and F. D. Wills, "Test of relativistic gravitation with a space-borne hydrogen maser," *Phys. Rev. Lett.*, vol. 45, pp. 2081–2084, Dec 1980. [Online]. Available: http://link.aps.org/doi/10.1103/PhysRevLett.45.2081

[72] M. Schioppo, G. Tino, N. Poli, M. Tarallo, D. Sutyrin, C. Lisdat, J. Vellore Winfred, S. Falke, U. Sterr, T. Legero, F. Riehle, and L. Cacciapuoti, "Development of a transportable laser cooled strontium source for future applications in space," in *24th European Frequency and Time Forum*, 2010, pp. 1–6.

[73] M. Lombardi, L. Nelson, A. Novick, and V. Zhang, "Time and frequency measurements using the global positioning system," *Cal Lab: International Journal of Metrology*, vol. 8, no. 3, pp. 26–33, July 2001.

[74] [Online]. Available: http://www.glonass-ianc.rsa.ru/en/

[75] [Online]. Available: http://www.esa.int/Our_Activities/Navigation/The_future_-_Galileo/The_first_four_satellites

[76] D. Matsakis, "Report from the U.S. Naval Observatory," *Timing Session of the Civil GPS Service Interface Committee*, 2011.

[77] D. W. Allan and M. A. Weiss, "Accurate time and frequency transfer during common-view of a GPS satellite," in *Proc. of the 34th Ann. Freq. Control Symposium, Ft. Monmouth, WJ 07703*, 1980.

[78] T. Feldmann, "Advances in GPS based Time and Frequency Comparisons for Metrological Use," Ph.D. dissertation, Gottfried Wilhelm Leibniz Universität Hannover, 2011.

[79] W. Lewandowski, J. Azoubib, G. de Jong, J. Nawrocki, and J. Danaher, "A new approach to international satellite time and frequency comparisons: 'all-in-view' multichannel GPS + GLONASS observations," in *Proc. of the 10th International Technical Meeting of the Satellite Division of The Institute of Navigation (ION GPS 1997)*, 1997.

[80] M. Weiss, G. Petit, and Z. Jiang, "A comparison of GPS common-view time transfer to all-in-view," in *Proceedings of the 2005 IEEE International Frequency Control Symposium and Exposition, 2005.*, 2005.

[81] S. W. Lee, B. E. Schutz, C.-B. Lee, and S. H. Yang, "A study on the common-view and all-in-view GPS time transfer using carrier-phase measurements," *Metrologia*, vol. 45, no. 2, p. 156, 2008. [Online]. Available: http://stacks.iop.org/0026-1394/45/i=2/a=005

[82] D. Piester and H. Schnatz, "Novel techniques for remote time and frequency comparisons," *Special Issue / PTB-Mitteilungen*, vol. 119, pp. 33–44, 2009.

[83] D. Hanson, "Fundamentals of two-way time and frequency transfer by satellite," *43rd Annual Symposium on Frequency Control*, pp. 174–178, 1989.

[84] D. Piester, A. Bauch, M. Fujieda, T. Gotoh, M. Aida, H. Maeno, M. Hosokawa, and S. H. Yang, "Studies on instabilities in long-baseline two-way satellite time and frequency transfer (TWSTFT) including a troposphere delay model," *Proc. 39th Annual Precise Time and Time Interval (PTTI) Systems and Applications Meeting*, pp. 211–222, 2008.

[85] D. Piester, M. Rost, M. Fujieda, T. Feldmann, and A. Bauch, "Remote atomic clock synchronization via satellites and optical fibers," *Adv. Radio Sci.*, vol. 9, pp. 1–7, 2011.

[86] M. Fujieda, T. Gotoh, F. Nakagawa, R. Tabuchi, M. Aida, and J. Amagai, "Carrier-phase-based two-way satellite time and frequency transfer," *IEEE Transactions on Ultrasonics, Ferroelectrics and Frequency Control*, vol. 59, no. 12, pp. 2625 –2630, dec. 2012.

[87] M. Fujieda, D. Piester, T. Gotoh, J. Becker, M. Aida, and A. Bauch, "Carrier-phase two-way satellite frequency transfer over a very long baseline," *Metrologia*, vol. 51, no. 3, p. 253, 2014. [Online]. Available: http://stacks.iop.org/0026-1394/51/i=3/a=253

[88] N. Hinkley, J. A. Sherman, N. B. Phillips, M. Schioppo, N. D. Lemke, K. Beloy, M. Pizzocaro, C. W. Oates, and A. D. Ludlow, "An atomic clock with $10^{-18}$ instability," *Science*, vol. 341, no. 6151, pp. 1215–1218, 2013. [Online]. Available: http://www.sciencemag.org/content/341/6151/1215.abstract

[89] O. Lopez, A. Amy-Klein, C. Daussy, C. Chardonnet, F. Narbonneau, M. Lours, and G. Santarelli, "86-km optical link with a resolution of $2 \times 10^{-18}$ for RF frequency transfer," *The European Physical Journal D - Atomic, Molecular, Optical and Plasma Physics*, vol. 48, pp. 35–41, 2008. [Online]. Available: http://dx.doi.org/10.1140/epjd/e2008-00059-5

[90] G. Marra, H. S. Margolis, and D. J. Richardson, "Dissemination of an optical frequency comb over fiber with $3 \times 10^{-18}$ fractional accuracy," *Opt. Express*, vol. 20, no. 2, pp. 1775–1782, Jan 2012. [Online]. Available: http://www.opticsexpress.org/abstract.cfm?URI=oe-20-2-1775

[91] F. R. Giorgetta, W. C. Swann, L. C. Sinclair, E. Baumann, I. Coddington, and N. R. Newbury, "Optical two-way time and frequency transfer over free space," *Nature Photonics*, vol. 7, no. 6, pp. 434–438, Jun. 2013. [Online]. Available: http://dx.doi.org/10.1038/nphoton.2013.69

[92] M. Xin, K. Şafak, M. Y. Peng, P. T. Callahan, and F. X. Kärtner, "One-femtosecond, long-term stable remote laser synchronization over a 3.5-km fiber link," *Opt. Express*, vol. 22, no. 12, pp. 14 904–14 912, Jun 2014. [Online]. Available: http://www.opticsexpress.org/abstract.cfm?URI=oe-22-12-14904

[93] D. R. Leibrandt, M. J. Thorpe, M. Notcutt, R. E. Drullinger, T. Rosenband, and J. C. Bergquist, "Spherical reference cavities for frequency stabilization of lasers in non-laboratory environments," *Opt. Express*, vol. 19, no. 4, pp. 3471–3482, Feb 2011. [Online]. Available: http://www.opticsexpress.org/abstract.cfm?URI=oe-19-4-3471

[94] R. Wu, V. R. Supradeepa, C. M. Long, D. E. Leaird, and A. M. Weiner, "Generation of very flat optical frequency combs from continuous-wave lasers using cascaded intensity and phase modulators driven by tailored radio frequency waveforms," *Opt. Lett.*, vol. 35, no. 19, pp. 3234–3236, Oct 2010. [Online]. Available: http://ol.osa.org/abstract.cfm?URI=ol-35-19-3234

[95] P. Del'Haye, A. Schliesser, O. Arcizet, T. Wilken, R. Holzwarth, and T. J. Kippenberg, "Optical frequency comb generation from a monolithic microresonator," *Nature*, vol. 450, no. 7173, pp. 1214–1217, Dec. 2007. [Online]. Available: http://dx.doi.org/10.1038/nature06401

[96] F. Tauser, A. Leitenstorfer, and W. Zinth, "Amplified femtosecond pulses from an Er:fiber system: Nonlinear pulse shortening and selfreferencing detection of the carrier-envelope phase evolution," *Opt. Express*, vol. 11, no. 6, pp. 594–600, Mar 2003. [Online]. Available: http://www.opticsexpress.org/abstract.cfm?URI=oe-11-6-594

[97] T. Wilken, T. W. Hänsch, R. Holzwarth, P. Adel, and M. Mei, "Low phase noise 250 MHz repetition rate fiber fs laser for frequency comb applications," in *Conference on Lasers and Electro-Optics*. Optical Society of America, 2007, p. CMR3. [Online]. Available: http://www.opticsinfobase.org/abstract.cfm?URI=CLEO-2007-CMR3

[98] C. V. Raman and K. S. Krishnan, "A New Type of Secondary Radiation," *Nature*, vol. 121, pp. 501–502, 1928.

[99] C. Headley and G. Agrawal, *Raman Amplification in Fiber Optical Communication Systems*, ser. Electronics & Electrical. Elsevier Academic Press, 2005. [Online]. Available: http://books.google.de/books?id=llzJB8qKGBEC

[100] E. Ippen and R. Stolen, "Stimulated Brillouin scattering in optical fibers," *Applied Physics Letters*, vol. 21, no. 11, pp. 539–541, 1972. [Online]. Available: http://scitation.aip.org/content/aip/journal/apl/21/11/10.1063/1.1654249

[101] G. B. Hocker, "Fiber-optic sensing of pressure and temperature," *Appl. Opt.*, vol. 18, no. 9, pp. 1445–1448, May 1979. [Online]. Available: http://ao.osa.org/abstract.cfm?URI=ao-18-9-1445

[102] G. Ghosh, "Model for the pressure-optic coefficients in optical materials," *Phys. Rev. B*, vol. 57, pp. 8178–8180, Apr 1998. [Online]. Available: http://link.aps.org/doi/10.1103/PhysRevB.57.8178

[103] L.-S. Ma, P. Jungner, J. Ye, and J. L. Hall, "Delivering the same optical frequency at two places: accurate cancellation of phase noise introduced by an optical fiber or other time-varying path," *Opt. Lett.*, vol. 19, no. 21, pp. 1777–1779, Nov 1994. [Online]. Available: http://ol.osa.org/abstract.cfm?URI=ol-19-21-1777

[104] A. Kersey, M. Marrone, and M. Davis, "Polarisation-insensitive fibre optic Michelson interferometer," *Electronics Letters*, vol. 27, pp. 518–520, 1991.

[105] T. Okoshi, K. Kikuchi, and A. Nakayama, "Novel method for high resolution measurement of laser output spectrum," *Electronics Letters*, vol. 16, no. 16, pp. 630–631, July 1980.

[106] N. R. Newbury, P. A. Williams, and W. C. Swann, "Coherent transfer of an optical carrier over 251 km," *Opt. Lett.*, vol. 32, no. 21, pp. 3056–3058, Nov 2007. [Online]. Available: http://ol.osa.org/abstract.cfm?URI=ol-32-21-3056

[107] F. M. Gardner, *Phaselock techniques; 3nd ed.* New York, NY: Wiley, 1979.

[108] O. Lopez, A. Haboucha, B. Chanteau, C. Chardonnet, A. Amy-Klein, and G. Santarelli, "Ultra-stable long distance optical frequency distribution using the internet fiber network," *Opt. Express*, vol. 20, no. 21, pp. 23 518–23 526, Oct 2012. [Online]. Available: http://www.opticsexpress.org/abstract.cfm?URI=oe-20-21-23518

[109] C. E. Calosso, E. Bertacco, D. Calonico, C. Clivati, G. A. Costanzo, M. Frittelli, F. Levi, A. Mura, and A. Godone, "Frequency transfer via a two-way optical phase comparison on a multiplexed fiber network," *Opt. Lett.*, vol. 39, no. 5, pp. 1177–1180, Mar 2014. [Online]. Available: http://ol.osa.org/abstract.cfm?URI=ol-39-5-1177

[110] S. W. Schediwy, D. Gozzard, K. G. H. Baldwin, B. J. Orr, R. B. Warrington, G. Aben, and A. N. Luiten, "High-precision optical-frequency dissemination on branching optical-fiber networks," *Opt. Lett.*, vol. 38, no. 15, pp. 2893–2896, Aug 2013. [Online]. Available: http://ol.osa.org/abstract.cfm?URI=ol-38-15-2893

[111] G. Grosche, "Eavesdropping time and frequency: phase noise cancellation along a time-varying path, such as an optical fiber," *Opt. Lett.*, vol. 39, no. 9, pp. 2545–2548, May 2014. [Online]. Available: http://ol.osa.org/abstract.cfm?URI=ol-39-9-2545

[112] A. Bercy, S. Guellati-Khelifa, F. Stefani, G. Santarelli, C. Chardonnet, P.-E. Pottie, O. Lopez, and A. Amy-Klein, "In-line extraction of an ultrastable frequency signal over an optical fiber link," *J. Opt. Soc. Am. B*, vol. 31, no. 4, pp. 678–685, Apr 2014. [Online]. Available: http://josab.osa.org/abstract.cfm?URI=josab-31-4-678

[113] K. Predehl, "A 920 km optical fiber link for frequency metrology at the 19th decimal place," Ph.D. dissertation, Ludwig-Maximilians-Universität München, 2012.

[114] International Telecommunication Union. (2009) Characteristics of a single-mode optical fibre and cable. [Online]. Available: http://www.itu.int/rec/T-REC-G. 652-200911-I/en

[115] H. Jiang, F. Kéfélian, P. Lemonde, A. Clairon, and G. Santarelli, "An agile laser with ultra-low frequency noise and high sweep linearity," *Opt. Express*, vol. 18, no. 4, pp. 3284–3297, Feb 2010. [Online]. Available: http://www.opticsexpress.org/abstract.cfm?URI=oe-18-4-3284

[116] R. Drever, J. Hall, F. Kowalski, J. Hough, G. Ford, A. Munley, and H. Ward, "Laser phase and frequency stabilization using an optical resonator," *Applied Physics B*, vol. 31, no. 2, pp. 97–105, 1983. [Online]. Available: http://dx.doi.org/10.1007/BF00702605

[117] E. D. Black, "An introduction to Pound–Drever–Hall laser frequency stabilization," *American Journal of Physics*, vol. 69, no. 1, pp. 79–87, 2001. [Online]. Available: http://scitation.aip.org/content/aapt/journal/ajp/69/1/10. 1119/1.1286663

[118] N. Gisin, J. P. Von der Weid, and J. p. Pellaux, "Polarization mode dispersion of short and long single-mode fibers," *Lightwave Technology, Journal of*, vol. 9, no. 7, pp. 821–827, Jul 1991.

[119] G. Grosche, O. Terra, K. Predehl, R. Holzwarth, B. Lipphardt, F. Vogt, U. Sterr, and H. Schnatz, "Optical frequency transfer via 146 km fiber link with $10^{-19}$ relative accuracy," *Opt. Lett.*, vol. 34, no. 15, pp. 2270–2272, Aug 2009. [Online]. Available: http://ol.osa.org/abstract.cfm?URI=ol-34-15-2270

[120] O. Lopez, A. Haboucha, F. Kéfélian, H. Jiang, B. Chanteau, V. Roncin, C. Chardonnet, A. Amy-Klein, and G. Santarelli, "Cascaded multiplexed optical link on a telecommunication network for frequency dissemination," *Opt.*

*Express*, vol. 18, no. 16, pp. 16 849–16 857, Aug 2010. [Online]. Available: http://www.opticsexpress.org/abstract.cfm?URI=oe-18-16-16849

[121] S. Raupach, T. Legero, C. Grebing, C. Hagemann, T. Kessler, A. Koczwara, B. Lipphardt, M. Misera, H. Schnatz, G. Grosche, and U. Sterr, "Subhertz-linewidth infrared frequency source with a long-term instability below $5 \times 10^{-15}$," *Appl. Phys. B.*, vol. 110, pp. 465–470, 2012.

[122] T. Udem, J. Reichert, T. W. Hänsch, and M. Kourogi, "Accuracy of optical frequency comb generators and optical frequency interval divider chains," *Opt. Lett.*, vol. 23, no. 17, pp. 1387–1389, Sep 1998. [Online]. Available: http://ol.osa.org/abstract.cfm?URI=ol-23-17-1387

[123] W.-K. Lee, D.-H. Yu, C. Y. Park, and J. Mun, "The uncertainty associated with the weighted mean frequency of a phase-stabilized signal with white phase noise," *Metrologia*, vol. 47, no. 1, p. 24, 2010. [Online]. Available: http://stacks.iop.org/0026-1394/47/i=1/a=004

[124] L. C. Sinclair, F. R. Giorgetta, W. C. Swann, E. Baumann, I. Coddington, and N. R. Newbury, "Optical phase noise from atmospheric fluctuations and its impact on optical time-frequency transfer," *Phys. Rev. A*, vol. 89, p. 023805, Feb 2014. [Online]. Available: http://link.aps.org/doi/10.1103/PhysRevA.89.023805

[125] B. S. Sheard, M. B. Gray, and D. E. McClelland, "High-bandwidth laser frequency stabilization to a fiber-optic delay line," *Appl. Opt.*, vol. 45, no. 33, pp. 8491–8499, Nov 2006. [Online]. Available: http://ao.osa.org/abstract.cfm?URI=ao-45-33-8491

[126] G. P. Agrawal, *Fiber-Optic Communication Systems*, 3rd ed. John Wiley & Sons, 2002.

[127] C. A. Greenhall, "Spectral ambiguity of Allan variance," *IEEE T. Instrumentation and Measurement*, vol. 47, no. 3, pp. 623–627, 1998.

[128] O. Terra, "Dissemination of ultra-stable optical frequencies over commercial fiber networks," Ph.D. dissertation, Gottfried Wilhelm Leibniz Universität Hannover, 2010.

[129] D. Calonico, E. K. Bertacco, C. E. Calosso, C. Clivati, G. A. Costanzo, M. Frittelli, A. Godone, A. Mura, N. Poli, D. V. Sutyrin, G. Tino, M. E. Zucco, and F. Levi, "Coherent optical frequency transfer at $5 \times 10^{-19}$ over a doubled 642 km fiber link," *arXiv:1404.0395v1 [physics.optics]*, 2014.

[130] G. Beutler, M. Rothacher, T. Springer, J. Kouba, and R. Neilan, "The international GPS service (IGS): An interdisciplinary service in support of earth sciences," *32nd Cospar Scientific Assembly, Nagoya, Japan*, 1998.

[131] J. Kouba and P. Héroux, "GPS precise point positioning using IGS orbit products," *GPS Solutions Quarterly Technical Journal*, vol. 5, pp. 12–28, 2001.

[132] [Online]. Available: http://www.nrcan.gc.ca/earth-sciences/geomatics/geodetic-reference-systems/tools-applications/10925#ppp

[133] C. Hackman, J. Levine, T. Parker, D. Piester, and J. Becker, "A new technique for estimating frequency from GPS carrier-phase time transfer data," in *Proceedings of the 2004 IEEE International Frequency Control Symposium and Exposition, 2004.*, Aug 2004, pp. 341–349.

[134] A. Bauch, S. Weyers, D. Piester, E. Staliuniene, and W. Yang, "Generation of UTC(PTB) as a fountain-clock based time scale," *Metrologia*, vol. 49, no. 3, p. 180, 2012. [Online]. Available: http://stacks.iop.org/0026-1394/49/i=3/a=180

[135] J. Kouba, "A guide to using international GNSS service (IGS) products," May 2009. [Online]. Available: http://igscb.jpl.nasa.gov/components/usage.html

[136] S. M. F. Raupach, S. Droste, H. Schnatz, and G. Grosche, "Measuring the relative synchronization error of frequency counters with sub-$\mu$s accuracy via a phase-stabilized fiber link," in *Proceedings of the 26th European Frequency and Time Forum*, 2012.

[137] A. Matveev, C. G. Parthey, K. Predehl, J. Alnis, A. Beyer, R. Holzwarth, T. Udem, T. Wilken, N. Kolachevsky, M. Abgrall, D. Rovera, C. Salomon, P. Laurent, G. Grosche, O. Terra, T. Legero, H. Schnatz, S. Weyers, B. Altschul, and T. W. Hänsch, "Precision measurement of the hydrogen $1S$-$2S$ frequency via a 920-km fiber link," *Phys. Rev. Lett.*, vol. 110, p. 230801, Jun 2013. [Online]. Available: http://link.aps.org/doi/10.1103/PhysRevLett.110.230801

[138] J. Frisch, D. Bernstein, D. Brown, and E. Cisneros, "A high stability, low noise RF distribution system," *Conf.Proc.*, vol. C0106181, pp. 816–818, 2001.

[139] M. Y. Peng, P. T. Callahan, A. H. Nejadmalayeri, S. Valente, M. Xin, L. Grüner-Nielsen, E. M. Monberg, M. Yan, J. M. Fini, and F. X. Kärtner, "Long-term stable, sub-femtosecond timing distribution via a 1.2-km polarization-maintaining fiber link: approaching $10^{-21}$ link stability," *Opt. Express*, vol. 21, no. 17, pp. 19 982–19 989, Aug 2013. [Online]. Available: http://www.opticsexpress.org/abstract.cfm?URI=oe-21-17-19982

[140] D. Thacker and W. Shillue, "Atacama large millimeter array local oscillator: How photonics is enabling millimeter-wave astronomy," in *Optical Fiber Communication Conference/National Fiber Optic Engineers Conference 2011*. Optical Society of America, 2011, p. OThJ1. [Online]. Available: http://www.opticsinfobase.org/abstract.cfm?URI=OFC-2011-OThJ1

[141] K. Sato, T. Hara, M. Fujishita, S. Kuji, S. Tsuruta, Y. Tamura, T. Sasao, K. Sato, and S. Manabe, "Application of phase-stabilized optical fiber in transmission of reference and IF signals in VLBI observation," *Instrumentation and Measurement, IEEE Transactions on*, vol. 41, no. 3, pp. 385–389, Jun 1992.

[142] M. Calhoun, S. Huang, and R. Tjoelker, "Stable photonic links for frequency and time transfer in the deep-space network and antenna arrays," *Proceedings of the IEEE*, vol. 95, no. 10, pp. 1931–1946, Oct 2007.

[143] A. Derevianko and M. Pospelov, "Hunting for topological dark matter with atomic clocks," *arXiv:1311.1244 [physics.atom-ph]*, 2014.

# List of Publications

**Peer-reviewed publications**

1. **Optical-frequency transfer over a single-span 1840 km fiber link**
   S. Droste, F. Ozimek, Th. Udem, K. Predehl, T. W. Hänsch, H. Schnatz, G. Grosche,
   R. Holzwarth
   Physical Review Letters **111**, 110801 (2013)

2. **A 920 kilometer optical fiber link for frequency metrology at the 19th
   decimal place**
   K. Predehl, G. Grosche, S. M. F. Raupach, S. Droste, O. Terra, J. Alnis, Th.
   Legero, T. W. Hänsch, Th. Udem, R. Holzwarth, H. Schnatz
   Science **336**, 441 (2012)

**Non-peer-reviewed publications**

1. **High resolution characterization of a 450-km-baseline GPS carrier-phase
   link via optical fiber**
   S. Droste, C. Grebing, J. Leute, S. M. F. Raupach, A. Bauch, R. Holzwarth,
   G. Grosche
   in *Proceedings of the 28th European Frequency and Time Forum* (2014)

2. **Optical-frequency transfer via 1840 km fiber link with superior stability**
   S. Droste, F. Ozimek, Th. Udem, K. Predehl, T. W. Hänsch, H. Schnatz, G. Grosche,
   R. Holzwarth
   in *Proceedings of the 2014 IEEE International Frequency Control Symposium* (2014)

3. **Characterization of a 450-km-baseline GPS carrier-phase link using an
   optical fiber link**
   S. Droste, C. Grebing, J. Leute, S. M. F. Raupach, A. Bauch, G. Grosche, R. Holzwarth
   in *Proceedings of the 2014 IEEE International Frequency Control Symposium* (2014)

4. **Precision spectroscopy of atomic hydrogen**
   A. Beyer, Ch. G. Parthey, N. Kolachevsky, J. Alnis, K. Khabarova, R. Pohl, E. Pe-
   ters, D. C. Yost, A. Matveev, K. Predehl, S. Droste, T. Wilken, R. Holzwarth,
   T. W. Hänsch, M. Abgrall, D. Rovera, Ch. Salomon, Ph. Laurent, Th. Udem
   in *Proceedings of the International Conference on Optics, Lasers and Spectroscopy*
   (2013)

5. **Optical frequency transfer over a single-span 1840-km fiber link**
   S. Droste, F. Ozimek, Th. Udem, T. W. Hänsch, S. M. F. Raupach, H. Schnatz,
   G. Grosche, R. Holzwarth
   in *Proceedings of the 27th European Frequency and Time Forum* (2013)

6. **Measuring the relative synchronization error of frequency counters with sub-$\mu$s accuracy via a phase stabilized fiber link**
   S. M. F. Raupach, S. Droste, H. Schnatz, G. Grosche
   in *Proceedings of the 26th European Frequency and Time Forum* (2012)

7. **High performance frequency comparisons over optical fibre**
   G. Grosche, K. Predehl, S. M. F. Raupach, H. Schnatz, O. Terra, S. Droste,
   R. Holzwarth
   in *Proceedings of CLEO/IQEC* (2011)

# Conference Contributions

- 2014 European Frequency and Time Forum (EFTF), Neuchatel, Switzerland

- 2014 Conference on Lasers and Electro-Optics (CLEO), San Jose, California, USA

- 2014 International Frequency Control Symposium (IFCS), Taipei, Taiwan

- 2014 Spring meeting of the German Physical Society, Berlin, Germany

- 2013 Nippon Telegraph and Telephone (NTT) Corporation BRL School, Tokyo,
  Japan

- 2013 Joint IEEE-International Frequency Control Symposium (IFCS) and European Frequency and Time Forum (EFTF), Prague, Czech Republic

- 2013 Conference on Lasers and Electro-Optics (CLEO), **Invited Talk**, San Jose,
  California, USA

- 2013 Spring meeting of the German Physical Society, Hanover, Germany

- 2012 Workshop on Optical Networks for Accurate Time and Frequency Transfer,
  Hoofddorp, The Netherlands

- 2012 Conference on Lasers and Electro-Optics (CLEO), San Jose, California, USA

- 2012 Spring meeting of the German Physical Society, Stuttgart, Germany

# Danksagung

Zunächst einmal möchte ich mich sehr bei Herrn Prof. Hänsch dafür bedanken, Teil seiner tollen Arbeitsgruppe gewesen sein zu dürfen. Die wissenschaftliche Expertise und die enormen Freiheiten bilden das ideale Umfeld für jeden Doktoranden. Nicht zuletzt deswegen war es eine spannende, lehrreiche und vor allem schöne Zeit am MPQ.

Betreut wurde ich größtenteils von Ronald Holzwarth. Von Dir, Ronald, habe ich in unseren wöchentlichen Diskussionen sicherlich am meisten gelernt. Egal ob es um experimentelle Details ging oder darum, das Gesamtbild nicht aus den Augen zu verlieren; Du hattest immer Antworten parat, die letztlich Stück für Stück zum Ziel geführt haben. Ich weiß noch, wie wir uns auf der Photonics West das erste Mal unterhalten haben und nur kurze Zeit später feierte ich dann auch schon meinen Einstand. Dafür, dass Du mir die Chance gegeben hast hier zu promovieren, möchte ich mich noch einmal herzlich bedanken.

Wenn es um wissenschaftliche Fragen ging, war Thomas Udem meist in greifbarer Nähe und stets bereit sich meiner Fragen anzunehmen. Auch wenn ich des Öfteren von Deinem geballten Wissen nahezu erschlagen wurde, so hast Du doch immer einen Weg gefunden, mir Deine Gedanken und Ideen verständlich zu machen. Abgesehen davon habe ich unsere Radtouren von und nach Ringberg immer sehr genossen. Sogar so sehr, dass ich Dir regelmäßig an der Mauer von Emmerkofen selbstlos den Vortritt überlassen habe ☺

Übernommen habe ich das "Link-Projekt" von meiner Vorgängerin Katharina Predehl. Katha, Du warst anfangs wohl die einzige Person, die sich in dem Gewirr von Fasern zurecht gefunden hat. Der erste Eindruck eines großen Durcheinanders sollte sich aber schnell verflüchtigen, denn Du hast mir ein ausgesprochen gut funktionierendes und einzigartiges System hinterlassen. Unvergessen sind auch unsere Aktivitäten außerhalb des Labors; allen voran die Abende auf der Wiesn, an die ich mich immer wieder gern zurück erinnere.

Eine Besonderheit meiner Arbeit war, dass sich das Experiment über zwei Labore und eine fast 1000 km lange Strecke dazwischen erstreckte. Bei allen Messungen waren daher meine Kollegen von der PTB beteiligt, zu denen Harald Schnatz, Gesine Grosche, Sebastian Raupach und zuletzt auch Christian Grebing, Julia Leute und Andreas Bauch zählten. Bei Euch allen möchte ich mich ebenfalls herzlich für die gute Zusammenarbeit bedanken. Darüber hinaus ein großes Dankeschön an Fritz Riehle für die Bereitschaft, Teil meines Prüfungskomitees zu sein und vor allem für seine Unterstützung beim Abschluss meiner Promotion.

Zu einer meiner wichtigsten Anlaufstellen bei Fragen zu so ziemlich allen erdenklichen Dingen hat sich mein Bürokollege Andreas Vernaleken entwickelt. Andy, Du standest

mir nicht nur stets mit Rat und Tat zur Seite, sondern wir hatten auch außerhalb des Instituts eine verdammt gute Zeit. Du hast ganz entscheidend dazu beigetragen die Stimmung bei der Arbeit zu erhellen. Wenn ich frustriert war, hast Du immer einen Weg gefunden mich aufzuheitern und fast täglich warst Du an diversen lustigen Situationen beteiligt. Oft resultierten diese Situationen aus irgendwelchen Witzen heraus. Auch wenn die meisten dieser Witze durch ein eher niedriges Niveau auffielen, wofür wir alle zweifellos großes Talent hatten, so waren es doch gerade diese Momente, die den Alltag ganz entscheidend erheitert haben. Es gab so viele Szenen, über die ich mich heute noch kaputt lachen könnte. Vielen Dank für die schöne Zeit, yeeesss!

Etwa nach der Hälfte meiner Promotion bekam ich Dylan Yost als neuen Bürokollegen. Wer Dylan kennt, der weiß, dass man ihn eigentlich nur mögen kann. Seine offene und lustige Art macht ihn nach kürzester Zeit zum Mittelpunkt jeder Konversation. Dylan, ich kann mich an keinen einzigen Tag erinnern, an dem ich nicht über irgendeinen Witz von Dir gelacht hätte. Genauso erinnere ich mich nicht daran mal einen Tag erlebt zu haben, an dem Du kein Youtube Video geschaut hast. Auch wenn Du sicherlich für den einen oder anderen kurzzeitigen Blutdruckanstieg während des Schreibens meiner Dissertation verantwortlich bist, so hatten wir doch auch immer mächtig Spaß sowohl bei der Arbeit als auch am Wochenende.

In den ersten Jahren meiner Promotion hatte ich das Vergnügen, Guido Saathoff meinen Bürokollegen nennen zu dürfen. Als bekennender HSV-Fan hattest Du es wahrlich nicht immer leicht, was Deiner unterhaltsamen Persönlichkeit allerdings keinerlei Abbruch tat. Deine geistreichen Sprüche und die vielen Pizzaabende in der Kurfürstenarena gehören zweifellos zu den Höhepunkten meiner Zeit in München. Desweiteren hab ich durch Dich gelernt, dass Whiskey nicht nur durch den Zusatz von Cola genießbar wird. Man kann nämlich auch Red Bull reinkippen. Aber sowas machen wir natürlich nicht.

Apropos Red Bull: Axel Beyer, der Mann am Wasserstoff-Experiment, hat etwa zeitgleich mit mir am MPQ als Masterstudent begonnen. Somit hat er mich durchgängig von Anfang bis Ende als Kollege begleitet. Zusammen haben wir Ringberg-Seminare, DPG-Tagungen und einige Wiesnabende erlebt. Besonders stolz hat mich gemacht, als Du gelernt hast, den Kamm selbstständig wieder zu locken. Inzwischen bist du natürlich längst ein Profi darin. Deswegen: Axel ganz alleine gut gemacht!

Unseren Technikern Charly Linner und Wolfgang Simon sowie unserem Elektroniker Helmut Brückner gebührt ein großes Dankeschön für all die Werkstücke und elektronischen Schaltungen, die für jedes Experiment unerlässlich sind. Bei allen administrativen Angelegenheiten war der unermüdliche Einsatz von Ingrid Hermann unerlässlich und eine große Erleichterung. Vielen Dank für all Eure Hilfe!

Seitens der Universität Hannover war Silke Ospelkaus meine Betreuerin und somit ganz entscheidend für meine Promotion. Für Dein Vertrauen und Deine Hilfsbereitschaft kann ich mich gar nicht genug bedanken. Ich hätte mir wahrlich keine bessere Betreuerin wünschen können!

Abschließend möchte ich mich nochmal bei der gesamten Hänsch-Gruppe für die gute Atmosphäre, den Zusammenhalt und den netten Umgang miteinander bedanken. Das haben wir gut hinbekommen! Stark 👍👍

# Curriculum Vitae

## Stefan Droste

### Personal Information

| | |
|---|---|
| Hans-Kopfermann-Strasse 1 | ☎ +49 89 32905 266 |
| D-85748 Garching, Germany | ✉ stefan.droste@mpq.mpg.de |

| | |
|---|---|
| Date of birth: | 11 September 1984 |
| Place of birth: | Muenster, Germany |
| Nationality: | German |

### Scientific Education

| | |
|---|---|
| Since Oct 2010 | Max Planck Institute of Quantum Optics, Garching, Germany<br>*Research towards the doctoral degree in the laser spectroscopy division of Prof. Theodor Hänsch* |
| Mar 2009 - Sep 2010 | Coherent Inc., Santa Clara, CA, USA<br>Research Laser Systems (RLS) department, R&D group |
| Sep 2007 - Oct 2009 | Muenster University of Applied Sciences, Steinfurt, Germany<br>*Master of Science in Photonics* |
| Mar 2007 - Mar 2009 | Photonics Laboratory, Steinfurt, Germany |
| Aug 2003 - Sep 2007 | Muenster University of Applied Sciences, Steinfurt, Germany<br>*Diploma in Physical Engineering* |

### General Education

| | |
|---|---|
| Aug 2001 - Jul 2003 | Berufskolleg Warendorf, Germany<br>– A - level<br>– Main area: Electrical Engineering |
| Aug 1995 - Jun 2001 | Johann-Heinrich-Schmülling-Schule, Warendorf, Germany |
| Aug 1991 - Jun 1995 | Overbergschule, Warendorf, Germany |